Stony Brook University

Solid state NMR study of protonic conductors for applications as electrolyte materials in Solid Oxide Fuel Cells

A Dissertation Presented

by

Lucienne Buannic

to

The Graduate School

in Partial Fulfillment of the

Requirements

for the Degree of

Doctor of Philosophy

In

Chemistry

Stony Brook University

August 2011

Stony Brook University

The Graduate School

Lucienne Buannic

We, the dissertation committee for the above candidate for the

Doctor of Philosophy degree, hereby recommend

acceptance of this dissertation.

Clare P. Grey – Dissertation Advisor
Professor, Department of Chemistry

John B. Parise - Chairperson of Defense
Professor, Department of Chemistry

Peter Khalifah – Third Member of Defense
Assistant Professor, Department of Chemistry

Tatyana Polenova – Outside Member of Defense
Associate Professor, Department of Chemistry and Biochemistry, University of Delaware

This dissertation is accepted by the Graduate School

Lawrence Martin
Dean of the Graduate School

Abstract of the Dissertation

Solid state NMR study of protonic conductors for applications as electrolyte materials in Solid Oxide Fuel Cells

by

Lucienne Buannic

Doctor of Philosophy

in

Chemistry

Stony Brook University

2011

In the context of the current energy crisis, we need to develop cleaner and more efficient energy conversion devices. The Solid Oxide Fuel Cell is one of the most promising conversion devices currently under study: it creates electricity by reduction of either fossil fuels or biofuels with an efficiency of up to 60% (compared to 30% for a combustion engine). In order to render this application viable for commercialization, we need to reduce the operating temperature of the device. This will decrease the fabrication cost and considerably extend the lifetime of the device, however the ionic conduction has to be kept as high as possible. Electrolyte materials used in the first commercialized devices were based on oxygen conduction and are active for temperatures above 700°C. These materials can be replaced by protonic conductors, which show similar conductivities but in the range of 200 to 400°C. This dissertation aims at explaining the structural differences and protonic conduction pathways between three of the most promising candidates: $BaZr_{1-x}Sc_xO_{3-\ y}(OH)_y$, $BaSn_{1-x}Y_xO_{3-y}(OH)_y$ and $BaZr_{1-x}Y_xO_{3-\ y}(OH)_y$. The combination of substitution level, cationic arrangement and protonic distribution strongly influences the protonic conduction of each. In $BaZr_{1-x}Sc_xO_{3-y}(OH)_y$, the scandium substitution is limited by the instability of the Sc-O-Sc environments, which exist but in a limited amount. These environments act as energetic traps for protons: the charge carriers are strongly bonded to these Sc-O-Sc environments considerably reducing their mobility. In $BaSn_{1-x}Y_xO_{3-\ y}(OH)_y$, Y^{3+}

and Zr^{4+} tend to alternate in the structure for high substitution levels (50%) leading to the presence of mostly one oxygen site, Sn-O-Y. This should facilitate the conduction of protons; however some unordered regions lead to the trapping of protons on Sn-O-Sn sites, reducing the protonic conductivity. Finally in $BaZr_{1-x}Y_xO_{3-\ y}(OH)_y$, the yttrium cations are distributed randomly in the structure and the larger size of Y^{3+} combined with its smaller electronegativity - as compared to Sc^{3+} - prevents the protons from being trapped on Y-O-Y environments. Our study explains why $BaZr_{0.80}Y_{0.20}O_{2.90-y}(OH)_y$ is the best protonic conductor as reported by impedance spectroscopy.

Table of Contents

List of Figures

List of Tables

List of Abbreviations

CSA	Chemical Shift Anisotropy
CT	Central Transition
HETCOR	HETeronuclear CORrelation
IT	Intermediate Temperature
MAS	Magic Angle Spinning
MQ	Multiple Quantum
NMR	Nuclear Magnetic Resonance
SOFC	Solid Oxide Fuel Cell
ST	Satellite Transition
TRAPDOR	TRAnsfer of Population in DOuble Resonance
XRD	X-Ray Diffraction

Acknowledgments

First, I would like to acknowledge Professor Clare Grey for her guidance throughout my PhD. She is a brilliant scientist and she has led me through my very first steps in research. Her patience and kindness are infinite and without her assistance, none of this research would have made any sense to me.

I would like to thank all my past and present fellows in the Grey lab. It has been a pleasure working with all of you; I am so glad we were able to share parts of this scientific journey together. I would like to dedicate special thanks to Dr. Frédéric Blanc, who has motivated me during this experience and offered me a hand with the research on many occasions.

I would like to express gratitude to Dr. Zhehong Gan (National High Magnetic Field Laboratory in Tallahassee), Dr. Boris Itin (New York Structural Biology Center), Dr. Dinu Iuga (The UK 850 MHz Solid-State NMR Facility) for sharing their expertise in running high field NMR. I would like to acknowledge Drs. Yoshihiro Yamazaki and Sossina Haile for the fruitful discussions and collaboration shared throughout the years.

I am extremely grateful to all of my friends who have been a crucial part of this process. Without their continuous support, I would not be writing this manuscript today. Special thanks to Kellie Aldi, who has put a smile on my face so many times when the world was crumbling and shared these five years with me, to Pranav Nawani for initiating me to the madness of Indian parties, to Abhishek Rao for his kindness, patience, attention and support throughout many of those years, to Ramón Fernández for his encouragement, love, presence and the discussions we shared about changing the world, to Kanishk Kapilashrami for the craziness he brought to my life and openly sharing his opinions, to YanYan Hu for bringing me support and comfort in the last steps of this tortuous journey and to Jack Lam and Kunal Shroff for all the hiking trips in the Catskills. I have discovered myself through all of you, gone behind what I thought I was capable of doing thanks to you, and we will always share the same passion for Science.

Finally, I would like to thank my parents for their open mind which has led me here to the USA, for their continuous trust in me, for their love of life and their incessant optimism. Without both of you, I would have never completed this amazing journey.

Chapter 1:

Introduction

This chapter describes the context in which this research was performed. The development of Solid Oxide Fuel Cells over the last decade has led to the need for better protonic conductors to render this application commercially viable on a larger scale. The best available protonic conductors and their characteristic structure will be described here. This research has been performed using solid-state NMR spectroscopy. This versatile technique has led to a large contribution in the understanding of the material science world. The second half of this chapter will describe the theory behind the different interactions to be considered while performing NMR and various methods to extract structural information from the studied materials in order to understand their limitations and propose better candidates.

I. Solid Oxide Fuel Cells

A. The next generation of highly efficient energy converter devices

In the last decade, a major concern of scientists has been to resolve the world's energy crisis. We are slowly using up all of our resources of fossil fuels while at the same time facing problems related to global warming making it a priority to find newer and cleaner ways to produce energy. Fuel cells offer a good alternative to the current power generation devices such as combustion engines found in cars and stationary heating appliances like household boilers: they allow the conversion of chemical energy into electrical energy with high efficiency and limited production of toxic by-products. In addition to emitting smaller quantities of CO_2 compared to current power generation devices, fuel cells are also a lot quieter and provide fuel flexibility. [1-5]

Solid Oxide Fuel Cells (SOFCs) are fuel cells constituted of only solid state materials and gases operating at high temperatures. The anode, electrolyte and cathode materials are made of ceramics which allow electronic and/or ionic transport at elevated temperatures. Each cell is extremely thin, only a couple of millimeters, can provide approximately 1 $W.cm^{-2}$ [3]and can be connected to the next cell via the interconnect. In this way, single cells can be stacked up to deliver more energy. As described in *Figure 1.1*, SOFCs are based on the reduction of dioxygen contained in the air at the cathode:

$$\tfrac{1}{2}\, O_2(g) + 2\, e^- \rightarrow O^{2-}(s) \qquad \text{cathode,}$$

followed by the transport of oxygen anions through the solid electrolyte and finally the oxidation of H_2 at the anode by the oxygen anions:

$$O^{2-}(s) + H_2(g) \rightarrow H_2O(g) + 2\, e^- \qquad \text{anode.}$$

If H_2 is directly provided to the cell (at the anode), the only resulting by-products consist of water at the anode and N_2 from the air at the cathode; however this requires the extraction of H_2 from hydrocarbons prior to use in the cell. Due to the high working temperature required for oxygen conduction through the ceramic materials, from 500°C to 1000°C, hydrocarbons and biofuels can be refined in situ the cell preventing the use of external reformers and reducing the complexity of the system; [2, 6-9] in such case CO_2 becomes an additional by-product. The

efficiency of the conversion compared to a combustion engine is significantly improved, from 30% to 60%.[10] The requirement for high operating temperatures can be seen as a major drawback for the application of this device. However, the community has thought of many ways to make use of this thermal energy, for example by combining the SOFC to a steam turbine where the hot exhaust gases would be used to drive the turbine and produce additional electricity, hereby increasing the overall efficiency of the device to 70%.[1, 11-12]

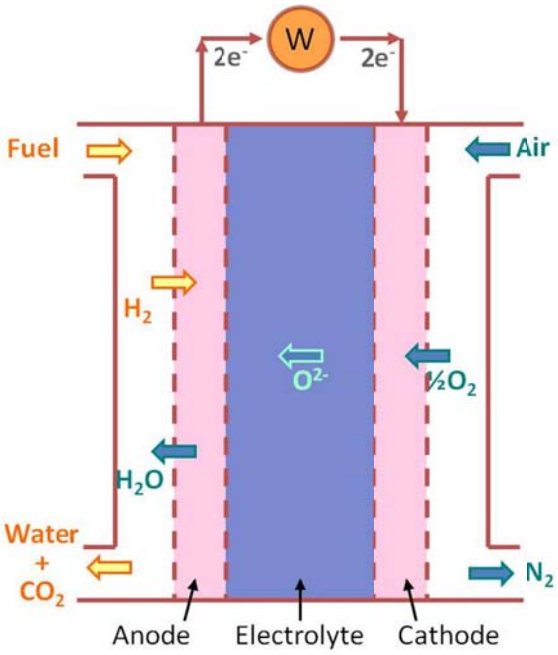

Figure 1.1. Scheme of a solid oxide fuel cell based on oxygen conduction.

Even though there are ways to enhance the efficiency of SOFCs operated at high temperature, this characteristic still limits the extended commercial development of SOFCs. Indeed operation at elevated temperature implies long start up and shut down times, high corrosion rate of metallic compounds and disparities in thermal expansion behaviors of the different parts of the cell leading to high wear and tear and therefore, expensive fabrication costs.[4, 13] In terms of applications, it confines the SOFCs to stationary power generators. In order to reduce the fabrication cost and expand the use of SOFCs to portable applications, it is necessary to lower the operating temperature of the cell and move on to Intermediate Temperature SOFCs (IT-SOFCs) which function in between 200 and 400°C. Achieving such a transformation requires the development of electrolyte materials that can conduct ions at similar

rates obtained today but at lower temperatures. Such a challenge requires the understanding of ionic conduction pathways in the electrolyte which led to the research presented in this dissertation.

B. Electrolyte materials: oxide conductors and possibly protonic conductors?

The high temperature SOFCs rely on the conduction of oxygen through the electrolyte material traditionally based on ZrO_2, CeO_2 and $LaGaO_3$. In order to reduce the operating temperature of SOFCs, new materials characterized by high ionic conduction (with no electronic conduction) at lower temperatures need to be developed. In the 1960s, Stotz and Wagner[14] discovered that some oxides were hosting protons as minor charge carriers. Further studies[15-17] outlined that perovskite based materials already known for their oxygen conductivity also presented potential applications as protonic conductors. Since the size of proton is significantly smaller than the one of oxygen and its charge is 1+ *vs.* 2-, high protonic conductivities can be achieved at lower temperatures in SOFCs. *Figure 1.2* illustrates that the protonic conductivity of yttrium substituted $BaZrO_3$ at 400°C is higher than the oxygen conductivity observed in the best oxygen conductors, hereby showing the strong potential of perovskite based materials as protonic conductor electrolytes for IT SOFCs.

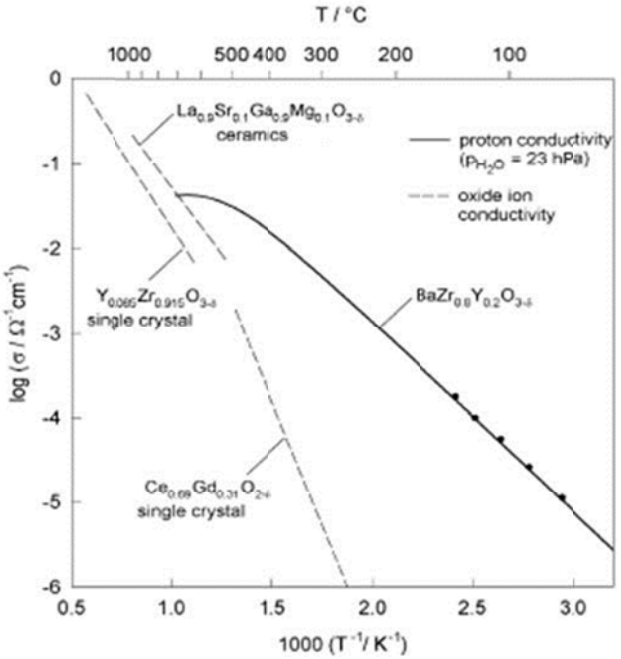

Figure 1.2. Proton conductivity of $BaZrO_3$ compared to the best oxide ion conductors. Figure taken from reference 18.

IT-SOFCs differ from SOFCs by the reactions occurring at the anode and the cathode due to the fact that the charge carriers traveling through the electrolyte are now protons rather than oxygen ions:

$$H_2(g) \rightarrow 2\,H^+(s) + 2\,e^- \qquad \text{anode}$$

$$2\,H^+(s) + \tfrac{1}{2}\,O_2(g) + 2\,e^- \rightarrow H_2O(g) \qquad \text{cathode}$$

The by-products are still the same but water is now released at the cathode (*Figure 1.3*). Note that the ions are now traveling through the electrolyte from the anode to the cathode.

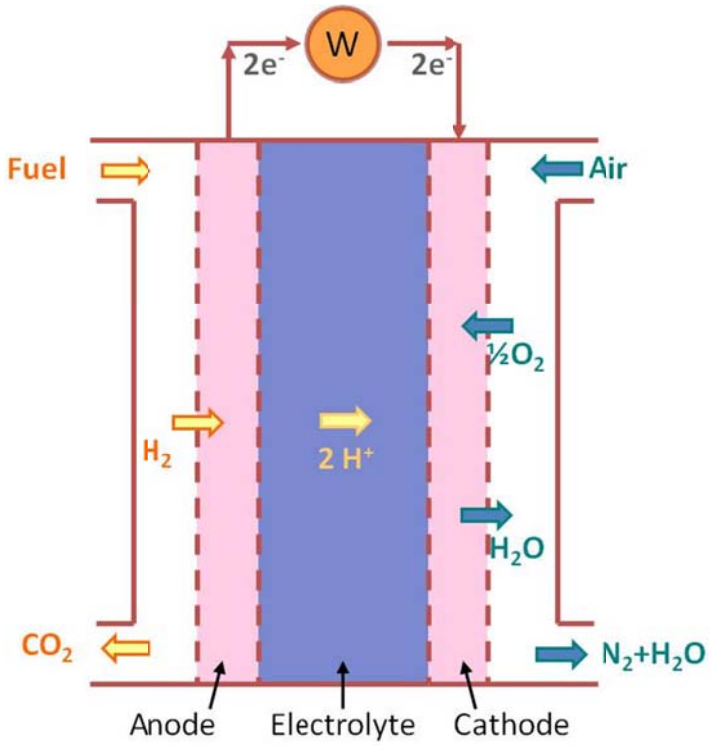

Figure 1.3. Scheme of a solid oxide fuel cell based on protonic conduction.

Kreuer reported in a detailed review[19] the characteristics of a large range of perovskite based protonic conductors. Aside from high conductivity behavior, in order to be applied in the SOFCs, the perovskite based candidates need to be stable under the various environments present in the cell: the material should not decompose under H_2O atmosphere or in the presence of CO_2 nor be reduced when exposed to the cathode environment. Although $BaCeO_3$, $BaTbO_3$, $BaThO_3$ and $SrCeO_3$ are good protonic conductors once hydrated (*Figure 1.4*), they are not very stable under carbon dioxide atmospheres.[20-23] $SrTiO_3$ and $BaTiO_3$ are more stable, but they do not incorporate protonic defects readily.[19] In contrast, $BaZrO_3$ is stable in the presence of CO_2 and it

can readily incorporate protonic defects, making this perovskite material the strongest candidate for this application so far.[24] $BaSnO_3$ is also stable under CO_2 and H_2O atmospheres which makes this material another potential candidate even though the conductivity reached by this material is smaller than the one for $BaZrO_3$.[19] However, the stability under H_2 atmosphere has not yet been extensively studied.

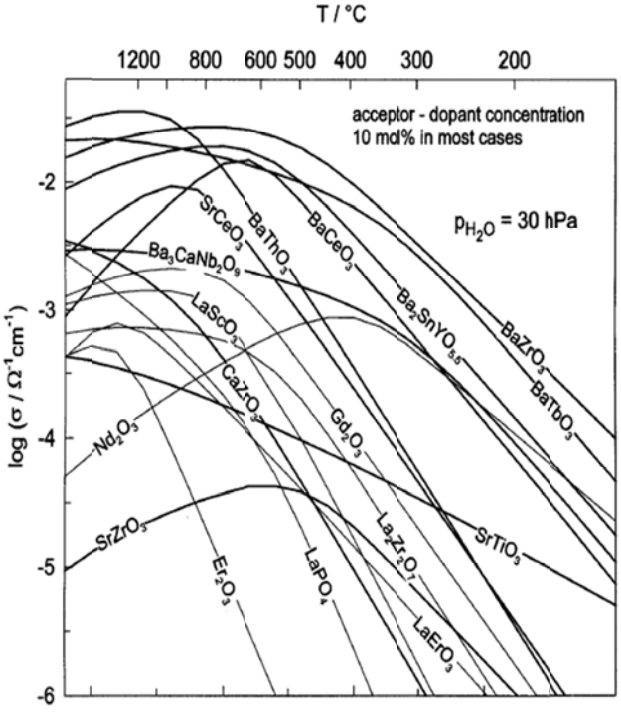

Figure 1.4. Proton conductivities of various oxides. Conductivities of perovskite type oxides are shown by bold lines. Figure taken from reference 19.

In order to improve the current properties of these materials, it is important to understand how protonic conduction works. Our aim is to determine the local structure of these materials and explain the pathway undergone by protons during the conduction mechanism. Since the materials most likely to be applied as electrolytes in IT SOFCs are $BaZrO_3$ and $BaSnO_3$, we will mainly focus our efforts on those two materials.

C. Perovskite structure and implications for protonic transport

One of the ways to lower the high operating temperatures of SOFCs is to replace oxygen-ion conducting electrolytes by protonic conductors. Most of the perovskite-type materials, originally studied as anionic conductors, are also potential protonic conductors after hydration. The general formula for a perovskite structure is ABX_3 where A is a large cation 12-fold coordinated to the anion X while B is a smaller cation occupying the centre of an octahedral unit surrounded by 6 X anions (*Figure 1.5*). Both $BaZrO_3$ and $BaSnO_3$ are cubic perovskites with space group Pm3m where the A cation (Ba) is divalent and the B cation (Zr or Sn) is tetravalent, i.e., $A^{+II}B^{+IV}O_3$.[25]

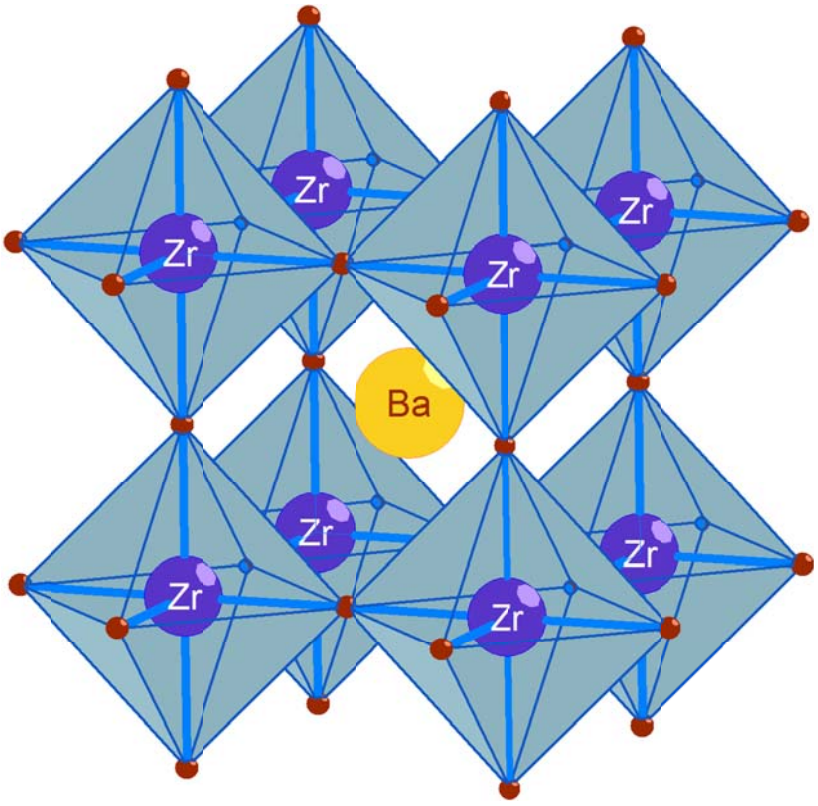

Figure 1.5. Cubic perovskite structure of $BaZrO_3$.

The substitution of some of the B^{4+} cations by M^{3+} cations leads to the creation of oxygen vacancies for charge balance reasons, one vacancy being formed for every two M^{3+} cations incorporated. The new structure can now be written as $A(B_{1-x}M_x)O_{3-x/2}\square_{x/2}$ where □ represents the oxygen vacancy. These oxygen vacancies, which lead to the oxygen motion at high temperatures, also allow for the hydration of the structure at lower temperatures: one molecule of

water can react with an oxygen vacancy to form two OH groups, generally referred to as the protonic defects as illustrated in *Figure 1.6*. The proton ions of these defects can hop from oxygen anion to oxygen anion at intermediate temperatures giving rise to protonic conduction.

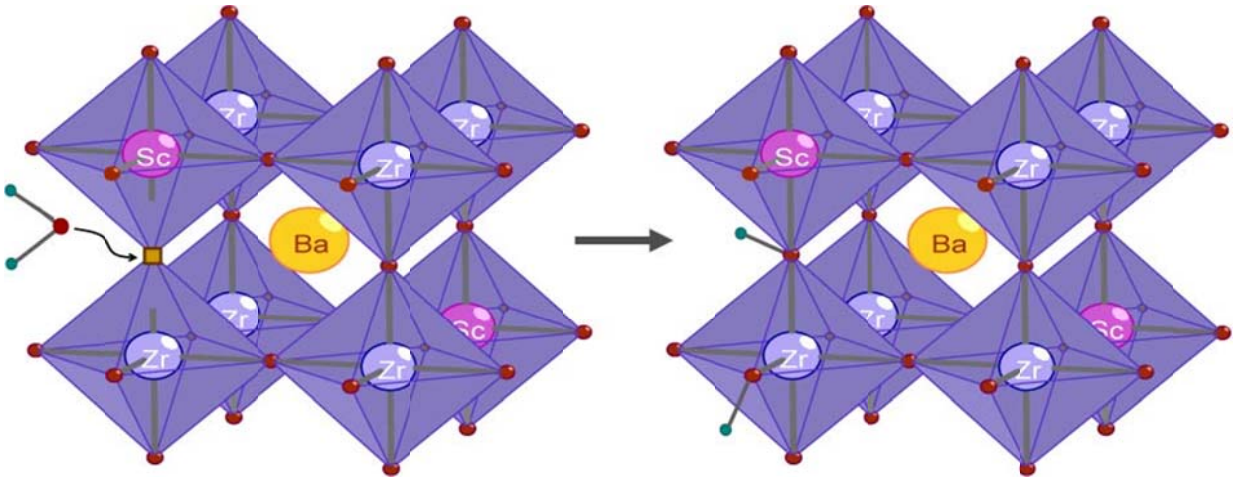

Figure 1.6. Hydration process of the $BaZr_{1-x}Sc_xO_{3-x/2}$ crystal structure. The yellow, blue, pink, red and green atoms respectively represent barium, zirconium, scandium, oxygen and hydrogen atoms.

The choice of the substituting cation will determine the symmetry and the conductivity of the new structure. In the case of $BaZrO_3$, a large range of substituting cations has been studied. The best results were obtained for substituting cations having a radius close to the one of Zr^{4+} (*Figure 1.7*), which limits the loss of symmetry resulting from the substitution,[19] the most promising acceptor substituting element for $BaZrO_3$ being yttrium. $BaZr_{1-x}Y_xO_{3-\delta}$ has been extensively studied by impedance spectroscopy;[26-37] however there is still a lack of understanding on the local structure and protonic motion occurring in this material. This research aims at clarifying the protonic conduction pathways in $BaZr_{1-x}Y_xO_{3-\delta}$ with the use of solid-state nuclear magnetic resonance (NMR) spectroscopy, a technique that will be introduced in the second half of this chapter. Since yttrium is not the easiest nucleus to investigate using solid-state NMR, we will also focus on scandium-substituted $BaZrO_3$. While a large literature exists on yttrium-substituted $BaZrO_3$, very little has been reported for the scandium-substituted analogue.[18-19] Yttrium has been reported to solubilise at least up to 40% in $BaZrO_3$,[38] while the scandium substitution is limited to approximately 29%.[39-40]

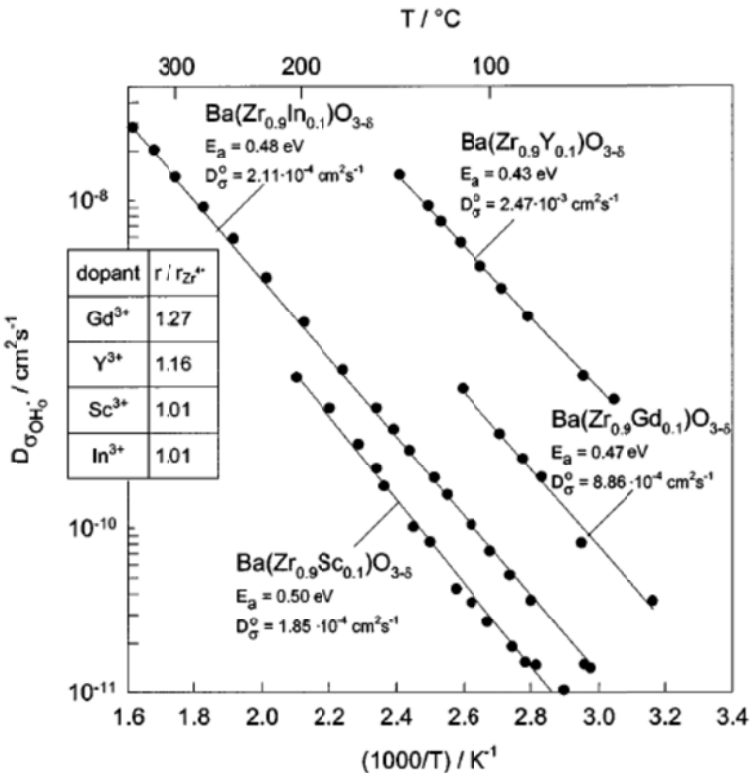

Figure 1.7. Proton mobility in $BaZrO_3$ substituted with different acceptor dopants. Figure taken from reference 19.

For most perovskite-type protonic conductors, the best conductivity values are obtained for low M^{3+} substitution levels, usually between 5 and 20%. The case of $BaSn_{0.50}Y_{0.50}O_{2.75}$ is more unusual as very high conductivities have been obtained for an exceptionally high substitution level of 50%.[19, 41] $BaSn_{0.50}Y_{0.50}O_{2.75}$ has been much less studied as a protonic conductor, although it reaches conductivity values comparable to $BaZr_{1-x}Y_xO_{3-\delta}$[19, 41] and shows good stability under CO_2 and H_2O atmospheres. The understanding of the local structure of $BaSn_{0.50}Y_{0.50}O_{2.75}$ and its protonic conduction mechanism will also be an extended part of this research.

II. Solid State Nuclear Magnetic Resonance Spectroscopy

Most structural studies of materials utilize diffraction methods, which provide long-range structural information such as the extent of tilting of the BO_6 octahedra. However, it is difficult to determine directly the structure of the defects and the relaxation around these defects from these methods. In contrast, solid state nuclear magnetic resonance (NMR) spectroscopy probes the local environments surrounding different nuclei in the structure, and variable temperature methods can be used to investigate the dynamics, complementing impedance spectroscopy measurements. NMR spectroscopy can sometimes separate the dynamics of different species and/or local environments, allowing motional processes seen by impedance spectroscopy to be assigned unambiguously to specific dynamical processes and local environments. In this section, we will introduce the various interactions involved in solid state NMR spectroscopy and review a couple of techniques that allow more information to be extracted from our systems.

A. Magnetic interactions in the solid

1. Zeeman interaction

NMR spectroscopy relies on the existence of a quantized property of the nucleus called nuclear spin angular momentum, I. Nuclei are charged particles and they can, depending on the nuclear structure, possess the property of spin; therefore they produce a small magnetic field and are associated with a magnetic moment, μ. For a nucleus with a spin quantum number I, there are (2I+1) allowed spin states, m_I = -I, (-I+1), ..., (I-1), I. In the absence of a magnetic field, all the states have the same energy level, they are degenerate. The energy levels split in the presence of a magnetic field; this is called the *Zeeman interaction*. For example, in the absence of a magnetic field a hydrogen nucleus (I = 1/2) has two spin states, m_I = +1/2 and m_I = -1/2, both corresponding to the same energy. When this nucleus is placed in an external magnetic field $\mathbf{B_0}$, its magnetic moment couples to the field $\mathbf{B_0}$ causing the two spin states into non-degenerate energy levels (*Figure 1.8*). The difference in energy between states is proportional to the strength of the field $\mathbf{B_0}$ and the corresponding transition occurs in the radio frequency region of the electromagnetic spectrum.[42]

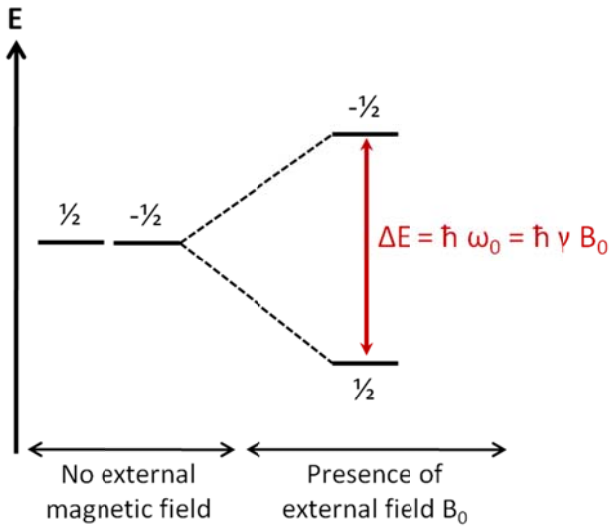

Figure 1.8. The Zeeman Effect on the spin state energy levels.

When NMR active nuclei (*i.e.* nuclei possessing spin) encounter a magnetic field, they will tend to align their magnetic moment along the field in order to minimize their energy. In the quantum mechanical picture, the nuclei will precess about the magnetic field (*Figure 1.9*) at the Larmor frequency ω_0. The Larmor frequency depends on the gyromagnetic ratio γ of the specific nucleus and the strength of the magnetic field $\mathbf{B_0}$, *i.e.* the strength of the magnet used :[43]

$$\boldsymbol{\omega_0 = \hbar\, \gamma\, B_0}$$

The gyromagnetic ratio γ is the ratio between the magnetic moment μ and the angular momentum I; this ratio is therefore unique for each nucleus.

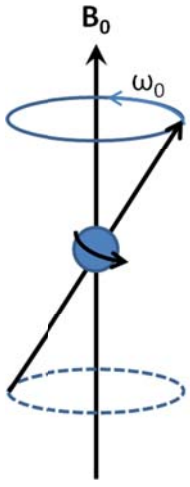

Figure 1.9. Precession of a spinning nucleus resulting from the influence of an applied magnetic field.

2. Effect of a temporary radio-frequency field

Once the spins have reached thermal equilibrium under the external field $\mathbf{B_0}$, an additional magnetic field $\mathbf{B_1}$ is applied via a radio frequency pulse generated by the spectrometer through a coil oriented along a different axis from the direction of the external field $\mathbf{B_0}$. The precession of the spins is now occurring along the axis resulting from $\mathbf{B_0} + \mathbf{B_1}$, i.e. away from the direction of $\mathbf{B_0}$. Once $\mathbf{B_1}$ is removed, only $\mathbf{B_0}$ remains and the axis of precession will relax until it is aligned with $\mathbf{B_0}$, so that thermal equilibrium is regained. The precession frequency and relaxation process are both influenced by the surroundings of the spins and will therefore differ slightly from spin to spin. The local magnetic fields generated by the precession and relaxation of each spin can be captured by the coil and recorded by the spectrometer. After Fourier transform, the evolution of the precession frequency with time gives rise to the NMR spectrum, the differences in frequency leading to different resonances. Interactions of the spin with its local environment affect the resulting lineshape of the NMR signal; the interactions at the origin of lineshape perturbations are detailed in the following sections. The application of the additional magnetic field $\mathbf{B_1}$ is often referred to as applying a $\pi/2$ pulse to the sample, since the strength of the $\mathbf{B_1}$ field is adjusted to flip the sample's magnetization by 90° from the direction of the $\mathbf{B_0}$ field.

3. Chemical Shift Anisotropy

One important interaction of the spin with its local environment occurs through the surrounding electrons. The nucleus is not the only one to have a magnetic moment the electrons also do; therefore not only does the nucleus experience the presence of a magnetic field but the electrons do as well. Even in a diamagnetic system, the presence of a magnetic field will create circulating currents of electrons which will in turn induce small magnetic fields and these small magnetic fields will be felt by the nucleus. As a consequence this will change the total magnetic field experienced by the nucleus and thus its resonance frequency.[44] The strength of the field felt by the electrons changes depending on the orientation of the electron density with respect to the magnetic field; therefore different orientations may give rise to different chemical shifts. This is called the *chemical shift anisotropy* (CSA). While in liquids all molecular orientations are encountered due to the rapid tumbling of the molecules averaging out the CSA, in solids the atomic motion is limited and therefore there is no natural averaging of the CSA. In a single crystal, there are only a limited number of orientations for the nucleus with respect to the

magnetic field leading to sharp resonances. However in a powder, there is a wide range of possible orientations, each interaction resulting in a sharp isotropic resonance at a different shift. The orientation dependence of the CSA contributes to the broadening of the isotropic peak leading to a particular shape illustrated in *Figure 1.10* that is generated by the sum of all the isotropic resonances arising from every single orientation present in the powder. Averaging of the different orientations leads to an isotropic distribution, *i.e.* a distribution for which the interaction between the electron density and the magnetic field is independent of their relative orientation.[45]

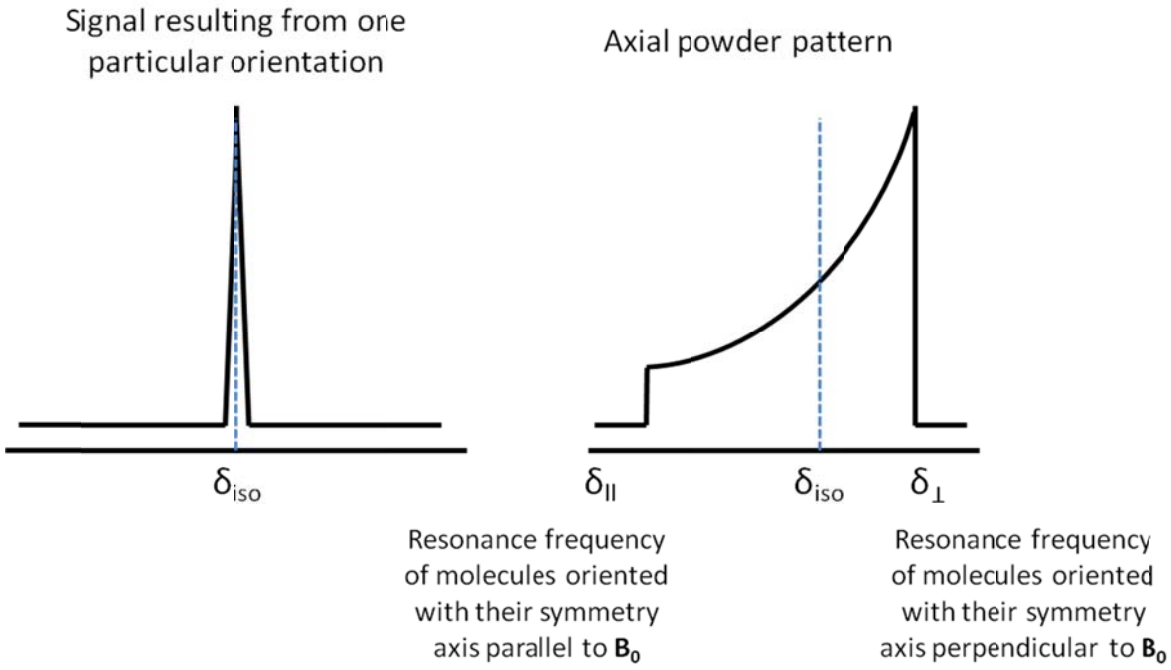

Figure 1.10. The Chemical Shift Anisotropy. On the left, a single crystal with isotropic chemical shift. On the right, a powder pattern with CSA. Figure reprodced from reference 46.

4. Dipolar coupling

In addition to being influenced by the local electronic density, the nucleus will also interact with other nearby nuclei if these nuclei are magnetic. For a first spin I, the magnetic interaction between the nucleus and the external field $\mathbf{B_0}$ results in the presence of a magnetic field at the nucleus; the same happens to a spin S located in spatial proximity to the spin I. If

these two spins are spatially close enough, they can interact with one another, modifying the resulting magnetic field at each nucleus. This interaction is called *dipolar coupling*, and can be homonuclear, if I and S are the same isotope, or heteronuclear. The strength of the interaction between two spins depends on their gyromagnetic ratio, the distance between the two spins - the interaction is inversely proportional to the cube of the internuclear distance - and the orientation of the I-S internuclear vector with respect to the external field $\mathbf{B_0}$. The last property gives rise to the particular lineshape for a powder called Pake doublet, illustrated in *Figure 1.11*.[44]

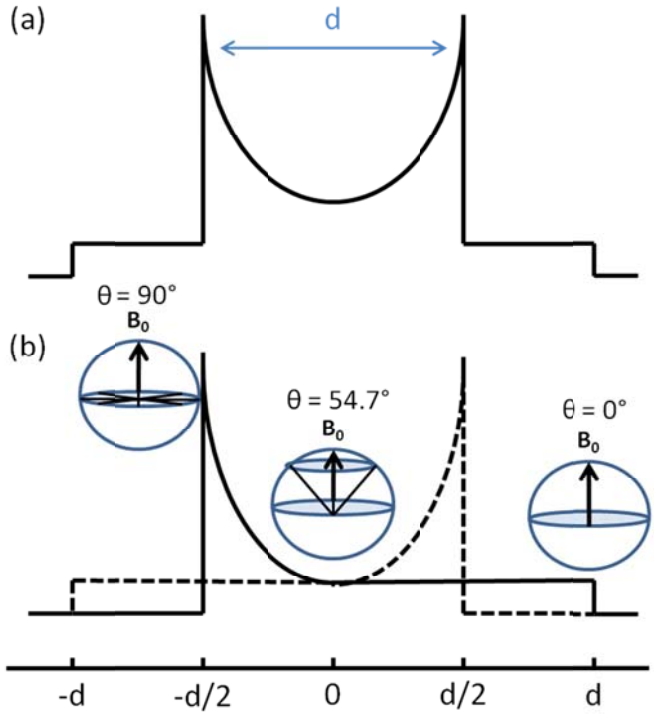

Figure 1.11. Dipolar Pake pattern for two coupled spins in a powder sample. (a) Overall shape and (b) Contribution of the different spin pair orientation to the lineshape. Figure reproduced from reference 44.

The two complementary patterns of the Pake doublet (*Figure 1.11 b*) arise from different energy contributions depending on the alignment of spin I with respect to spin S. The intensity of each pattern reflects the percentage of one particular orientation of the spin pair related to the external field $\mathbf{B_0}$.

5. Quadrupolar interaction

There are 120 NMR active nuclei in the periodic table, amongst which 80 have spin > 1/2.[47] These nuclei are called quadrupolar due to their non-spherical charge distribution; this particular charge distribution leads to the presence of a nuclear quadrupole moment eQ that can interact with the electric field gradient at the nucleus. The resulting interaction is called *quadrupolar coupling* and depends on both the strength of the quadrupolar moment and the electric field gradient at the nucleus. The quadrupolar coupling constant C_Q can be expressed as:

$$C_Q = \frac{e\,Q * V_{zz}}{\hbar} = \frac{e^2\,Q\,q}{\hbar},$$

where eq and V_{zz} represent the electric field gradient. There are two categories of quadrupolar nuclei, ones with integer spins and ones with half-integer spins; from now one we will only focus on the second category since this work will not involve integer spin quadrupolar nuclei. The quadrupolar interaction has a considerable effect on the NMR spectrum; its dependence on the orientation of the nuclear spins with respect to $\mathbf{B_0}$ affects the nuclear energy level splitting as depicted in *Figure 1.12* for a spin 3/2 nucleus.

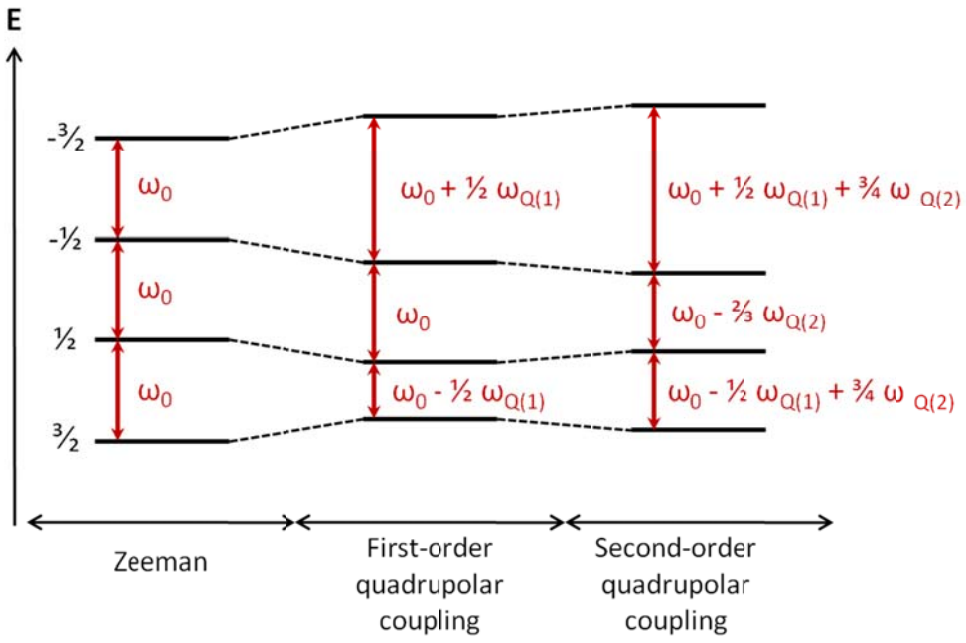

Figure 1.12. Effect of the Zeeman splitting and first- and second-order quadrupolar coupling on the energy levels of a spin 3/2 nucleus.

The first order of the quadrupolar interaction shifts the $m_I = -1/2$ and $m_I = 1/2$ levels by the same amount in the same direction leaving the frequency of the central transition (1/2 to -1/2) unchanged. However the other transitions, 3/2 → 1/2 and -1/2 → 3/2 for a spin 3/2, known as satellite transitions, are both affected by an amount proportional to ω_Q, called the first order quadrupolar frequency, resulting in a shift and a broadening of these resonances.[44] The second order of the quadrupolar interaction does, however, affect the central transition: it leads to its broadening and adds a contribution to the isotropic shift δ_{iso}, in addition to the chemical shift δ_{CS}, which depends on the strength of the quadrupolar coupling.[46] The isotropic shift can now be expressed as:

$$\delta_{iso} = \delta_{CS} + \delta_{QIS}$$

where δ_{QIS} is for the quadrupolar induced shift. The lineshape of the central transition is related to the local symmetry of the site and can be described by the asymmetry parameter:

$$\eta_Q = \frac{V_{xx} - V_{yy}}{V_{zz}}$$

where V_{xx}, V_{yy} and V_{zz} describe the electric field gradient tensor. It is possible to simulate a quadrupolar lineshape and determine both the C_Q and η parameters which are related to the local structure at the nucleus. Depending on the size of the C_Q value, the satellite transitions may be too broad and only the central transition will be observed. One way to confirm the quadrupolar parameters determined from the fit is to acquire the same spectrum at a different field as the second-order quadrupolar interaction is inversely proportional to the strength of the field. However it remains non-trivial to quantify site ratios when the sites have very different sizes of C_Q since some of the signal intensity is contained in the spinning sidebands and it is not always straightforward to separate the contribution of the central transition to the sidebands from that of the satellite transitions. Care needs to be taken when setting up experiments for samples containing sites with very different C_Q as the larger the C_Q the faster the nutation of the spin. The length of the pulse should be chosen accordingly so that the two sites have a linear response in terms of intensity; usually $\pi/2$ pulses are shortened to $\frac{\pi/2}{I+1}$ to ensure such conditions.

B. NMR techniques for solids

1. Magic Angle Spinning

In solution NMR molecules are subject to rapid motion. This leads to the averaging of the different anisotropic interactions such as dipolar coupling and chemical shift anisotropy; this is the reason why, for liquid samples, peaks resulting from the signal are generally very narrow. This is not applicable to solids where molecular motions are much slower than the dominant internal interactions (CSA, dipolar, quadrupolar) which leads to peak broadening and difficulties in extracting isotropic shifts. The effect of the CSA and the dipolar coupling are strongly related to the orientation of the local environment of the nucleus with respect to the external magnetic field $\mathbf{B_0}$ through the following factor: $(3\cos^2\Theta - 1)$ where Θ is the angle between the principal axis of the interaction and the external magnetic field $\mathbf{B_0}$. In order to remove the impact of these two interactions on the NMR lineshape, the angle Θ has to be equal to 54.74°, *i.e.* all residual nuclear magnetic fields should align at this angle with respect to the external field $\mathbf{B_0}$. Rotating the sample fast enough around an axis at an angle of 54.74° from the external field $\mathbf{B_0}$ creates the illusion that all the residual nuclear magnetic fields are parallel to this axis, removing the CSA and dipolar interactions (*Figure 1.13*). This angle is called Magic Angle and gives its name to the NMR technique, *Magic Angle Spinning* (MAS).[43]

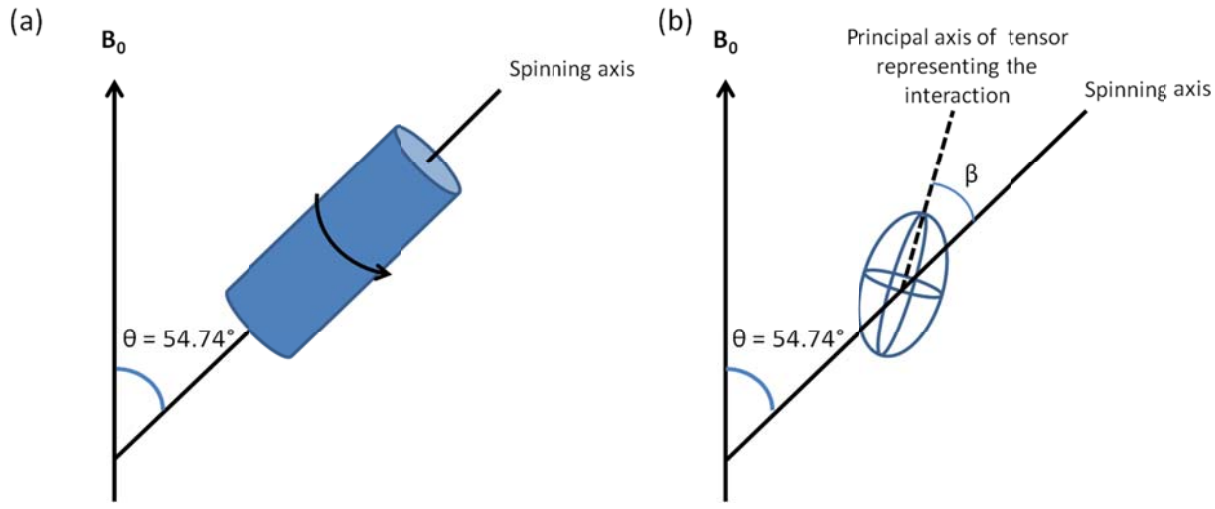

Figure 1.13. The Magic Angle Spinning experiment. (a) The sample is spun rapidly in a cylindrical rotor about a spinning axis at the magic angle (Θ = 54.74°) with respect to the external field $\mathbf{B_0}$. (b) The nuclear interaction tensor is represented by an ellipsoid; it is fixed to the molecular frame to which it applies and so rotates with the sample. Figure reproduced from reference 46.

If the spinning speed is fast enough to completely average the interactions, then a sharp resonance whose shift corresponds to the isotropic chemical shift is observed (*Figure 1.14*). For slower spinning speeds, the signal breaks down into the isotropic resonance surrounded by a set of spinning sidebands separated by the spinning frequency; these sidebands are the result of the remaining non-averaged terms of these interactions.

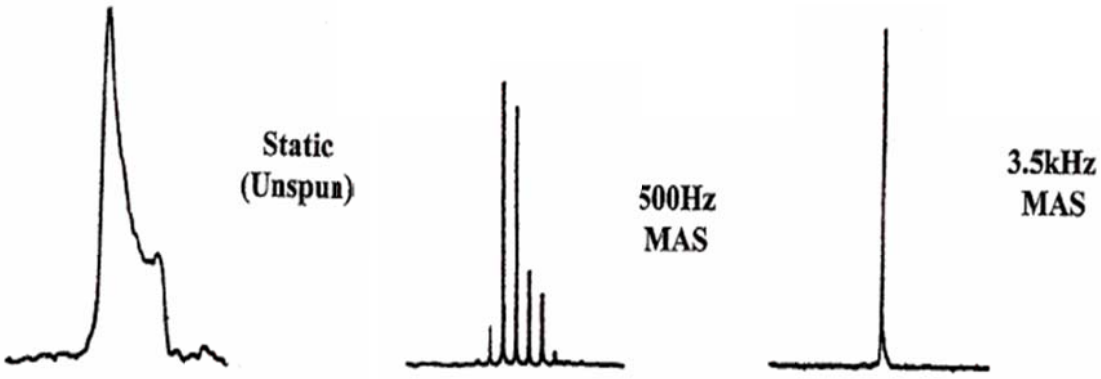

Figure 1.14. Effect of MAS at various speeds on an NMR spectrum. Figure from reference 48.

In the case of the quadrupolar interaction, MAS is generally never enough to completely average this interaction due to the size of the first-order quadrupolar interaction and the incomplete averaging of the second-order quadrupolar interaction; therefore various pulse sequences have been developed to facilitate the analysis of the local structure surrounding quadrupolar nuclei. We will detail two of those in the next sections: the first one is used to reduce the effect of the quadrupolar coupling and clarify peak assignment (MQMAS) and the second one to identify the quadrupole's neighbors by reintroduction of the dipolar coupling interaction (TRAPDOR).

2. MQMAS

Most of the initial techniques developed to increase the spectral resolution of quadrupolar nuclei relied on spinning the sample at two different angles simultaneously; it is evident that achieving such technical performances is extremely challenging. Multiple-Quantum Magic angle Spinning[49] (MQMAS) was a considerable breakthrough in the world of quadrupolar nuclei since it was the first pulse sequence leading to high spectral resolution while spinning the rotor at only one angle, the magic angle.[46] MQMAS is a two-dimensional experiment which correlates a

multiple quantum transition ($m_I \rightarrow -m_I$) to the central transition ($1/2 \rightarrow -1/2$) (*Figure 1.15*). It consists of the excitation of a symmetric <m,-m> multiple quantum transition by a single high power radio frequency pulse followed by an evolution time t_{1a} during which the quadrupolar interaction is allowed to evolve. A selective pulse is applied to convert the multiple quantum transition $<m_I,-m_I>$ into an observable coherence, <1/2,-1/2>. The single quantum coherence is allowed to refocus during a time t_{1b} after which the acquisition starts.[47] Simultaneous increments of t_{1a} and t_{1b} lead to the two-dimensional spectrum; the increment is preferably set to integer or half integer rotor periods to prevent excessive spinning sideband manifolds. The selection of a particular multiple quantum transition is achieved through predefined phase cycling of the excitation sequence.

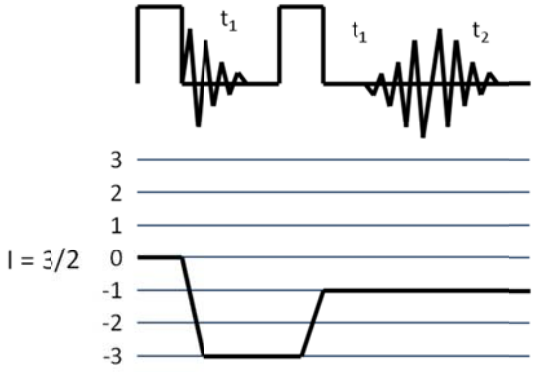

Figure 1.15. MQMAS pusle sequence and coherence pathways. The selected coherence pathways selected here are $0 \rightarrow -3/2 \rightarrow -1/2$ for a spins 3/2. During the time t_1, the second quadrupolar coupling is averaged to zero leaving a scaled isotropic spectrum in the indirect dimension. Figure reproduced from reference 44.

After a 2D Fourier transform and shearing, the resonances will appear as ridges along the diagonal. The projection of each 2D spectrum along the F_1 dimension - *i.e.* the vertical projection - yields an isotropic spectrum free from quadrupolar broadening, the shifts of the resonances in this dimension reflecting the combination of both the isotropic shift δ_{iso} and the quadrupolar induced shift δ_{QIS}. In addition, a one dimensional spectrum can be extracted along the F_2 dimension for each resonance, and fit to yield an estimation of the quadrupolar interaction parameters and chemical shift δ_{CS} for each individual resonance.[44] Examples will be given in the following chapters.

3. TRAPDOR

The transfer of populations in double resonance (TRAPDOR) pulse sequence[50] was developed to study the heteronuclear dipolar coupling between a spin ½ nucleus I and a quadrupolar nucleus S under MAS conditions. The principle of this experiment consists of acquiring a rotor synchronized echo ($\pi/2$ - τ - π - τ) of the spin ½ nucleus I, while continuously irradiating the quadrupolar nucleus S during the τ times (*Figure 1.16*). The irradiation of the quadrupolar spin prevents the refocusing of the echo by modulating the heteronuclear dipolar coupling interaction under MAS. The spectrum of the spin ½ I resulting from acquisition under irradiation of the quadrupolar nucleus S is compared to the spectrum of the spin ½ I obtained from a regular rotor synchronized echo experiment, *i.e.* without S spin irradiation. The differences in the spectra only affect the environment involving the I-S dipolar coupling interaction. Increasing the number of rotor periods in between pulses, *i.e.* increasing the τ values, leads to a stronger dephasing of the spin ½ signal, the spectral differences becoming more obvious.[46-47, 50]

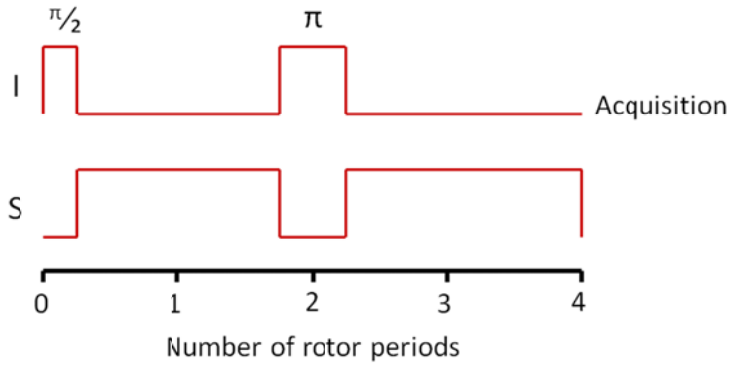

Figure 1.16. Schematic representation of the TRAPDOR pulse sequence.

4. Time scales in NMR

NMR spectroscopy gives access to three different time regimes which relate to various physical processes in the solid (*Figure 1.17*). The *Larmor timescale* is in the same range as molecular rotations, in the 10^{-9} to 10^{-11} s timeframe. Similar to the liquid state, such molecular motion will prevent the CSA from being refocused and will lead to the loss of spinning sidebands if any were previously observed under slower molecular motion. The *spectral*

timescale which ranges from 10^{-4} to 10^{-6} s will be affected by chemical exchange leading to broadening of spectral width and even coalescence of resonances (*Figure 1.18*). Finally slow molecular *relaxation processes* occur in the 10^{-3} to 1 s range and are in the same regime as macroscopic diffusion. Several experiments have been developed to accurately determine the relaxation times as described in the following section.

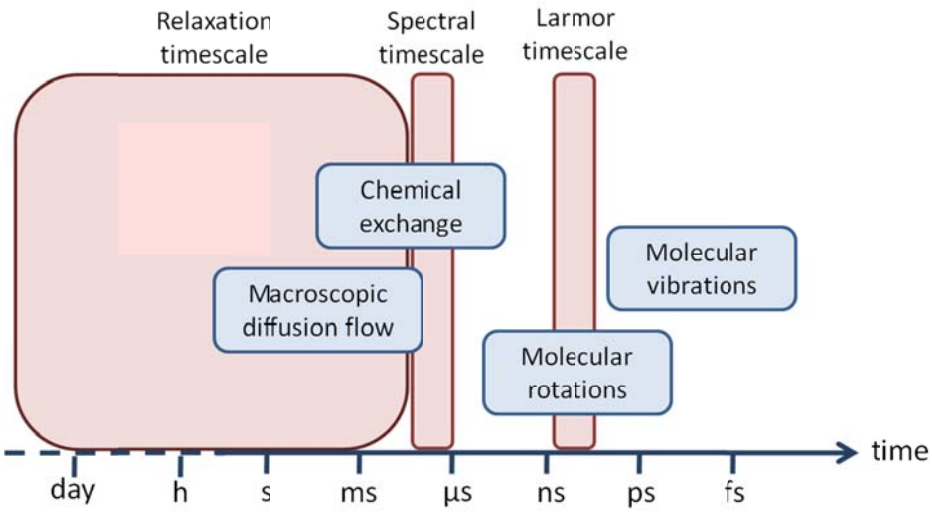

Figure 1.17. Typical motional timescale for physical processes and how they compare to the NMR timeframe. Figure reproduced from reference 45.

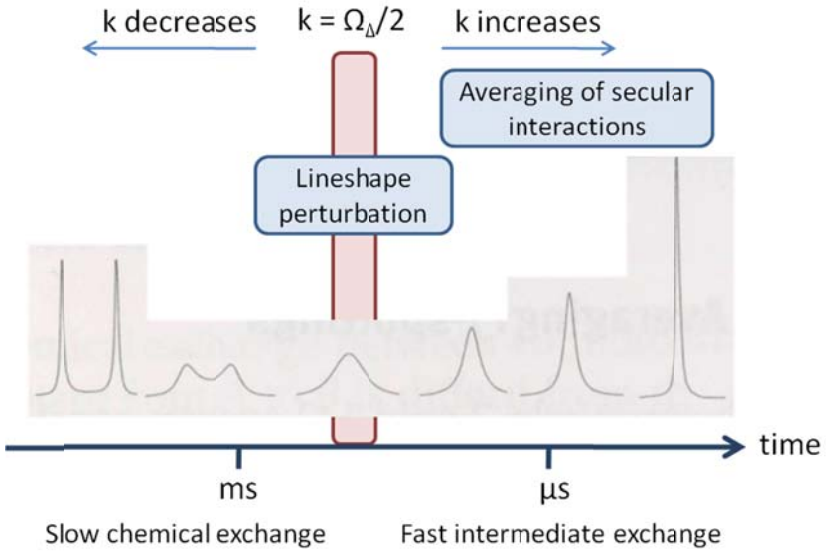

Figure 1.18. Intermediate two site exchange and its effect on the NMR lineshape depending on the regime. Figure reproduced from reference 45.

5. Relaxation times

Once the bulk magnetization has been rotated away from the magnetic field $\mathbf{B_0}$, it will relax back to thermal equilibrium towards the $\mathbf{B_0}$ field by giving up energy to the surroundings, *i.e.* to the lattice. The time constant for the magnetization to recover parts its initial magnetization along the z direction is called the *spin-lattice relaxation time, T_1*. Once the bulk magnetization has been rotated away from the magnetic field $\mathbf{B_0}$, the spins will start precessing at different frequencies leading to the dephasing of the spins magnetization in the x-y plane; the intensity of the bulk magnetization in the x-y plane decreases. The time constant for the magnetization to vanish in the x-y plane is called *spin-spin relaxation, T_2*. Both the T_1 and T_2 time constants are illustrated in *Figure 1.19*. In general for solids, the bulk magnetization is fully recovered along the z direction after its component in the x-y plane has vanished which means that $T_2 < T_1$.[43]

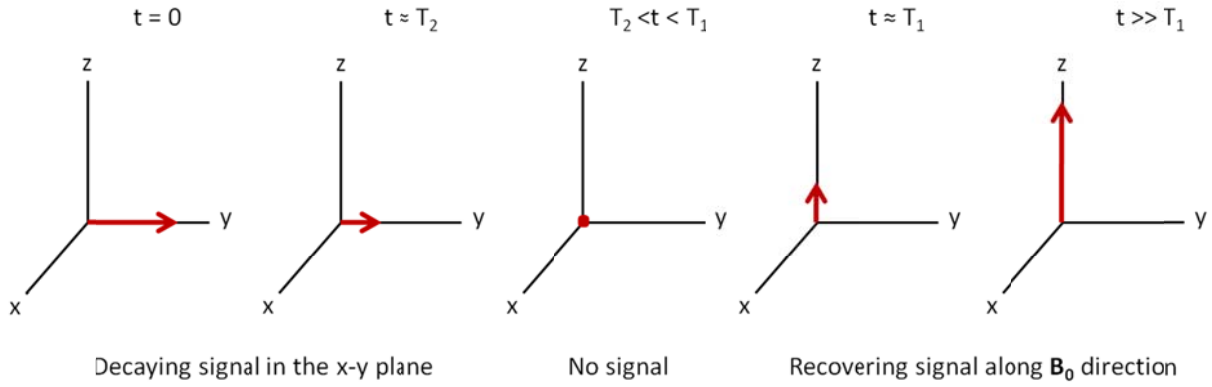

Figure 1.19. T_1 and T_2 relaxation processes. Figure reproduced from reference 43.

The spin-lattice relaxation time T_1 can be determined by using an inversion recovery experiment. The magnetization is inverted by a π pulse, allowed to evolve for a time τ and then rotated by a π/2 pulse. The pulse sequence is repeated with increasing τ times to observe the change of the magnetization intensity in the x-y plane versus τ. For such an experiment, the magnetization obeys the following equation:

$$M(\tau) = M_0 * \left(1 - 2 * \exp\left(\frac{-\tau}{T_1}\right)\right).$$

After extraction of M_0 and $M(\tau)$, the following plot will readily give access to the T_1 value:

$$\ln\left(1 - \frac{M(\tau)}{M_0}\right) = \frac{-\tau}{T_1} * \ln(2).$$

The spin-spin relaxation time T_2 can be measured by using a Hahn echo experiment ($\pi/2$ - τ - π - τ) with increasing values of τ. The magnetization decreases exponentially and can be readily be extracted by fitting the following equation:

$$M(\tau) = \exp\left(-\frac{\tau}{T_2}\right).$$

III. How do we proceed from here?

After this introduction, the second chapter will be dedicated to solving the local structure of $BaZr_{1-x}Sc_xO_{3-x/2}$ and drawing a first assignment of the different protonic environments encountered in the material using solid state NMR. The third chapter will attempt to understand the differences observed in $BaZr_{1-x}Y_xO_{3-x/2}$ compared to $BaZr_{1-x}Sc_xO_{3-x/2}$. The fourth chapter will cover the unusual characteristics of the $BaSn_{0.50}Y_{0.50}O_{2.75}$ structure observed by solid-state NMR and their consequences on protonic conduction. Finally the fifth chapter will consist of a detailed protonic study of the three materials.

IV. References

1. S. C. Singhal, *MRS Bulletin*, 2000, **25**, 16.

2. R. M. Ormerod, *Chemical Society Reviews*, 2003, **32**, 17.

3. A. Lashtabeg and S. J. Skinner, *Journal of Materials Chemistry*, 2006, **16**, 3161.

4. D. J. L. Brett, A. Atkinson, N. P. Brandon and S. J. Skinner, *Chemical Society Reviews*, 2008, **37**, 1568.

5. J. C. Ruiz-Morales, D. Marrero-Lopez, M. Galvez-Sanchez, J. Canales-Vazquez, C. Savaniu and S. N. Savvin, *Energy and Environmental Science*, 2010, **3**, 1670.

6. Z. Zhan and S. A. Barnett, *Science*, 2005, **308**, 844.

7. M. D. Gross, J. M. Vohs and R. J. Gorte, *Journal of Materials Chemistry*, 2007, **17**, 3071.

8. W. Jamsak, S. Assabumrungrat, P. L. Douglas, N. Laosiripojana, R. Suwanwarangkul, S. Charojrochkul and E. Croiset, *Chemical Engineering Journal*, 2007, **133**, 187.

9. E. D. Wachsman and S. C. Singhal, *Electrochemical Society Interface*, 2009, **18**, 38.

10. G. W. Crabtree and M. S. Dresselhaus, *MRS Bulletin*, 2008, **33**, 421.

11. J. Larminie and A. Dicks, *Fuel Cell Systems Explained* John Wiley & Sons, 2nd edition, 2003.

12. D. Tucker, M. Shelton and A. Manivannan, *Electrochemical Society Interface*, 2009, **18**, 45.

13. S. M. Haile, *Acta Materialia*, 2003, **51**, 5981.

14. S. Stotz and C. Wagner, *Berichte der Bunsengesellschaft für Physikalische Chemie*, 1966, **70**, 781.

15. T. Takahashi and H. Iwahara, *Revue de Chimie Minerale*, 1980, **17**, 243.

16. H. Iwahara, H. Uchida and S. Tanaka, *Solid State Ionics*, 1983, **9-10**, 1021.

17. H. Iwahara, H. Uchida, K. Ono and K. Ogaki, *Journal of the Electrochemical Society*, 1988, **135**, 529.

18. K. D. Kreuer, S. Adams, W. Münch, A. Fuchs, U. Klock and J. Maier, *Solid State Ionics*, 2001, **145**, 295.

19. K. D. Kreuer, *Annual Review of Materials Research*, 2003, **33**, 333.

20. M. J. Scholten, J. Schoonman, J. C. van Miltenburg and H. A. J. Oonk, *Solid State Ionics*, 1993, **61**, 83.

21. K. H. Ryu and S. M. Haile, *Solid State Ionics*, 1999, **125**, 355.

22. H. Iwahara, T. Yajima, T. Hibino, K. Ozaki and H. Suzuki, *Solid State Ionics*, 1993, **61**, 65.

23. K. A. Furøy, R. Haugsrud, M. Hänsel, A. Magrasó and T. Norby, *Solid State Ionics*, 2007, **178**, 461.

24. M. J. Scholten, J. Schoonman, J. C. van Miltenburg and H. A. J. Oonk, *Proceedings - Electrochemical Society*, 1993, **93-4**, 146.

25. I. Naray-Szabo, *Naturwissenschaften*, 1943, **31**, 202.

26. T. Schober and H. G. Bohn, *Solid State Ionics*, 2000, **127**, 351.

27. H. G. Bohn and T. Schober, *Journal of the American Ceramic Society*, 2000, **83**, 768.

28. A. Magrez and T. Schober, *Solid State Ionics*, 2004, **175**, 585.

29. F. M. M. Snijkers, A. Buekenhoudt, J. Cooymans and J. J. Luyten, *Scripta Materialia*, 2004, **50**, 655.

30. P. Babilo, T. Uda and S. M. Haile, *Journal of Materials Research*, 2007, **22**, 1322.

31. F. Iguchi, N. Sata, T. Tsurui and H. Yugami, *Solid State Ionics*, 2007, **178**, 691.

32. S. B. C. Duval, P. Holtappels, U. F. Vogt, E. Pomjakushina, K. Conder, U. Stimming and T. Graule, *Solid State Ionics*, 2007, **178**, 1437.

33. S. Tao and J. T. S. Irvine, *Journal of Solid State Chemistry*, 2007, **180**, 3493.

34. R. B. Cervera, Y. Oyama, S. Miyoshi, K. Kobayashi, T. Yagi and S. Yamaguchi, *Solid State Ionics*, 2008, **179**, 236.

35. S. Higgins, N. M. Sammes, A. Smirnova, J. A. Kilner and G. Tompsett, *Journal of Fuel Cell Science and Technology*, 2008, **5**, 027001/1.

36. F. Iguchi, T. Tsurui, N. Sata, Y. Nagao and H. Yugami, *Solid State Ionics*, 2009, **180**, 563.

37. Y. Yamazaki, R. Hernandez-Sanchez and S. M. Haile, *Chemistry of Materials*, 2009, **21**, 2755.

38. Y. Yamazaki, P. Babilo and S. M. Haile, *Chemistry of Materials*, 2008, **20**, 6352.

39. S. Imashuku, T. Uda and Y. Awakura, *ECS Transactions*, 2007, **7**, 2321.

40. S. Imashuku, T. Uda, T. Ichitsubo, E. Matsubara and Y. Awakura, *Journal of Phase Equilibria and Diffusion*, 2007, **28**, 517.

41. P. Murugaraj, K. D. Kreuer, T. He, T. Schober and J. Maier, *Solid State Ionics*, 1997, **98**, 1.

42. D. L. Pavia, G. M. Lampman and G. S. Kriz, *Introduction to spectroscopy*, 3rd edn., Hartcourt College Publisher, Orlando, 2001.

43. E. Fukushima and S. B. W. Roeder, *Experimental pulse NMR - A nuts and bolts approach*, Massachusetts, 1981.

44. D. D. Laws, H.-M. L. Bitter and A. Jerschow, *Angewandte Chemie, International Edition*, 2002, **41**, 3096.

45. M. H. Levitt, *Spin Dynamics: Basics of Nuclear Magnetic Resonance*, John Wiley & Sons, 2001.

46. M. J. Duer, *Introduction to Solid-State NMR Spectroscopy*, Blackwell Publishing Ltd, Oxford, 2004.

47. M. E. Smith and E. R. H. Van Eck, *Progress in Nuclear Magnetic Resonance Spectroscopy*, 1999, **34**, 159.

48. K. J. D. MacKenzie, *Solid State Ionics*, 2004, **172**, 383.

49. L. Frydman and J. S. Harwood, *Journal of the American Chemical Society*, 1995, **117**, 5367.

50. C. P. Grey and A. J. Vega, *Journal of the American Chemical Society*, 1995, **117**, 8232.

Chapter 2:

Probing the local structures and protonic conduction pathways in scandium substituted $BaZrO_3$ by multinuclear solid-state NMR spectroscopy

A comprehensive multinuclear solid-state NMR study of scandium-substituted $BaZrO_3$ is reported. Static low field and MQMAS very high field ^{45}Sc NMR data revealed the presence of both 5 and 6 coordinated scandium atoms, the vacancies not being very strongly bound to scandium. ^{17}O NMR spectra showed the presence of up to three different chemical oxygen environments assigned to Zr-O-Zr, Zr-O-Sc and Sc-O-Sc. From the ratios of these different oxygen sites, the distribution of the scandium cations appeared to be close to random but indicated that the scandium incorporation was lower than expected, consistent with the observation of Sc_2O_3 impurities at higher substitution levels. ^{1}H and ^{45}Sc NMR data on the hydrated materials revealed the presence of scandium next to protonic defects. Finally, variable temperature ^{1}H NMR showed the presence of at least two different proton environments in between which proton transfer occurs at ambient temperatures (300 K).

This chapter is adapted from an article published in the Journal of Materials Chemistry.[1]

I. Introduction

As described in the first chapter, lowering the operating temperature of SOFCs may be achieved by using protonic conductors instead of oxygen conductors as the electrolyte material. It was pointed out that one of the strongest candidate so far for such an application is derived from the perovskite $BaZrO_3$ since this material is stable in the presence of CO_2 and can readily incorporate protonic defects.[2] While the best conductivities are reported for yttrium substituted $BaZrO_3$, this material is rather unfriendly from an NMR point of view: the NMR of the elements of interest, Y and Zr, is difficult to perform, therefore studying the structural characteristics of scandium substituted $BaZrO_3$ appeared to be a better starting point in order to understand oxygen deficiency and protonic trapping arrangements in the dry and hydrated structures respectively. A large literature exists on yttrium-substituted $BaZrO_3$[3-14] but to date very little has been reported for the scandium substituted analogue.[15-16] $BaZrO_3$ crystallizes in a cubic perovskite structure,[17] space group *Pm3m* and remains cubic upon substitution.[15] Yttrium has been reported to solubilise at least up to 40 % in $BaZrO_3$,[18] while the scandium substitution is limited to only 29 %.[19-20] This chapter focuses on the application of NMR methods to investigate the local structure of a series of scandium-substituted barium zirconate ($BaZr_{1-x}Sc_xO_{3-x/2}$, x = 0.05, 0.15 and 0.30). ^{45}Sc, ^{17}O and ^{1}H NMR spectra of both dry and hydrated structures are acquired to investigate cation ordering, the locations of the vacancies, and the mobility of the protons in the hydrated materials.

^{45}Sc chemical shifts are sensitive to the coordination number of the cation and the lineshape of the resonance of this spin I = 7/2 nucleus to the local distortion of the environment.[21-22] Thus, we use ^{45}Sc to determine whether the oxygen vacancies are nearby the scandium cations, the presence of a 5 coordinated scandium atom indicating the existence of an oxygen vacancy in the scandium 1st coordination shell. ^{45}Sc NMR is relatively straightforward to perform since ^{45}Sc has a natural abundance of 100 %, a gyromagnetic ratio γ of 6.50880×10^7 $rad.T^{-1}.s^{-1}$, close to that of ^{13}C, and a moderate nuclear quadrupolar moment Q of 0.22×10^{-28} m^2. While ^{45}Sc NMR spectra are often broad due to the large anisotropic interactions, NMR parameters including the quadrupolar interactions (EFG) and the chemical shielding anisotropy (CSA) can be readily extracted to determine the symmetry, structure and dynamics of various materials.[21, 23-27]

^{17}O (I = 5/2) NMR is used to probe the cation ordering, since the ^{17}O chemical shift is sensitive to the nature of the nearby cations (Sc^{3+} and Zr^{4+} in this case). Natural abundance ^{17}O NMR is challenging in part due to the very low concentration of ^{17}O (≈ 0.037 %) and ^{17}O enrichments are required. Enrichment is, however, very easily performed in this type of materials via an exchange reaction between the solid itself and ^{17}O-labeled O_2 gas at moderate to high temperatures.[28]

Finally, ^{1}H NMR is widely used for the characterization of structure and dynamics of molecules due to its very high sensitivity (spin quantum number I = ½, almost 100 % natural abundance and high γ). Highly resolved spectra are easily obtained from liquids because of fast molecular tumbling, which in most cases fully averages out the anisotropic interactions. However, in static solids the dominant homonuclear ^{1}H - ^{1}H dipolar interaction generally leads to broad proton resonances unless dilution,[29-30] very fast Magic Angle Spinning (MAS)[31-32] or CRAMPS (Combined Rotation And Multiple Pulse Spectroscopy) techniques [33] are used.[34] ^{1}H MAS NMR spectra of the hydrated samples are acquired at room and low temperatures, to directly observe the protonic defects and to characterize their motional processes.

II. Experimental section

A. Sample Preparation

$BaZr_{1-x}Sc_xO_{3-x/2}$ (x = 0.05, 0.15, 0.30) samples were synthesized through a glycine-nitrate combustion route[35] using $Ba(NO_3)_2$ (Alfa Aesar, 99.999 %), $ZrO(NO_3)$. x H_2O (Alfa Aesar, 99.9%), $Sc(NO_3)_3$. x H_2O (Alfa Aesar, 99.9 %) and glycine (Alfa Aesar, 99.7 %) as starting materials. Stoichiometric ratios of the reactants were mixed in a small amount of deionized water with a nitrate to glycine ratio of 2:1. Mixtures were then dehydrated on a hot plate and auto-ignition followed. Powders were then ground and fired at 1200 °C for 10 hours, pressed into pellets, buried in $BaZrO_3$ powder to prevent barium evaporation, sintered at 1600 °C for another 15 hours and finally slowly cooled to room temperature. ^{17}O enrichment was performed by heating the freshly dried samples (1 hour at 950 °C under vacuum) under 50 % ^{17}O enriched O_2 gas (Isotec, 99 %) for 2 days at 950 °C. Purity of the samples was checked by X-ray diffraction using a Scintag diffractometer with Cu-Kα radiation. Diffraction patterns were compared to the

JCPDS (Joint Committee on Powder Diffraction Standards) card for $BaZrO_3$ (# 06-0399). Even though the reported solubility of scandium into $BaZrO_3$ is limited to 29 %,[19-20] no Sc_2O_3 was detected in the diffraction pattern, except for the ^{17}O enriched $BaZr_{0.70}Sc_{0.30}O_{2.85}$. Hydration of the powders was carried out in a tube furnace. The powders were first dried at 1000 °C for 2 hours and then cooled down by steps of 100 °C every 2 hours until the temperature reached 200 °C with wet N_2 flowing over the samples at a rate of 60 mL min^{-1}. The cycle was repeated again from 800 to 200 °C, to increase the hydration levels of the powders.

B. ^{45}Sc NMR experiments

Static ^{45}Sc NMR experiments were performed on a 8.5 T wide bore magnet with a single channel static probe tuned to 87.46 MHz. Quadrupolar echo experiments were performed using a selective $\pi/2$ = 0.9 μs at a radio-frequency (rf) field amplitude of 71 kHz with an evolution period of 20 μs and a recycle delay of 1 s. Additional static ^{45}Sc NMR experiments were performed on a 11.7 T wide bore with a double resonance 5 mm MAS probe tuned to 127.47 MHz. The dry samples used for the ^{45}Sc static NMR were dehydrated under vacuum at 950 °C overnight and packed in well sealed rotors under N_2 atmosphere before the experiments were recorded, to remove any water absorbed during storage of the samples. High field ^{45}Sc NMR experiments were performed at 19.6 T on a ultra narrow bore Bruker DRX 830 MHz spectrometer at the National High Magnetic Field Laboratory, Tallahassee, Florida, USA using a home-built 1.8 mm single channel probe[36] tuned to 202.44 MHz. All samples were packed inside 1.8 mm rotors and spun at a spinning frequency ω_r of 33 kHz. t_1 rotor synchronized two-dimensional (2D) Multiple-Quantum MAS (MQMAS) experiments [37] - in this case triple-quantum - were performed using a shifted echo pulse sequence and the Soft-Pulse-Added-Mixing (SPAM) enhancement pulse.[38] Excitation and reconversion pulse lengths of 2 and 0.5 μs, respectively, were used at an rf field amplitude of 150 kHz, while a pulse length of 1.5 and 0.75 μs were used for the selective 180° echo and the 90° SPAM pulses, respectively, corresponding to an rf field amplitude of approximately 50 kHz. The experiments were optimized for $BaZr_{0.70}Sc_{0.30}O_{2.85}$ and performed under the same conditions for all the other samples. The chemical shift was externally referenced to a 1 M solution of $Sc(NO_3)_3$ in water at 0.0 ppm.

C. ^{17}O NMR experiments

^{17}O NMR experiments were carried out on a 14.1 T wide bore Bruker Avance 600 MHz spectrometer equipped with a 4 mm HX probehead and operating at 81.36 MHz. All samples were packed inside 4 mm rotors and spun at a spinning frequency ω_r of 15 kHz. ^{17}O one-dimensional spectra were recorded using the rotor synchronized Hahn echo experiments with an evolution period of one rotor period, *i.e.* τ_r = 66.7 μs, to avoid probe ringing and selective pulse widths of $\pi/6$ = 0.28 μs and $\pi/3$ = 0.57 μs at a rf field amplitude of 100 kHz. Two-dimensional triple-quantum ^{17}O MAS NMR experiments were recorded at a spinning frequency of 15 kHz using the *z-filtered* pulse sequence.[39] Excitation and reconversion pulse lengths of 4.8 to 5 μs and 1.4 μs, respectively, corresponding to an rf field amplitude of 100 kHz, and selective 90° pulses of 20 μs (rf field amplitude of 15 kHz) were used. Multiple-quantum transfer was optimized on every sample to ensure efficient excitation of the 3Q coherences, the t_1 increment was rotor synchronized to one rotor period. High field ^{17}O NMR experiments were performed on a 21.1 T standard bore Bruker Avance III 900 MHz spectrometer equipped with a 3.2 mm HX probehead and operating at 122.04 MHz. The samples were packed inside 3.2 mm rotors and spun at a spinning frequency ω_r of 22 kHz. ^{17}O one-dimensional spectra were recorded using a simple one pulse experiment. 15000 transients were accumulated using selective pulse widths of $\pi/6$ = 1 μs at an rf field amplitude of 30 kHz. Further experimental details are given in the figure captions. The recycle delay was set to 5 s for all experiments and the chemical shift was externally referenced to water at 0.0 ppm.

D. ^{1}H NMR experiments

^{1}H NMR experiments were carried out on a 14.1 T wide bore Bruker Avance III 600 MHz spectrometer equipped with a 3.2 mm HXY low temperature probehead. All samples were packed inside 3.2 mm rotors and spun at a spinning frequency ω_r of 12.5 kHz. Spectra were recorded using a rotor synchronized Hahn echo experiments with an evolution period of one rotor period. The spin lattice relaxation times T_1 were estimated by fitting a recycle delay array curve. The chemical shift was externally referenced to TMS at 0.0 ppm. All temperatures given here correspond to the sample temperatures and have been corrected for MAS mechanical friction.[40]

E. NMR simulation

MatLab and MatNMR[41] were used to process the data. Simulations and fits were performed using Winsolid[42] or SIMPSON[43] and standard numerical techniques.[44] The quadrupolar lineshapes were only simulated using the quadrupolar interaction, no CSA was introduced.

III. Results

A. Thermogravimetric Analysis

Prior to the description of the NMR data, the thermogravimetric analyses (TGA) of the hydrated samples are presented in order to quantify the amount of protonic defects contained in the structure (*Figure 2.1*). For all $BaZr_{1-x}Sc_xO_{3-x/2}$ samples, we used the total mass loss to calculate the total water content of the hydrated material. Assuming full hydration of the structures, which is not always achievable, a maximum amount of *x/2* H_2O molecules can be incorporated leading to *x* OH defects. Thus we label the hydrated materials $BaZr_{1-x}Sc_xO_{3-x/2-y}(OH)_{2y}$ where the subscript 2y indicates the quantity of protonic defects (2y should be ≤ x) leading to the following formulas: $BaZr_{0.95}Sc_{0.05}O_{2.97}(OH)_{0.01}$, $BaZr_{0.85}Sc_{0.15}O_{2.875}(OH)_{0.10}$ and $BaZr_{0.70}Sc_{0.30}O_{2.75}(OH)_{0.20}$, for the three samples studied here. At all substitution levels, the incorporation of water is lower than expected theoretically, which is ascribed to slow mobilities of the oxygen vacancies in the lower temperature regimes where the proton defects are more stable. For the lowest scandium substitution, the hydration level is noticeably lower, and this may be due to poorer conductivity of this material, which has the fewest oxygen vacancies.

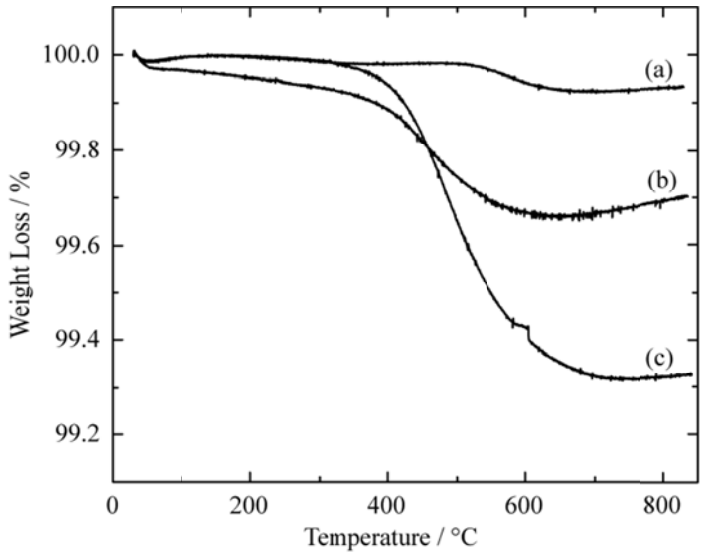

Figure 2.1. Thermogravimetric analysis of $BaZr_{1-x}Sc_xO_{3-x/2-y}(OH)_{2y}$. (a) $BaZr_{0.95}Sc_{0.05}O_{2.97}(OH)_{0.01}$. (b) $BaZr_{0.85}Sc_{0.15}O_{2.875}(OH)_{0.10}$. (c) $BaZr_{0.70}Sc_{0.30}O_{2.75}(OH)_{0.20}$.

B. Defect chemistry by ^{45}Sc NMR

Figure 2.2 shows the static ^{45}Sc spectra of dry and hydrated $BaZr_{1-x}Sc_xO_{3-x/2}$ obtained at 8.5 T along with their respective simulations (dashed lines). The spectra of the dry samples consist of a resonance at 140 ppm comprising a sharper component due to the central transition, along with broader features due to the satellite transitions, and a second broader signal, whose concentration grows as the scandium substitution level increases. The chemical shift of the sharp signal is consistent with a 6 coordinated scandium environment, typically from 108 to 158 ppm,[21] while the lack of breadth of this signal indicates that the scandium ions are in a highly symmetric environment; the broad signal is ascribed to scandium in a highly distorted local environment. After hydration, the sharp signal is still present in the spectra of all samples, while the broader signal significantly reduces in intensity. We, therefore, assign the broad resonance to 5 coordinated scandium cations which, upon hydration, become six-fold coordinated and thus more symmetrically coordinated. These hypotheses are confirmed by numerical simulation of the spectra and by the MAS data presented in the next section. The broadening of the central transition of the 6 coordinated scandium signal after hydration along with the loss of the satellite transitions is largely due to an increase in the chemical shift distribution.

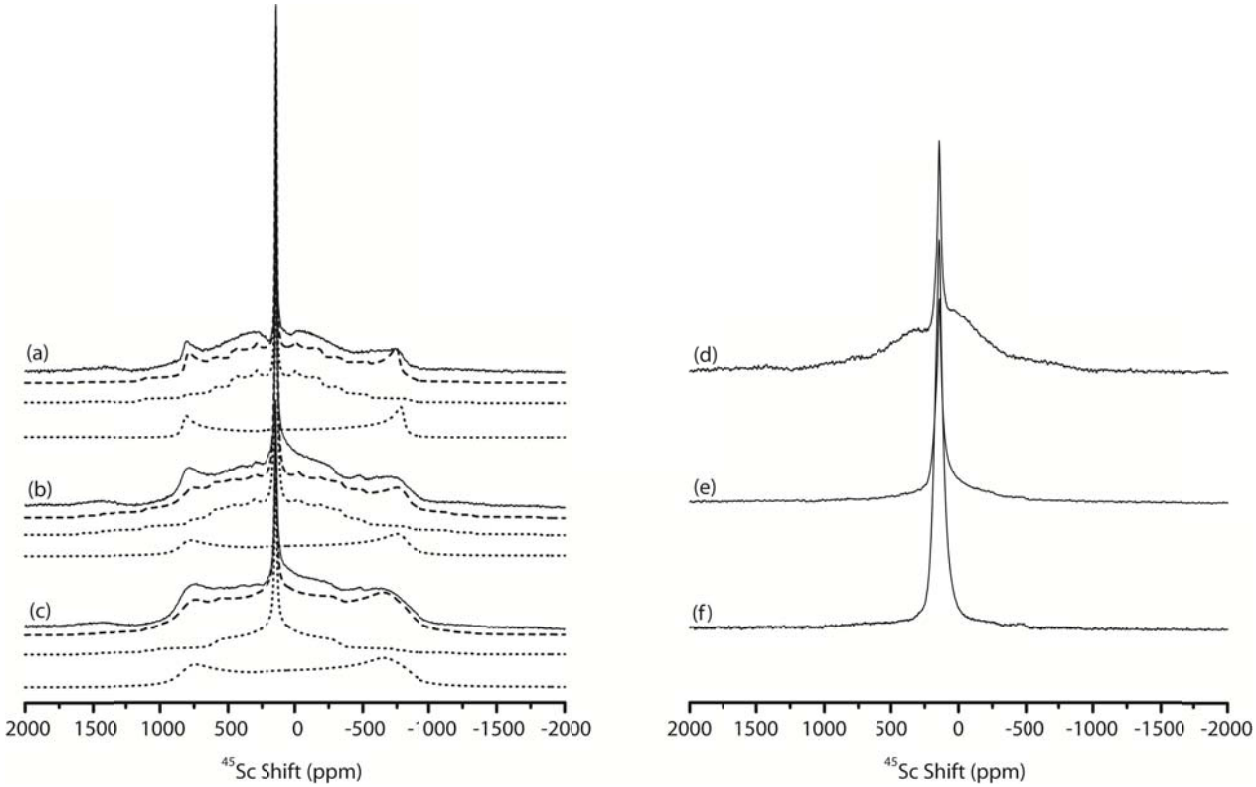

Figure 2.2. Static ^{45}Sc quadrupolar echo spectra of $BaZr_{1-x}Sc_xO_{3-x/2}$ and $BaZr_{1-x}Sc_xO_{3-x/2-y}(OH)_{2y}$ obtained at 8.5 T. (a) $BaZr_{0.95}Sc_{0.05}O_{2.985}$ (80944 transients). (b) $BaZr_{0.85}Sc_{0.15}O_{2.925}$ (60792 transients). (c) $BaZr_{0.70}Sc_{0.30}O_{2.85}$ (27464 transients). (d) $BaZr_{0.95}Sc_{0.05}O_{2.97}(OH)_{0.01}$ (56736 transients). (e) $BaZr_{0.85}Sc_{0.15}O_{2.875}(OH)_{0.10}$ (13228 transients). (f) $BaZr_{0.70}Sc_{0.30}O_{2.75}(OH)_{0.20}$ (11520 transients). Simulations performed with the parameters reported in Table 2.1, are shown below the spectra of the dry samples. The dotted lines represent the two individual components used to simulate each spectrum and the dashed lines are the sum of the two components.

The NMR lineshapes for the dry samples could be fit by using two different scandium environments, whose quadrupolar interaction parameters are listed in *Table 2.1*. Although the fits are good, the poor resolution at low magnetic field strengths, and the weak intensities of the satellite transitions render the determination of the quadrupolar asymmetry parameters, η_Q, somewhat difficult. Nonetheless the same parameters also give an excellent fit to the spectra of the dry samples recorded at a higher field of 11.7 T (*Figure 2.3*) providing further support for these simulations.

Table 2.1. Experimental ^{45}Sc NMR parameters (Isotropic Chemical Shifts δ_{iso}; Quadrupolar Coupling Constants C_Q and Quadrupolar Asymmetries η_Q) extracted from the static and MQMAS spectra of $BaZr_{1-x}Sc_xO_{3-x/2}$ (x = 0.05-0.30) obtained at 8.5 and 19.6 T.

x	δ_{iso} (ppm)	C_Q / MHz	η_Q	Assignments
0.05	139(1)	0.6(1)	0.4(1)	Sc^{VI}
	167(1)[a]	-[a, b]	-[a, b]	Sc^{VI} OH
	240(5)	31(1)	0.0(1)	Sc^{V}
0.05 Hyd[c]	142(2)	1.1(1)	0.9(1)	Sc^{VI}
	160(1)	8(1)	0.0(3)	Sc^{VI} OH
0.15	138(2)	0.8(2)	0.5(2)	Sc^{VI}
	235(5)	31(1)	0.0(1)	Sc^{V}
0.15 Hyd [c]	144(2)	1.5(4)[d]	- [d, e]	Sc^{VI}
	162(1)[a]	7(1)[a]	0.0(3)[a]	Sc^{VI} OH
0.30	142(1)	0.6(2)	0.8(1)	Sc^{VI}
	240(10)	31(2)	0.0(1)	Sc^{V}
0.30 Hyd [c]	144(2)	1.5(8)[d]	-[d, e]	Sc^{VI}
	162(2)[a]	7(1)[a]	7(1)[a]	Sc^{VI} OH

[a] Signal not observed at 8.5 T. [b] Signal too weak and at the limit of detection of the MQMAS experiment, and hence cannot be fit with any degree of certainty. [c] Hydrated samples. [d] Not determined at 8.5 T due to the lack of satellite transitions. [e] Not determined at 19.6 T due to the lack of signal lineshape.

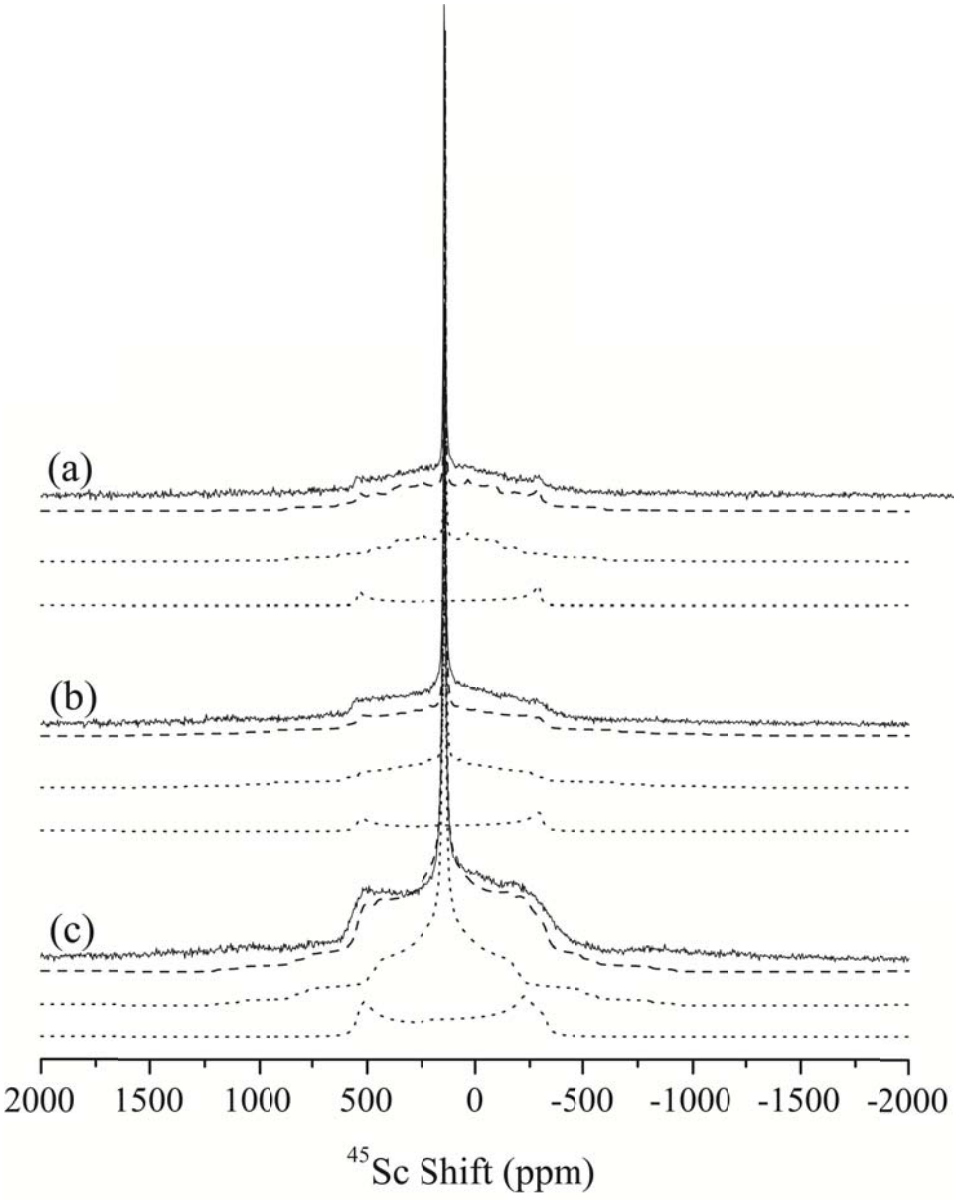

Figure 2.3. Static ^{45}Sc quadrupolar echo spectra of $BaZr_{1-x}Sc_xO_{3-x/2}$ obtained at 11.7 T with a relaxation delay of 1.5 s. (a) $BaZr_{0.95}Sc_{0.05}O_{2.985}$ (6104 transients). (b) $BaZr_{0.85}Sc_{0.15}O_{2.925}$ (4512 transients). (c) $BaZr_{0.70}Sc_{0.30}O_{2.85}$ (6224 transients). Simulations performed with the parameters reported in Table 2.1, are shown below the spectra of the dry samples. The dotted lines represent the two individual components used to simulate each spectrum and the dashed lines are the sum of the two components.

The sharp peak has a small quadrupolar coupling constant C_Q, consistent with a symmetric ScO_6 site; however, the value of η_Q (0.5 – 0.8) is not consistent with the symmetry of the site: η_Q is expected to be 0 based on the crystallographic structure of the unsubstituted material. This may reflect the small local distortions that result from substituting a slightly larger Sc^{3+} ion (r = 0.89 Å) on the Zr^{4+} site (r = 0.86 Å)[45] and additional effects due to cation substitutions and oxygen vacancies in the 2nd and 3rd coordination shells, but may also be due to the inherent errors associated with this fitting. η_Q increases upon scandium substitution, perhaps reflecting the higher numbers of nearby defects.

The broad scandium resonance, whose relative intensity increases upon scandium substitution in the dry samples, has a much larger quadrupolar coupling constant (C_Q = 30 MHz, *Table 2.1*). Its isotropic chemical shift value of 245 ppm falls in the range predicted by Stebbins *et al.*[21] for a 5 coordinated scandium ion. The large C_Q value is consistent with the significant distortion, and thus electric field gradient, expected for a $ScO_5\square$ environment, ($\square$ is a vacancy) and provides strong evidence for the location of the vacancy nearby a scandium ion. Note that this $ScO_5\square$ environment is square pyramidal and although possessing a large distortion from the original octahedral environment and thus a Cq, it will still maintain a C_4 symmetry axis, and thus axial symmetry (*i.e.* $\eta = 0$).

Our results are in agreement with a previous high-field MAS NMR study, where a broad shifted ^{45}Sc resonance at approximately 230 ppm was observed, that was similarly assigned to a 5 coordinate scandium environment in substituted $BaZrO_3$, again the concentration of this resonance increasing on scandium doping.[46] The fitting of the static spectra of the hydrated samples is more challenging than for the dry ones and it is clear that the spectra contain multiple sites indicating considerable disorder.

Figure 2.4A shows the one pulse ^{45}Sc spectra of dry and hydrated $BaZr_{0.85}Sc_{0.15}O_{2.925}$ materials at a very high field strength of 19.6 T. While the resulting lineshape reveals several sites, in agreement with the static data obtained at 8.5 T, the signals are still very broad as MAS alone is not sufficient to fully average out the second-order quadrupolar broadening. The residual

second-order quadrupolar broadening can, however, be removed by performing a two-dimensional (2D) multiple-quantum magic angle spinning (MQMAS) experiment. [28, 39, 47-49]

For $BaZr_{0.85}Sc_{0.15}O_{2.925}$ (see *Figure 2.4, panel B*), the projection along the F_1 dimension clearly reveals the presence of two sites with shifts of 138 and 262 ppm. The slice at 138 ppm in the F_2 dimension contains a sharp signal with an isotropic chemical shift of 137 ppm that is assigned to the 6 coordinated scandium environment observed in the static data. Estimation of the quadrupolar coupling constant of this site is difficult since it is so small. The slice at 262 ppm contains a resonance with a much broader lineshape, due to a large quadrupolar coupling interaction (C_Q = 31 MHz; *Table 2.1*), and an isotropic resonance of 230 ppm. This broad signal, which was difficult to resolve clearly in the one pulse MAS experiment, corresponds to 5 coordinated scandium cations.

The MQMAS results are in very good agreement with the static NMR data obtained at 8.5 T (*Table 2.1*) and confirm the presence of a site with a very large quadrupolar coupling interaction, which is ascribed to the presence of an oxygen vacancy in the vicinity of a scandium atom, *i.e.* a 5 coordinate scandium site. Similar data were obtained for $BaZr_{0.70}Sc_{0.30}O_{2.85}$ and $BaZr_{0.95}Sc_{0.05}O_{2.975}$; an increase in the ratio of the 6:5 coordinated scandium environments is seen as the substitution level is decreased, although care must be taken in interpreting intensities of MQMAS data.

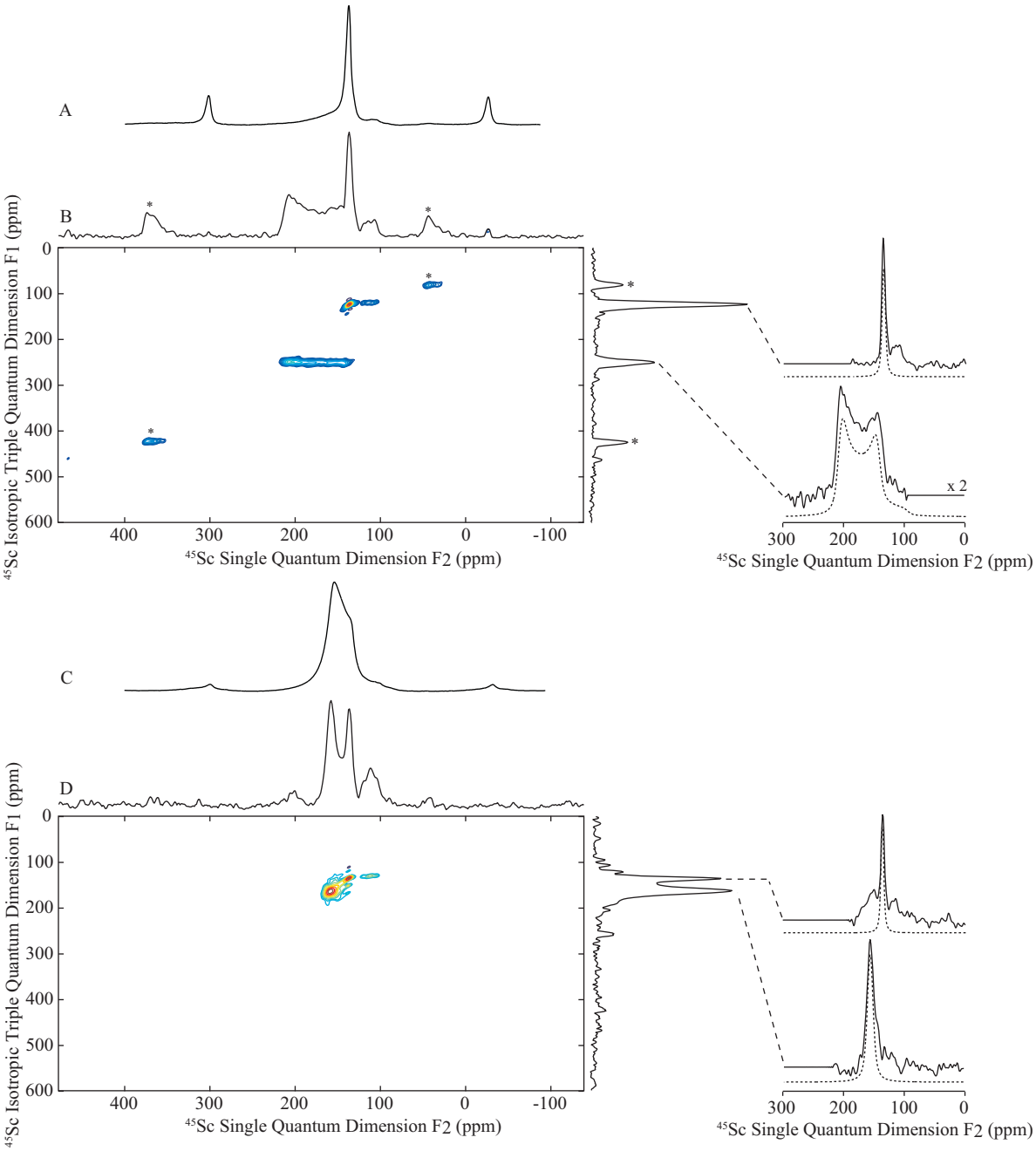

Figure 2.4. ^{45}Sc MAS NMR single pulse spectra of (A) $BaZr_{0.85}Sc_{0.15}O_{2.925}$ and (C) $BaZr_{0.85}Sc_{0.15}O_{2.875}(OH)_{0.10}$ and two-dimensional sheared triple-quantum ^{45}Sc MAS spectrum of (B) $BaZr_{0.85}Sc_{0.15}O_{2.925}$ and (D) $BaZr_{0.85}Sc_{0.15}O_{2.875}(OH)_{0.10}$ obtained at 19.6 T. 9600 transients were accumulated for each of 12 (for A) and 16 (for B) t_1 increments at a recycle rate of 0.5 s. Top: Anisotropic skyline projection. Right: Isotropic skyline projection of the 2D 3Q MAS. Cross sections (full lines) extracted parallel to F_2 of the 2D 3Q MAS spectrum at: (A) δ_1 = 137 (top) and 262 (bottom) ppm and (B) δ_1 = 142 (top) and 165 (bottom) ppm, along with the best fit simulation (dashed lines) using the parameters given in Table 2.1. The asterisks denote the spinning side bands.

The MQMAS ^{45}Sc data for the 15 % substituted compound after hydration, *i.e.* for $BaZr_{0.85}Sc_{0.15}O_{2.875}(OH)_{0.10}$, is plotted in Panel D of *Figure 2.4*. The projection along the F_1 dimension of the spectrum clearly shows the loss of the broad signal at 262 ppm associated with the 5 coordinated scandium environment. The spectrum is now dominated by resonances due to two six-coordinated scandium signals at 142 and 165 ppm for which slices were extracted along the F_2 dimension. The slice at 142 ppm reveals a sharp signal with δ_{iso} = 140 ppm corresponding to the six coordinated scandium environment observed in the dry sample, while the second slice at 165 ppm contains a much broader lineshape ascribed to a six coordinated scandium in the vicinity of a protonic defect, for example a $ScO_5(OH)$ environment.

The MQMAS spectra for $BaZr_{0.70}Sc_{0.30}O_{2.75}(OH)_{0.20}$ and $BaZr_{0.95}Sc_{0.05}O_{2.97}(OH)_{0.01}$ showed similar results, despite a poor signal to noise ratio for the latter (*Table 2.1*). Even though the hydrated samples still contain oxygen vacancies as revealed by the TGA and static ^{45}Sc NMR data, any remaining 5 coordinated scandium environments are barely observed by MQMAS as their concentration is probably beyond the limit of detection of the MQMAS experiments. Note that in both 15 and 30 % substituted $BaZrO_3$, some residual scandium oxide Sc_2O_3 is also observed, as revealed by the signal at around 120 ppm,[21, 27] even though it was not observed by XRD. The high field MAS ^{45}Sc data hereby confirm the presence of oxygen vacancies in the vicinity of the scandium cations that are filled during the hydration process creating protonic defects, some of which have been observed nearby the scandium cations.

C. Defect chemistry by ^{17}O NMR

^{17}O MAS NMR was performed to probe the cation ordering further (*Figure 2.5*). The spectrum of unsubstituted $BaZrO_3$ at 14.1 T contains only one sharp peak, along with its spinning sidebands, at an isotropic chemical shift of 376 ppm which is assigned to the single crystallographic site of oxygen, bound to two zirconium cations, Zr-O-Zr.[50] The $BaZr_{0.85}Sc_{0.15}O_{2.925}$ and $BaZr_{0.70}Sc_{0.30}O_{2.85}$ spectra contain an additional environment at around 405 ppm, which is assigned to an oxygen atom between a zirconium and a scandium atom, Zr-O-Sc, the substitution of a scandium ion in the oxygen local environment resulting in a shift of approximately 29 ppm. Two additional weak resonances can be observed in the

$BaZr_{0.70}Sc_{0.30}O_{2.85}$ spectrum. The first signal at approximately 430 ppm is assigned to an oxygen atom between two scandium atoms, Sc-O-Sc, based on an additional shift of approximately 25 ppm relative to the Sc-O-Zr environment while the second resonance observed at around 359 ppm is assigned to some residual Sc_2O_3 in agreement with the ^{45}Sc data at high field.[51]

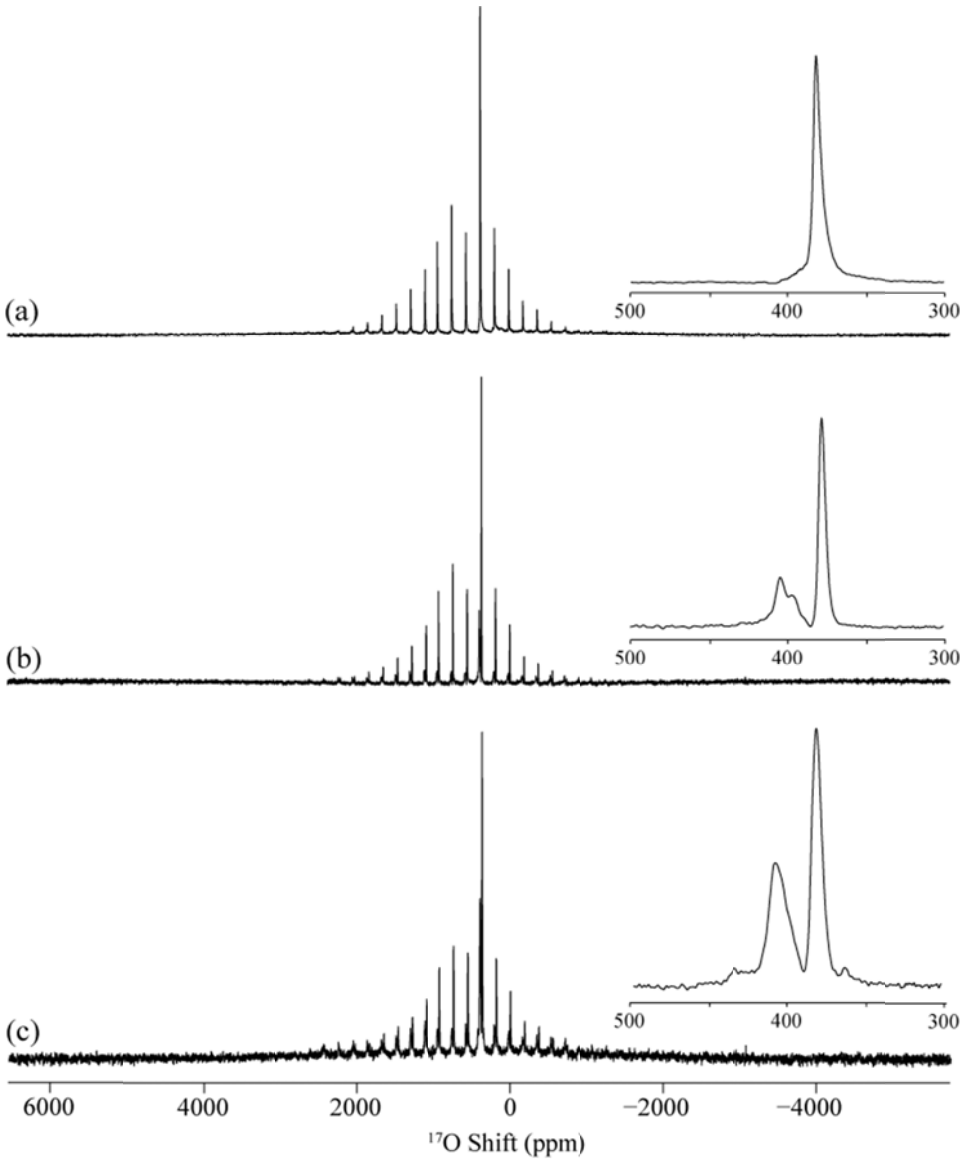

Figure 2.5. Rotor synchronised ^{17}O MAS NMR Hahn echo spectra of ^{17}O enriched $BaZr_{1-x}Sc_xO_{3-x/2}$ obtained at 14.1 T. (a) $BaZrO_3$ (15360 transients). (b) $BaZr_{0.85}Sc_{0.15}O_{2.925}$ (4096 transients). (c) $BaZr_{0.70}Sc_{0.30}O_{2.85}$ (3072 transients). The inserts show a zoom of the central transition region of the spectra.

The ^{17}O MQMAS NMR spectrum of $BaZr_{0.70}Sc_{0.30}O_{2.85}$ (*Figure 2.6*) confirms the presence of two oxygen environments, Zr-O-Zr and Zr-O-Sc, with isotropic chemical shifts of 386 and approximately 405 ppm, respectively, the concentration of the Sc-O-Sc in $BaZr_{0.70}Sc_{0.30}O_{2.85}$ presumably being below the MQMAS detection limit.

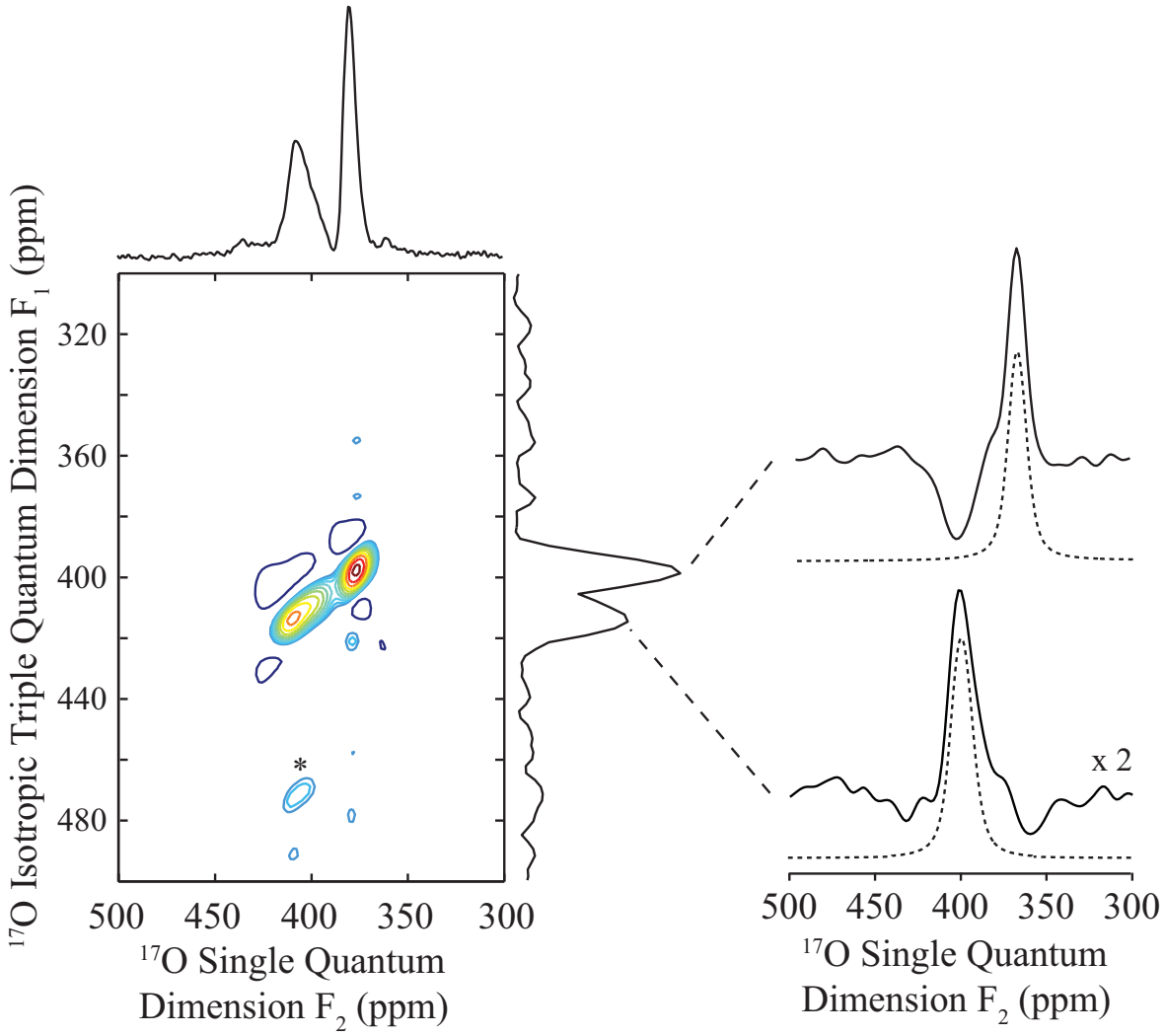

Figure 2.6. Two-dimensional sheared triple-quantum ^{17}O MAS spectrum of $BaZr_{0.70}Sc_{0.30}O_{2.85}$ obtained at 14.1 T. 2220 transients were accumulated for each of 16 t_1 increment. Top: NMR spectrum. Right: Isotropic skyline projection of the 2D 3Q MAS. Cross sections (full lines) extracted parallel to F_2 of the 2D 3Q MAS spectrum at δ_1 = 398 (top) and 414 (bottom) ppm along with the best fit simulation (dashed lines) using the parameters given in Table 2.2.

Fitting of the individual ridgeline shapes (*Table 2.2*) yield quadrupolar coupling constants C_Q of ≈ 1.6 and 3.0 MHz for the sites at 386 and 405 ppm, respectively, in line with values previously reported for other bridging oxygen atoms in perovskite structures.[52]

Table 2.2. Experimental ^{17}O NMR parameters (Isotropic Chemical Shifts δ_{iso}; Quadrupolar Coupling Constants C_Q and Quadrupolar Asymmetries η_Q) extracted from the MAS spectra of $BaZr_{1-x}Sc_xO_{3-x/2}$ (x = 0.05-0.30) obtained at 14.1 T.[a]

x	δ_{iso} (ppm)	C_Q / MHz	η_Q	Assignments
0 [b]	376	1.2(3)	-[c]	Zr-O-Zr
0.15	386(2)	1.5(2)	0.0(2)	Zr-O-Zr
	402(7)	3.2(2)	0.2(2)	Zr-O-Sc
0.30	386(2)	1.7(2)	0.0(3)	Zr-O-Zr
	408(4)	2.8(2)	0.2(2)	Zr-O-Sc

[a] Determined from the MQMAS experiment. [b] Determined from best fit simulation of the MAS spectrum. [c] Not determined.

Experiments performed at a very high field of 21.1 T (*Figure 2.7*) did not produce any enhancement in resolution but allowed us to estimate the ratios of the different oxygen environments (*Table 2.3*), which are close to the expected values for a random distribution of scandium cations and oxygen vacancies.

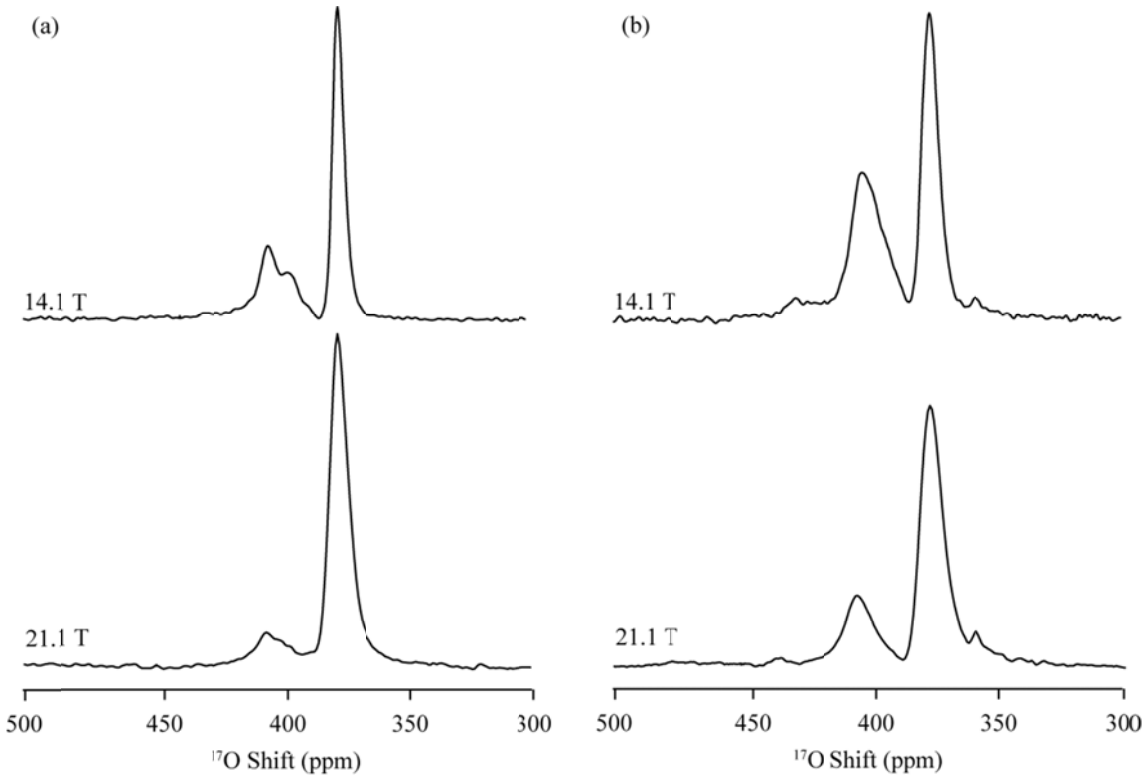

Figure 2.7. Comparison between the ^{17}O MAS NMR spectra of $BaZr_{1-x}Sc_xO_{3-x/2}$ obtained at 14.1 and 21.1 T. (a) $BaZr_{0.85}Sc_{0.15}O_{2.925}$. (b) $BaZr_{0.70}Sc_{0.30}O_{2.85}$. A zoom of the ^{17}O central transition of the spectra is only shown.

Table 2.3. Relative intensities of the different local environments extracted from experimental ^{17}O NMR data and expected ratios for a random distribution of the scandium cations in the $BaZr_{1-x}Sc_xO_{3-x/2}$ structure.[a]

x	Zr-O-Zr	Zr-O-Sc	Sc-O-Sc
0.15	0.7 - 0.9 (0.72)	0.1 - 0.3 (0.26)	-[b] (0.02)
0.30	0.67 - 0.73 (0.49)	0.23 - 0.33 (0.42)	0.01 - 0.05 (0.09)

[a] The experimental ratios have been obtained from spectral deconvolution and simulation of the ^{17}O data. The range of values represent the two different values obtained by fitting the high (21.1 T) and lower field (14.1 T) data. Values in parenthesis correspond to the expected ratios for a random distribution of cation and oxygen vacancies. [b] Not detected experimentally.

D. Protonic defects by ^{1}H NMR

The ^{1}H NMR spectra obtained for all the hydrated materials at 110 and 300 K are shown in *Figure 2.8*. At all substitution levels, the spectra recorded at 110 K contain a broad resonance with intense spinning sidebands, indicating that the protonic defects are rigid at this temperature. The broad signal can be simulated with two resonances at approximately 1.1 - 1.3 and 2.8 – 3.1 ppm suggesting that there are at least two types of protonic defects with different chemical environments and basicities (or hydrogen bonding strength). The ratio of the 1.1 - 1.3 ppm resonance to the 2.8 – 3.1 ppm signal increases upon substitution, from 0.3:1 to 0.5:1 and to 1:1 for $BaZr_{0.95}Sc_{0.05}O_{2.97}(OH)_{0.01}$, $BaZr_{0.85}Sc_{0.15}O_{2.875}(OH)_{0.10}$ and $BaZr_{0.70}Sc_{0.30}O_{2.75}(OH)_{0.20}$ respectively, the increasing level of scandium ions in the structure leading to a higher concentration of more basic (or more weakly hydrogen bonded) protonic defects.

It is clear that the protons at around 1.2 ppm are hosted by an oxygen atom next to a scandium; however there are still two possible assignments to this proton resonance. Indeed, this oxygen could be linked to either a Zr cation or another Sc atom. If we assume the proton at around 1.2 ppm is hosted by a Zr-O-Sc site, then we can attribute the resonance at around 2.9 ppm to a proton on a Zr-O-Zr environment. In this case the ratios of the two signals would be very close to those expected for a random distribution of protonic defects over these two environments: 0.1:1, 0.4:1 and 0.9:1 for $BaZr_{0.95}Sc_{0.05}O_{2.97}(OH)_{0.01}$, $BaZr_{0.85}Sc_{0.15}O_{2.875}(OH)_{0.10}$ and $BaZr_{0.70}Sc_{0.30}O_{2.75}(OH)_{0.20}$ respectively. However, the slightly higher concentration of the Zr-OH-Sc environment than that predicted, based on a random distribution, would suggest that there is a slight tendency of the protonic defect to order nearby a scandium ion.

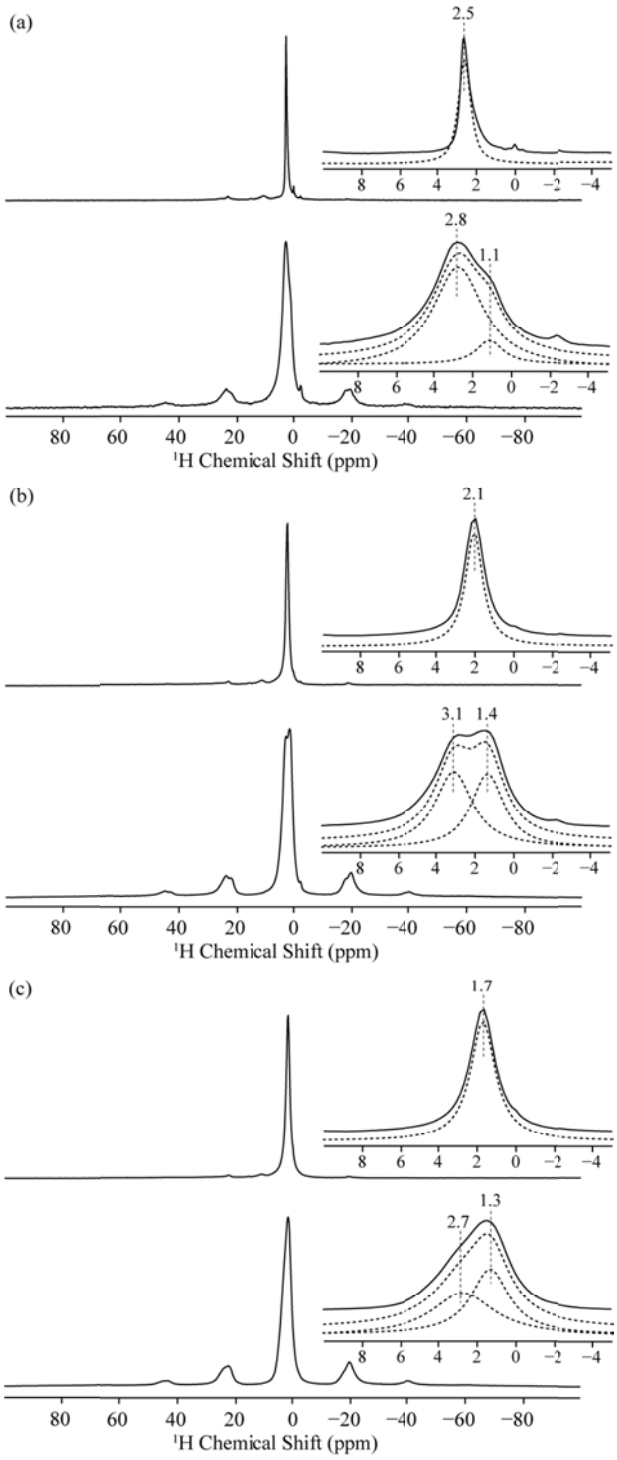

Figure 2.8. Variable temperature ^{1}H MAS NMR Hahn echo spectra of $BaZr_{1-x}Sc_xO_{3-x/2-y}(OH)_{2y}$. (a) $BaZr_{0.95}Sc_{0.05}O_{2.97}(OH)_{0.01}$. (b) $BaZr_{0.85}Sc_{0.15}O_{2.875}(OH)_{0.10}$ and (c) $BaZr_{0.70}Sc_{0.30}O_{2.75}(OH)_{0.20}$. Top: Spectra obtained at 300 K. The signal at around 12 ppm arises from the probe background. Bottom: Spectra obtained at 110 K. The inserts show a zoom in the 10 to -5 ppm range region.

For the second scenario where the proton at 1.2 ppm is hosted by a Sc-O-Sc anion, then the resonance at 2.9 ppm most likely arises from a proton on a Zr-O-Sc site. In this case, the protons would be strongly attracted to scandium since they preferentially associate on oxygen sites nearby scandium. However the number of protons that can be hosted on a Sc-O-Sc site is limited since the concentration of this particular oxygen site is rather small; therefore some protons are forced to locate on Zr-O-Sc site. Additionally this later hypothesis would imply that a large quantity of the oxygen vacancies are located in between two Sc cations, since we barely observed Sc-O-Sc in the dry samples. The concentration of those sites would therefore critically increase after hydration. Indeed if we assume that all the vacancies are located in between two Sc cations, i.e Sc-□-Sc, then the ratios of Sc-O-Sc to Zr-O-Sc upon hydration increase from 0:1 and 0.12:1 to 0.14:1 to 0.51:1 in $BaZr_{0.85}Sc_{0.15}O_{2.875}(OH)_{0.10}$ and $BaZr_{0.70}Sc_{0.30}O_{2.75}(OH)_{0.20}$ respectively. Therefore there would be enough Sc-O-Sc *vs.* Zr-O-Sc sites after hydration to host the reported amounts of proton ions, namely 0.08 vs. 0.58 and 0.29 vs. 0.57 in $BaZr_{0.85}Sc_{0.15}O_{2.875}(OH)_{0.10}$ and $BaZr_{0.70}Sc_{0.30}O_{2.75}(OH)_{0.20}$ respectively.

Although less likely, it is possible that the two resonances both arise from Sc-OH-Zr groups that differ in the nature and strength of H-bonding. In this case, the higher frequency resonance is assigned to a proton H-bonded to another Sc-O-Zr environment, while the lower frequency environment is only weakly H-bonded, possibly to a Zr-O-Zr environment, the least basic oxygen environment in the structure. The correct assignment will be identified in Chapter 5 via the use of appropriate ^{1}H-^{45}Sc double resonance experiments and comparison to ^{1}H NMR spectra of the other two studied systems, $BaZr_{1-x}Y_xO_{3-x/2-y}(OH)_{2y}$ and $BaSn_{1-x}Y_xO_{3-x/2-y}(OH)_{2y}$. A ^{1}H spin lattice relaxation time of 40 s is estimated for both sites in all samples at 110 K, consistent with the rigidity of the protonic defects at this temperature.

The spectra recorded at room temperature (300 K) show only one single resonance resulting from the coalescence of the two environments observed at 110 K, the single resonance moving from 2.5 to 1.7 ppm upon scandium substitution, in agreement with the increasing concentration of more basic oxygen sites, either Sc-O-Zr or Sc-O-Sc. Along with the absence of spinning sidebands and the presence of a line width of only 1 to 2 kHz, the coalescence of the two signals at 300 K is a clear proof of the local protonic motion. The spin lattice relaxation time

T_1 also corroborates the increased mobility of the protonic defects, decreasing from 40 s at 110 K to 1 s at 300 K for all samples. Our results demonstrate that the protonic motion already occurs at room temperature, on the timescale of these NMR experiments, at approximately 0.5 kHz, based on hopping rate between two sites required for coalescence of two resonances separated by approximately 1.6 ppm.[53]

IV. Discussion

Both sets of ^{45}Sc NMR experiments revealed the presence of 5 and 6 coordinated scandium environments. The hydration of the different materials lead to a noticeable drop of the number of 5 coordinated scandium sites. Although the MQMAS data did not resolve the remaining 5 coordinated sites due to their low concentrations, they were, however, detected in the static spectra in agreement with the partial hydration level determined from the TGA data. The study of the hydrated samples by MQMAS revealed the presence of a new resonance which was assigned to a 6 coordinated scandium atom near a protonic defect. The scandium NMR results, therefore, showed the presence of oxygen vacancies in the vicinity of the scandium cations and also the existence of protonic defects in the surrounding of scandium after hydration.

It is difficult, however, to estimate accurately the proportion of oxygen vacancies or protonic defects present in the surroundings of scandium as both the MQMAS and quadrupolar echo experiments are not quantitative pulse sequences, especially when the environments under investigation have very different quadrupolar environments. However, the trends in the ratios between the two environments, as a function of scandium doping level, should reflect the changes in relative proportions for experiments performed under similar conditions, even if the absolute ratios are not accurate. Both the MQMAS and static experiments reveal that the 5 coordinate scandium environments are present in significant concentrations and that the ratio of the concentration of the 5:6 coordinate sites increases upon scandium substitution; a similar increase in the 5:6 ratio was also observed in some earlier work.[46]

Assuming that the oxygen vacancies randomly occupy all possible oxygen sites leads to ratios, for the 6:5 coordinate scandium environments, of 95:5 and approximately 86:13 for 5 and 15 % substitution, respectively. For 30 % substitution, a small concentration (3 %) of 4 scandium

coordinate sites is also predicted (although unlikely), and hence the ratio of 6:(5+4) is 74:26. In contrast, if the vacancies are always coordinated to (*i.e.* are nearby) a scandium ion, then a ratio for the 6:5 sites of 1:1 is predicted for low substitution levels, since every scandium ion is, on average, associated with ½ a vacancy. A very slight increase in the number of 5-coordinate scandium environments will occur at high scandium substitution levels if Sc-O-Sc or Sc-□-Sc contacts exist, which will occur if there is a random or close to random distribution of scandium ions. The increase in the concentration of 5 coordinate environments with scandium substitution suggests that, although the vacancies do not avoid scandium (the 5 coordinate sites are seen), there is only a slight tendency, if any, for them to order nearby the scandium cations, for samples prepared at 1600 °C and cooled slowly to room temperature.

The oxygen results for $BaZr_{0.85}Sc_{0.15}O_{2.925}$ and $BaZr_{0.70}Sc_{0.30}O_{2.85}$ showed the presence of three different local environments for oxygen: Zr-O-Zr, Zr-O-Sc and Sc-O-Sc. Although the ratio of these sites is reasonably close to that expected for a random distribution of scandium cations in the structure (*Table 2.3*), there are significantly fewer Sc-O-Sc interactions than that predicted, based on a random model, and also fewer Sc-O-Zr sites, indicating that there is no tendency for scandium and zirconium to alternate in the lattice, unlike yttrium and tin in yttrium-substituted $BaSnO_3$ (Chapter 3).

There appear to be missing scandium ions, particularly at the highest doping level (*i.e.* more oxygen atoms nearby scandium should be seen experimentally), and the experimental ratios obtained for $BaZr_{0.70}Sc_{0.30}O_{2.85}$ are very close to the distribution of sites calculated for a substitution level of 15 to 21 %. This is ascribed to incomplete substitution of scandium in the lattice (supported by the observation of Sc_2O_3, particularly in the highest doped material by ^{45}Sc and ^{17}O NMR), the inherent errors associated with these measurements (which can be large when deconvoluting and simulating spectra containing resonances with very different quadrupolar coupling constants), and possibly the tendency for a vacancy to sit between two scandium ions, when they are located nearby. However this latter effect is much too small to account for all the missing scandium, since the vacancies only account for 1, 2.5 and 5 % of all oxygen sites for the 5, 15 and 30 % substituted samples respectively.

The tendency for the scandium cations to avoid energetically unfavourable Sc-O-Sc interactions, *i.e.* two nearby ScO_6 species, may very well explain the limit of the solid solution to 29 % (and only 15 to 21 % in this study). Above this substitution level, the structure would have to contain a significant number of Sc-O-Sc environments unless Sc-O-Zr ordering is favourable, which it is not. Even if the vacancies are preferentially located in between two scandium ions to form O_5Sc-□-ScO_5 linkages, the system appears unstable with respect to phase separation to form Sc_2O_3 and a barium zirconate with a lower substitution level.

The ^1H NMR results at low temperature showed the presence of at least two different protonic sites, the intensity of the more basic (or more weakly hydrogen bonded) environment, increasing upon substitution. There are still some uncertainties on the final assignment of these two resonances, whether we are observing protons on Zr-O-Zr and Zr-O-Sc or on Zr-O-Sc and Sc-O-Sc. The first hypothesis would suggest that the proton ions are only slightly preferentially attracted by the more basic (or more weakly hydrogen bonded) oxygen environments, *i.e.* Zr-O-Sc. Indeed if binding to a Sc-O-Zr oxygen atom were strongly thermodynamically favoured over binding to a Zr-O-Zr environment then the concentration of Sc-OH-Zr environments would dominate at all substitution levels, since there are always sufficient Sc-O-Zr oxygen sites for the protons to bind to. If there is only a small energy difference between binding to a Zr-O-Zr vs. a Sc-O-Zr site, then the additional configurational entropy gained by the occupancy of a much larger number of Zr-O-Zr environments may make binding to the Zr-O-Zr site favourable. Furthermore, the occupancy of protons on the Zr-O-Zr sites should increase with temperature; however, a greater range of temperatures is required to explore this phenomenon.The location of the proton positions is also in agreement with the original locations of the vacancies, where we did not see a strong tendency for clustering nearby scandium, although it is not strictly necessary that the two are related. The second hypothesis implies that the protons are strongly associated with scandium. It would also suggest that most of the oxygen vacancies are located in between two scandium atoms, since we do not observe enough Sc-O-Sc environments by ^{17}O NMR to host such a large concentration of protons. Additional experiments will be presented in Chapter 5 to clarify the assignment.

The coalescence of the protonic sites and the sharpness of the resonances observed for each compound at room temperature imply the presence of protonic motion even at this temperature. Furthermore, the motion related to the coalescence phenomenon must correspond to a transfer of a proton cation between the chemically distinct oxygen environments. The loss of spinning sidebands at 300 K, *i.e.* the loss of ^{1}H dipolar coupling, implies rotational motion of the protons about their oxygen sites. Although, to date, we have not performed detailed analyses of the motion, the onset of the rotational motion does not appear to occur at a temperature that is noticeably lower than that of the proton exchange process, but this suggestion must be more fully tested.

The proton transfer step between different oxygen sites was reported to be the rate-limiting step of the conduction mechanism in comparison to the rotational diffusion of the protons around their hosting oxygen in systems such as substituted $SrCeO_3$, $BaCeO_3$ and $BaTiO_3$, based on quantum molecular dynamics simulations and quasielastic thermal neutron scattering experiments.[54-58] In contrast, in a system with strong H-bonding, such as scandium-substituted $SrTiO_3$, quantum molecular dynamics simulations (albeit on the $SrTiO_3$ unsubstituted system) showed that very rapid proton transfer steps occurred between oxygen atoms.[59]

The smaller expansion of the lattice parameter on substitution by scandium, in comparison to substitution by the much larger yttrium ion, will result in shorter O…O distances and consequently stronger hydrogen bonds and easier proton transfer between oxygen sites; this may hinder reorientation of the proton ions around the oxygen atom in this system. Thus, in scandium-substituted $BaZrO_3$, the rotational diffusion step may be a possible hindrance to long-range conduction, *in addition* to the transfer step. This may help to explain the slightly poorer conductivity of this material compare to the yttrium-substituted analogue.

V. Conclusions

A comprehensive solid-state NMR study of scandium substituted $BaZrO_3$ has been reported. Five coordinated scandium cations were observed by ^{45}Sc NMR confirming the presence of oxygen vacancies in the vicinity of the substituting element. Scandium atoms nearby protonic defects were seen on hydration. No clear evidence for strong clustering of the vacancies nearby scandium was seen. The ^{17}O NMR results did not show any evidence for any Sc-O-Zr ordering and instead revealed a lower scandium substitution level than expected based on the initial scandium molar ratio, particularly at the higher doping levels, the system forming Sc_2O_3, presumably so as to avoid the formation of Sc-O-Sc environments in the perovskite structure. ^1H NMR at 110 K revealed the presence of at least two different types of protonic defects, due to sites with different basicity and/or hydrogen-bonding. Further experiments are in progress to examine the interaction of proton and scandium. The proton defects are rigid and strongly bonded at 110 K, while the coalescence of their respective resonances along with the loss of spinning sidebands at room temperature indicates that the protons undergo local motional modes. The coalescence of the two resolved signals corresponds to one possible proton transfer step in the conduction mechanism (involving two (or more) types of defect sites), which occurs at surprisingly low temperatures (300 K). The reorientation of the protons around their hosting oxygen atoms, which does not appear to be more rapid than the transfer step, may be hindered by the small expansion of the lattice parameter after scandium insertion and the presence of strong hydrogen bonds, thereby contributing an additional barrier to long-range conduction in the scandium-substituted $BaZrO_3$ systems. This may help to explain the lower conductivity of scandium-substituted $BaZrO_3$ as compared to the yttrium substituted analogue.

VI. References

1. L. Buannic, F. Blanc, I. Hung, Z. Gan and C. P. Grey, *Journal of Materials Chemistry*, 2010, **20**, 6322.

2. M. J. Scholten, J. Schoonman, J. C. van Miltenburg and H. A. J. Oonk, *Proceedings - Electrochemical Society*, 1993, **93-4**, 146.

3. T. Schober and H. G. Bohn, *Solid State Ionics*, 2000, **127**, 351.

4. H. G. Bohn and T. Schober, *Journal of the American Ceramic Society*, 2000, **83**, 768.

5. A. Magrez and T. Schober, *Solid State Ionics*, 2004, **175**, 585.

6. F. M. M. Snijkers, A. Buekenhoudt, J. Cooymans and J. J. Luyten, *Scripta Materialia*, 2004, **50**, 655.

7. P. Babilo, T. Uda and S. M. Haile, *Journal of Materials Research*, 2007, **22**, 1322.

8. F. Iguchi, N. Sata, T. Tsurui and H. Yugami, *Solid State Ionics*, 2007, **178**, 691.

9. S. B. C. Duval, P. Holtappels, U. F. Vogt, E. Pomjakushina, K. Conder, U. Stimming and T. Graule, *Solid State Ionics*, 2007, **178**, 1437.

10. S. Tao and J. T. S. Irvine, *Journal of Solid State Chemistry*, 2007, **180**, 3493.

11. R. B. Cervera, Y. Oyama, S. Miyoshi, K. Kobayashi, T. Yagi and S. Yamaguchi, *Solid State Ionics*, 2008, **179**, 236.

12. S. Higgins, N. M. Sammes, A. Smirnova, J. A. Kilner and G. Tompsett, *Journal of Fuel Cell Science and Technology*, 2008, **5**, 027001/1.

13. F. Iguchi, T. Tsurui, N. Sata, Y. Nagao and H. Yugami, *Solid State Ionics*, 2009, **180**, 563.

14. Y. Yamazaki, R. Hernandez-Sanchez and S. M. Haile, *Chemistry of Materials*, 2009, **21**, 2755.

15. K. D. Kreuer, S. Adams, W. Münch, A. Fuchs, U. Klock and J. Maier, *Solid State Ionics*, 2001, **145**, 295.

16. K. D. Kreuer, *Annual Review of Materials Research*, 2003, **33**, 333.

17. I. Naray-Szabo, *Naturwissenschaften*, 1943, **31**, 202.

18. Y. Yamazaki, P. Babilo and S. M. Haile, *Chemistry of Materials*, 2008, **20**, 6352.

19. S. Imashuku, T. Uda and Y. Awakura, *ECS Transactions*, 2007, **7**, 2321.

20. S. Imashuku, T. Uda, T. Ichitsubo, E. Matsubara and Y. Awakura, *Journal of Phase Equilibria and Diffusion*, 2007, **28**, 517.

21. N. Kim, C.-H. Hsieh and J. F. Stebbins, *Chemistry of Materials*, 2006, **18**, 3855.

22. K. J. D. MacKenzie and M. E. Smith, *Multinuclear Solid-State Nuclear Magnetic Resonance of Inorganic Materials*, Pergamon Oxford, 2002.

23. A. J. Rossini and R. W. Schurko, *Journal of the American Chemical Society*, 2006, **128**, 10391.

24. N. Kim and J. F. Stebbins, *Chemistry of Materials*, 2009, **21**, 309.

25. N. Kim, J. F. Stebbins, S. Quartieri and R. Oberti, *American Mineralogist*, 2007, **92**, 1875.

26. P. Jain, H. J. Avila-Paredes, C. Gapuz, S. Sen and S. Kim, *Journal of Physical Chemistry C*, 2009, **113**, 6553.

27. D. Riou, F. Fayon and D. Massiot, *Chemistry of Materials*, 2002, **14**, 2416.

28. S. E. Ashbrook and M. E. Smith, *Chemical Society Reviews*, 2006, **35**, 718.

29. A. E. McDermott, F. J. Creuzet, A. C. Kolbert and R. G. Griffin, *Journal of Magnetic Resonance*, 1992, **98**, 408.

30. D. H. Zhou, D. T. Graesser, W. T. Franks and C. M. Rienstra, *Journal of Magnetic Resonance*, 2006, **178**, 297.

31. A. Samoson, *Extended magic-angle spinning*, Wiley, Chichester, UK, 2002.

32. A. Samoson, T. Tuherm, J. Past, A. Reinhold, T. Anupold and I. Heinmaa, *Topics in Current Chemistry*, 2005, **246**, 15.

33. B. C. Gerstein, *CRAMPS*, Wiley, Chichester, U.K., 1996.

34. A. Lesage, *Physical Chemistry Chemical Physics*, 2009, **11**, 6876.

35. P. Babilo and S. M. Haile, *Journal of the American Ceramic Society*, 2005, **88**, 2362.

36. Z. Gan, P. L. Gor'kov, W. W. Brey, P. J. Sideris and C. P. Grey, *Journal of Magnetic Resonance*, 2009, **200**, 2.

37. L. Frydman, *Encyclopedia of Nuclear Magnetic Resonance*, 2002, **9**, 262.

38. Z. Gan and H.-T. Kwak, *Journal of Magnetic Resonance*, 2004, **168**, 346.

39. J.-P. Amoureux, C. Fernandez and S. Steuernagel, *Journal of Magnetic Resonance, Series A*, 1996, **123**, 116.

40. A. Bielecki and D. P. Burum, *Journal of Magnetic Resonance, Series A*, 1995, **116**, 215.

41. J. D. van Beek, *Journal of Magnetic Resonance*, 2007, **187**, 19.

42. K. Eichele and R. E. Wasylishen, Dalhousie University, Halifax, Canada.

43. M. Bak, J. T. Rasmussen and N. C. Nielsen, *Journal of Magnetic Resonance*, 2000, **147**, 296.

44. P. Hodgkinson and L. Emsley, *Progress in Nuclear Magnetic Resonance Spectroscopy*, 2000, **36**, 201.

45. R. D. Shannon, *Acta Crystallographica, Section A Crystal Physics, Diffraction, Theoretical and General Crystallography*, 1976, **A32**, 751.

46. I. Oikawa, M. Ando, Y. Noda, K. Amezawa, H. Kiyono, T. Shimizu, M. Tansho and H. Maekawa, *17th International Conference on Solid State Ionics*, Toronto, 2009.

47. L. Frydman and J. S. Harwood, *Journal of the American Chemical Society*, 1995, **117**, 5367.

48. A. Medek, J. S. Harwood and L. Frydman, *Journal of the American Chemical Society*, 1995, **117**, 12779.

49. I. Hung, J. Trébosc, G. L. Hoatson, R. L. Vold, J.-P. Amoureux and Z. Gan, *Journal of Magnetic Resonance*, 2009, **201**, 81.

50. T. J. Bastow, P. J. Dirken, M. E. Smith and H. J. Whitfield, *Journal of Physical Chemistry*, 1996, **100**, 18539.

51. E. Oldfield, C. Coretsopoulos, S. Yang, L. Reven, H. C. Lee, J. Shore, O. H. Han, E. Ramli and D. Hinks, *Physical Review B Condensed Matter and Materials Physics*, 1989, **40**, 6832.

52. D. S. Middlemiss, F. Blanc, C. J. Pickard and C. P. Grey, *Journal of Magnetic Resonance*, 2010, **204**, 1.

53. M. H. Levitt, *Spin Dynamics: Basics of Nuclear Magnetic Resonance*, John Wiley & Sons, 2001.

54. T. Matzke, U. Stimming, C. Karmonik, M. Soetratmo, R. Hempelmann and F. Güthoff, *Solid State Ionics*, 1996, **86-88**, 621.

55. M. Pionke, T. Mono, W. Schweika, T. Springer and H. Schober, *Solid State Ionics*, 1997, **97**, 497.

56. W. Münch, G. Seifert, K. D. Kreuer and J. Maier, *Solid State Ionics*, 1996, **86-88**, 647.

57. W. Münch, G. Seifert, K. D. Kreuer and J. Maier, *Solid State Ionics*, 1997, **97**, 39.

58. K. D. Kreuer, W. Münch, U. Traub and J. Maier, *Berichte der Bunsen-Gesellschaft*, 1998, **102**, 552.

59. F. Shimojo, K. Hoshino and H. Okazaki, *Journal of the Physical Society of Japan*, 1997, **66**, 8.

Chapter 3:

Evidence of mixed site cationic substitution in $BaZr_{1-x}Y_xO_{3-\delta}$ by NMR spectroscopy

The mixed site substitution of yttrium in $BaZrO_3$ is reported by XRD and solid-state NMR analyses. Due to its rather large ionic size, yttrium can substitute for both Zr and Ba in $BaZrO_3$. It is important to limit the amount of A site substitution occurring during sintering in order to keep the oxygen vacancies present in the dry structure. As observed by ^{89}Y NMR, the presence of 12-coordinated yttrium cations significantly decreases the amount of oxygen vacancies preventing the incorporation of proton ions in the material. The sintering conditions are critical to ensure the preparation of the best protonic conductor.

I. Introduction

The substitution of Y^{3+} for Zr^{4+} in $BaZrO_3$ leads to the formation of oxygen vacancies. After reaction of the vacancies with atmospheric water, the material conducts protons starting from approximately 200°C. For applications in IT-SOFCs, not only should the electrolyte material be a good protonic conductor but it should also be stable under CO_2, H_2O and reducing atmospheres. $BaZr_{1-x}Y_xO_{3-x/2}$ is one of the few materials to possess all of these characteristics, which explains why it is the most studied perovskite based protonic conductor.[1-13] From the point of view of solid state NMR, this material is difficult to study. ^{17}O is a quadrupolar nucleus (spin = 5/2) and the acquisition of ^{17}O NMR signal requires prior ^{17}O enrichment of the samples due to the low abundance of this isotope (≈ 0.037 %). While these characteristics would make such a nucleus quite unfriendly, the oxygen environments are the easiest to detect in the structure. ^{89}Y may be a 100% abundant spin ½, usually excellent qualities for an NMR nucleus; however yttrium has a particularly small gyromagnetic ratio rendering this nucleus rather insensitive to any change of magnetization and is also characterized by long T_1 relaxation times. This leads to time-consuming experiments in order to obtain a good signal to noise ratio for this particular nucleus. In addition the concentration of Y is rather limited in the studied materials, from 10 to 50 % of the B site cations, increasing the initial difficulty in detecting the various Y environments existing in our structure of interest. ^{91}Zr is another active nucleus; however not only is it a quadrupolar nucleus (spin = 5/2), it is also the main cation present in the rotors used to spin the samples. The most commons rotors are made of yttria stabilized ZrO_2, Si_3N_4 rotors are used only in particular occasions.

II. Experimental section

A. Sample Preparation

$BaZr_{1-x}Y_xO_{3-x/2}$ (x = 0.10, 0.30, 0.50) samples were synthesized through a glycine-nitrate combustion route[14] using $Ba(NO_3)_2$ (Alfa Aesar, 99.999 %), $ZrO(NO_3)$. x H_2O (Alfa Aesar, 99.9%), $Y(NO_3)_3$. x H_2O (Alfa Aesar, 99.99 %) and glycine (Alfa Aesar, 99.7 %) as starting materials. Stoichiometric ratios of the reactants were mixed in a small amount of deionized water with a nitrate to glycine ratio of 2:1. Mixtures were then dehydrated on a hot plate and auto-ignition followed. Powders were then ground and fired at 1200 °C for 10 hours, pressed into

pellets, buried in $BaZrO_3$ powder to prevent barium evaporation, sintered at 1600 °C for another 15 hours and finally slowly cooled to room temperature. ^{17}O enrichment was performed by heating the freshly dried samples (1 hour at 950 °C under vacuum) under 50 % ^{17}O enriched O_2 gas (Isotec, 99 %) for 2 days at 950 °C. Purity of the samples was checked by X-ray diffraction using a Scintag diffractometer with Cu-Kα radiation. Diffraction patterns were compared to the JCPDS (Joint Committee on Powder Diffraction Standards) card for $BaZrO_3$ (# 06-0399).

B. ^{17}O NMR spectroscopy

Room temperature ^{17}O NMR experiments were carried out on a 14.1 T wide bore Bruker Avance 600 MHz spectrometer equipped with a 4 mm HX probehead operating at 81.36 MHz. All samples were packed inside 4 mm MAS zirconia rotors and spun at a spinning frequency ω_r of 15 kHz. ^{17}O one-dimensional spectra were recorded using the rotor synchronized Hahn echo experiments with an evolution period of one rotor period, *i.e.* τ_r = 66.7 μs, to avoid probe ringing, selective pulse widths of $\pi/6$ = 0.83 μs and $\pi/3$ = 1.67 μs and recycle delay of 5 s. Two-dimensional triple-quantum MAS NMR experiments were performed using the *z-filtered* pulse sequence.[15] Hard and soft pulses were performed at ω_1^O = 100 kHz and approximately 15 kHz, respectively. The multiple-quantum transfer was optimized on every sample to increase the excitation sensitivity of the MQ coherences. The t_1 increment was rotor synchronized to one rotor period ω_r of 15 kHz, *i.e.* 66.67 μs. The recycle delay was set to 5 s for all the experiments. High temperature ^{17}O MAS NMR experiments were performed at 11.7 T on a wide bore Oxford 500 MHz spectrometer equipped with a 7 mm HX high temperature MAS probe from Doty Scientific, Inc tuned to 67.78 MHz. The samples were packed in a boron nitride BN insert which was then placed in a 7 mm silicon nitride Si_3N_4 rotor. Spinning was performed under nitrogen at 4 kHz at room temperature and at 6 kHz above 200 °C. Temperature calibration of the probe was carefully performed by using the ^{207}Pb resonance of $Pb(NO_3)_3$[16-17] below 400 °C and ^{119}Sn resonance of $Pr_2Sn_2O_7$[18] above 400 °C. The temperatures given in the text are actual sample temperatures and are given with an accuracy of ± 4 °C. One-pulse spectra were recorded with a $\pi/2$ pulse width of 3 μs and a recycle delay of 1 s was used for 200°C and above. Chemical shifts were externally referenced to H_2O at 0 ppm.

C. ^{89}Y NMR Spectroscopy

High field ^{89}Y NMR experiments were performed on a 20.0 T standard bore Bruker 850 MHz spectrometer in Warwick, UK equipped with a 7 mm probe tuned to 41.66 MHz using a Hahn echo pulse program with a $\pi/2 = 6$ μs and a π pulse of 15 μs with a pulse delay of 250 s. All samples were packed in 7 mm silicon nitride Si_3N_4 rotors and spun at a spinning frequency of 4 kHz. Chemical shifts were externally referenced to solid Y_2O_3 at 330 ppm for the main peak.

D. ^{91}Zr NMR Spectroscopy

High field ^{91}Zr NMR experiments were performed on a 21.1 T standard bore Bruker Avance III 900 MHz spectrometer equipped with a 3.2 mm HX probehead and operating at 83.69 MHz. The samples were packed inside 3 mm glass tubes to avoid rotor background; no spinning was performed. Static quadrupolar echo experiments ($\pi/2 - \tau - \pi/2 - \tau$) were recorded using a pulse widths of $\pi/2 = 3$ μs. The chemical shift was reference to $BaZrO_3$ at 317 ppm.

III. Results and discussion

A. XRD

Figure 3.1 shows the XRD pattern for the dry $BaZr_{1-x}Y_xO_{3-x/2}$ solid-solution. The samples do not contain Y_2O_3 impurities, usually observed at a 2Θ values of around 29°. We can observe a shift to lower 2Θ values upon yttrium substitution. The ionic radius of Y^{3+} is bigger than the one of Zr^{4+}, 0.90 Å and 0.72 Å respectively,[19] thereby increasing the lattice parameter upon substitution. While the lattice increase should be proportional to the yttrium concentration, it seems that this is not the case for our set of samples (*Table 3.1* and *Figure 3.2*). For instance the lattice parameter of $BaZr_{0.50}Y_{0.50}O_{2.75}$ is almost identical to the one of $BaZr_{0.70}Y_{0.30}O_{2.85}$; however we do not detect any impurity. The yttrium must be present in the structure but maybe not where we expect it. According to a recent report by *Haile et al.*,[13] there is a tendency for yttrium to not only substitute on the B site of the perovskite but also on the A site, particularly if Ba evaporation occurred during sintering. BaO loss has been reported at temperatures above 1250°C[20] and may very well be occurring in our samples since the sintering temperature is set to 1600°C. The small lattice parameter observed for $BaZr_{0.50}Y_{0.50}O_{2.75}$ may be an indication for the occurrence of such phenomenon in our sample. More information will be obtained from ^{89}Y NMR spectroscopy.

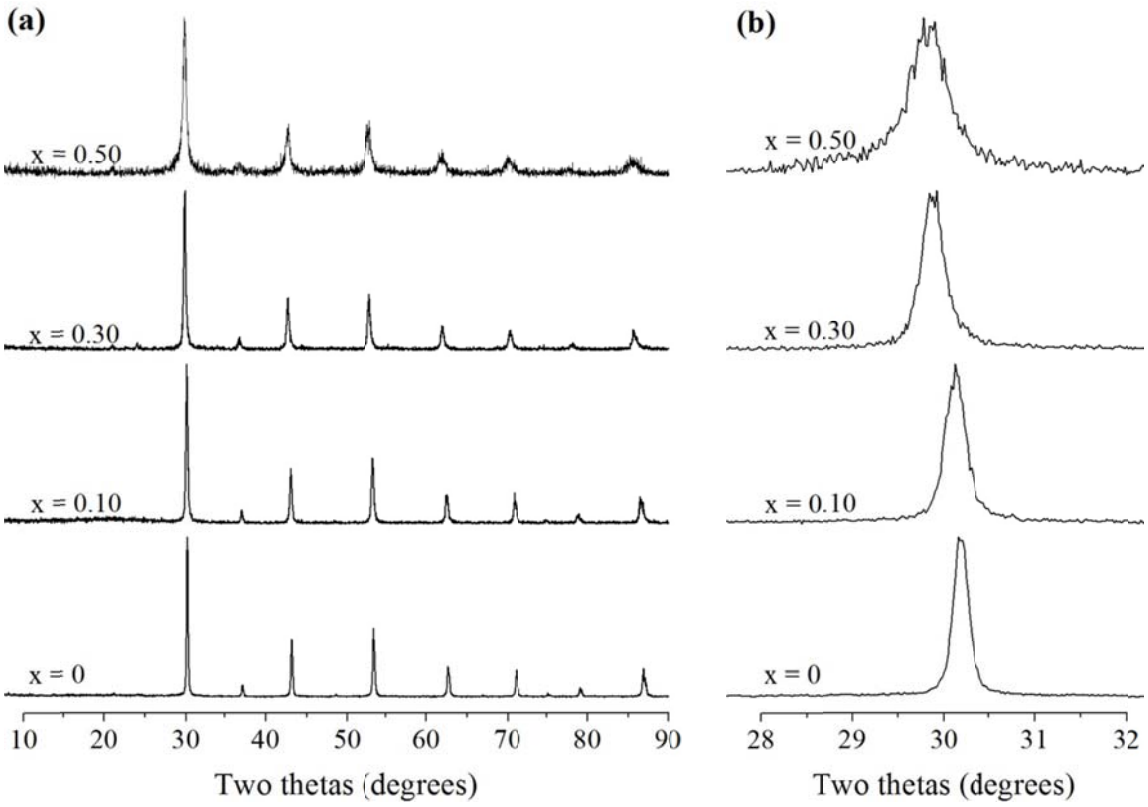

Figure 3.1. X-ray diffraction pattern of dry $BaZr_{1-x}Y_xO_{3-x/2}$. (a) For 2Θ values of 10° to 90° and (b) zoom in the 28° to 32° 2Θ region.

Table 3.1. Cell parameter extracted from XRD patterns for dry $BaZr_{1-x}Y_xO_{3-x/2}$.

x	0	0.10	0.30	0.50
Cell parameter (Å)	4.193(1)	4.200(2)	4.231(1)	4.234(1)

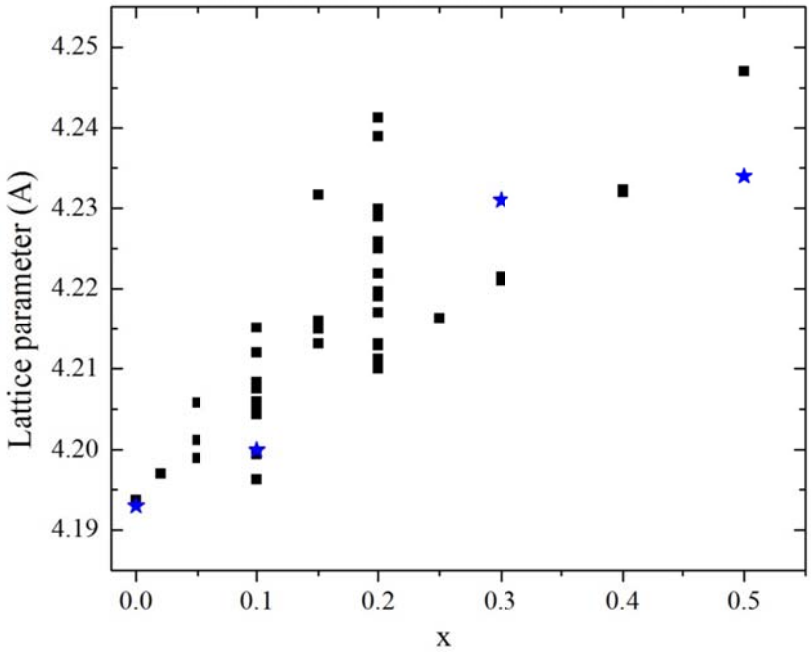

Figure 3.2. Comparison of the lattice parameter of our $BaZr_{1-x}Y_xO_{3-x/2}$ samples (blue stars) with the ones gathered by Yamazaki et al[20] from the literature. [6, 10, 13, 20-30]

B. ^{17}O NMR

Figure 3.3 illustrates the ^{17}O NMR results for the dry $BaZr_{1-x}Y_xO_{3-x/2}$ samples. $BaZrO_3$ contains only a single oxygen site, Zr-O-Zr, with a chemical shift of 376 ppm in agreement with the literature.[31] We observe two resonances for $x > 0$: at 375 and 395 ppm for $x = 0.10$, at 374 and 394 ppm for 0.30 and at 371 and 380 for $x = 0.50$. The lower frequency resonance (371 to 376 ppm) is the strongest resonance in both $BaZr_{0.90}Y_{0.10}O_{2.95}$ and $BaZr_{0.70}Y_{0.30}O_{2.85}$; we can therefore assign it to an oxygen atom surrounded by two Zr cations, *i.e.* Zr-O-Zr, in agreement with the Zr-O-Zr shift in $BaZrO_3$.[31] The resonance at higher frequency grows upon yttrium substitution; it can be assigned to an oxygen anion in between Zr and Y, *i.e.* Zr-O-Y. The shift resulting from the substitution of a zirconium ion by an yttrium cation induces a shift of 20 ppm, which is smaller than the one induced by substituting a scandium atom in the structure (29 ppm).

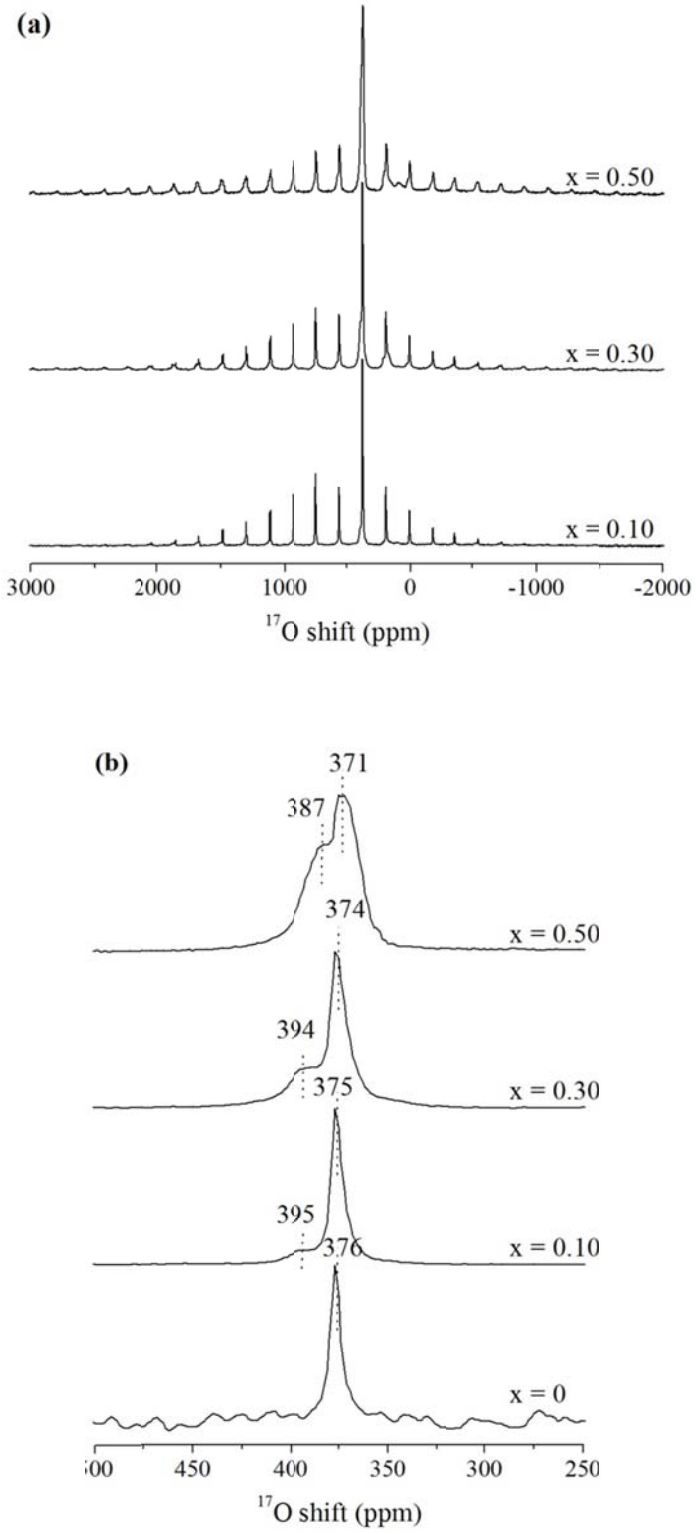

Figure 3.3. ^{17}O NMR of dry $BaZr_{1-x}Y_xO_{3-x/2}$ at room temperature with a spinning speed of 15 kHz. (a) Full Hahn Echo spectra, (b) zoom of the isotropic region.

Deconvolution results of the site ratios are gathered in *Table 3.2* and compared to the oxygen site ratio in the case of a random distribution of yttrium in the structure. Our samples seem to always contain less oxygen nearby yttrium as compared to the amount that should be detected. One possibility is that all the oxygen vacancies are located in between two yttrium cations forming Y-□-Y environments. However even in such a case we are still missing some yttrium cations. For $BaZr_{0.50}Y_{0.50}O_{2.75}$ if we assume that all the oxygen vacancies are located in between two yttrium cations (*Table 3.3*), then the experimental ratios of oxygen sites in the sample would be 0.49:0.43:0.08 for Zr-O-Zr:Zr-O-Y:Y-□-Y which are similar to those calculated for a substitution level of 30%, in agreement with the XRD results. A similar trend is seen for all substitution levels: we observe less yttrium on the B site of the perovskite than expected from calculation for the chosen substitution levels.

Table 3.2. Ratios of the different oxygen sites in $BaZr_{1-x}Y_xO_{3-\delta}$ extracted from Figure 3.3b.

x	Deconvolution results by site			Random distribution model		
	Zr-O-Zr	Zr-O-Y	Y-O-Y	Zr-O-Zr	Zr-O-Y	Y-O-Y
0.00	1.00	0.00	0.00	1.00	0.00	0.00
0.10	0.95(3)	0.05(2)	- [(a)]	0.81	0.18	0.01
0.30	0.80(4)	0.20(4)	- [(a)]	0.49	0.42	0.09
0.50	0.53(4)	0.47(3)	- [(a)]	0.25	0.50	0.25

[(a)] No such environment detected by Hahn Echo experiment.

Table 3.3. Ratios of the different oxygen sites in $BaZr_{1-x}Y_xO_{3-\delta}$ extracted from Figure 3.3b and assuming that all oxygen vacancies are located between two yttrium atoms. The ratio of Y-□-Y assuming all vacancies in between yttrium caitons can be calculated for each substitution level.

x	Deconvolution results by site			Random distribution model		
	Zr-O-Zr	Zr-O-Y	Y-□-Y	Zr-O-Zr	Zr-O-Y	Y-O-Y
0.00	1.00	0.00	0.00	1.00	0.00	0.00
0.10	0.93(3)	0.05(2)	0.02	0.81	0.18	0.01
0.30	0.76(4)	0.19(4)	0.05	0.49	0.42	0.09
0.50	0.49(4)	0.43(3)	0.08	0.25	0.50	0.25

Figure 3.4, 3.5 and 3.6 show the MQMAS spectra for $BaZr_{0.90}Y_{0.10}O_{2.95}$, $BaZr_{0.70}Y_{0.30}O_{2.85}$ and $BaZr_{0.50}Y_{0.50}O_{2.75}$ respectively. The two oxygen sites, Zr-O-Zr and Zr-O-Y, are clearly resolved for all substitution levels; however no third site that could potentially arise from a Y-O-Y configuration is observed, even for $BaZr_{0.50}Y_{0.50}O_{2.75}$. Such a site is expected to appear at a chemical shift around 411 ppm based on the other two shifts. Since the substitution of yttrium for zirconium in $BaZr_{0.50}Y_{0.50}O_{2.75}$ seems to actually be only approximately 30%, the amount of Y-O-Y environment present in the structure may very well be below the detection limit of the MQMAS experiment for this sample. In the case of a 30% substitution level, only 9% of the oxygen sites are predicted to be Y-O-Y environments assuming the distribution of Zr and Y cations is random, a concentration that may be difficult to observe by MQMAS.

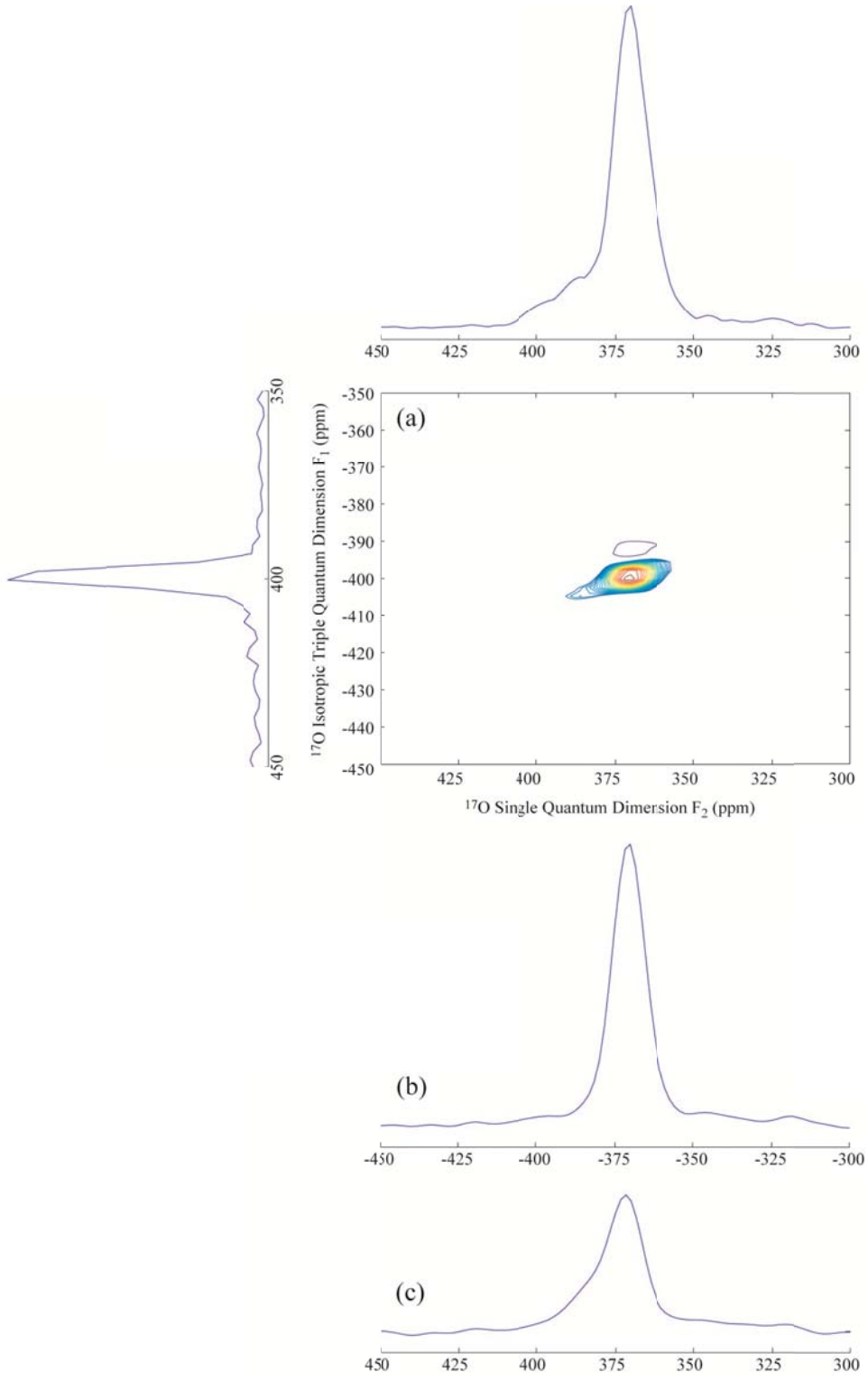

Figure 3.4. ^{17}O MQMAS of dry $BaZr_{0.90}Y_{0.10}O_{2.95}$ at room temperature. (a) Triple quantum MAS spectrum. On top is the skyline projection along the F_2 dimension and on the left the isotropic projection along the F_1 dimension. Cross sections extracted along the F2 dimension at (b) 399 ppm and (c) 403 ppm.

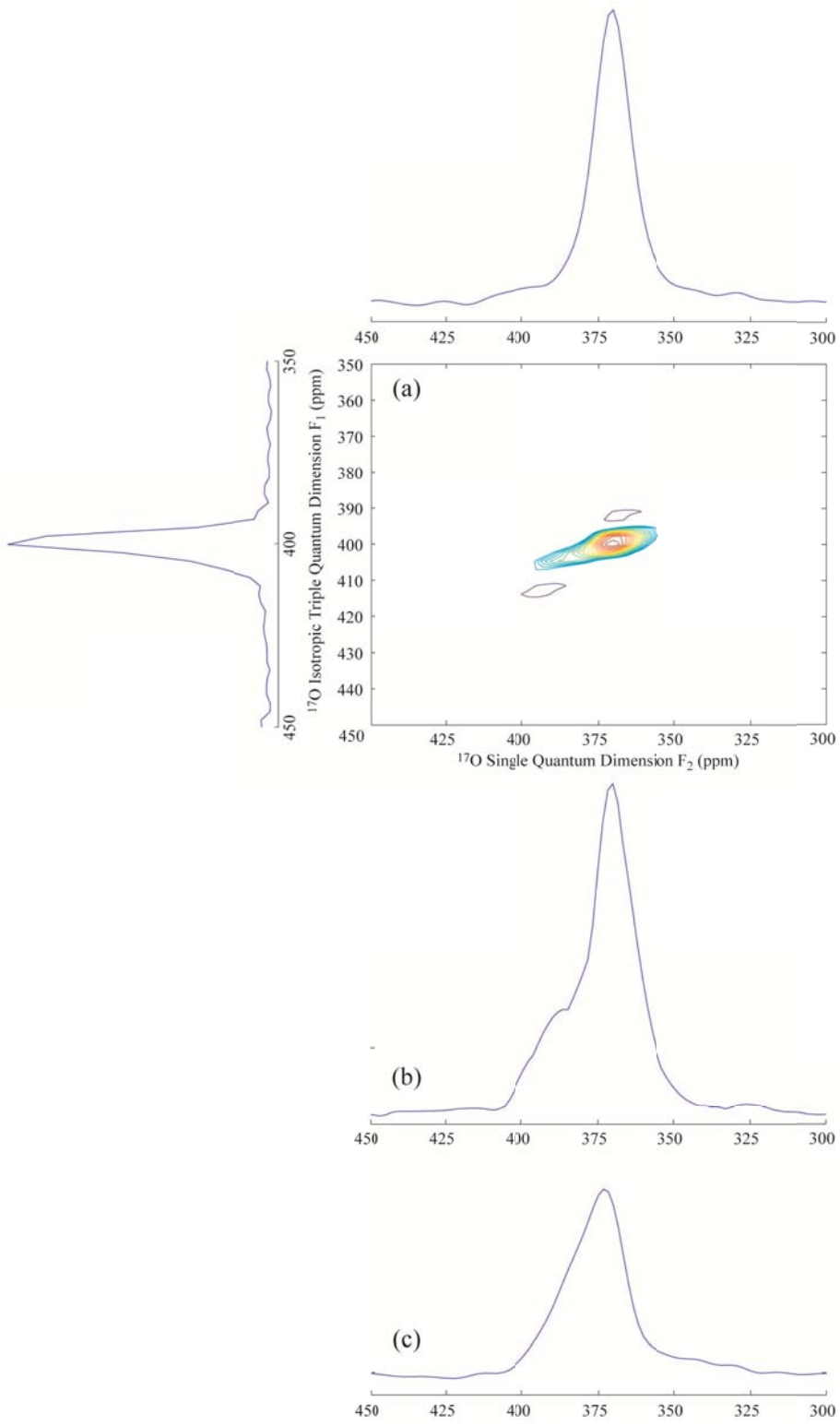

Figure 3.5. ^{17}O MQMAS of dry $BaZr_{0.70}Y_{0.30}O_{2.85}$ at room temperature. (a) Triple quantum MAS spectrum. On top is the skyline projection along the F_2 dimension and on the left the isotropic projection along the F_1 dimension. Cross sections extracted along the F2 dimension at (b) 400 ppm and (c) 404 ppm.

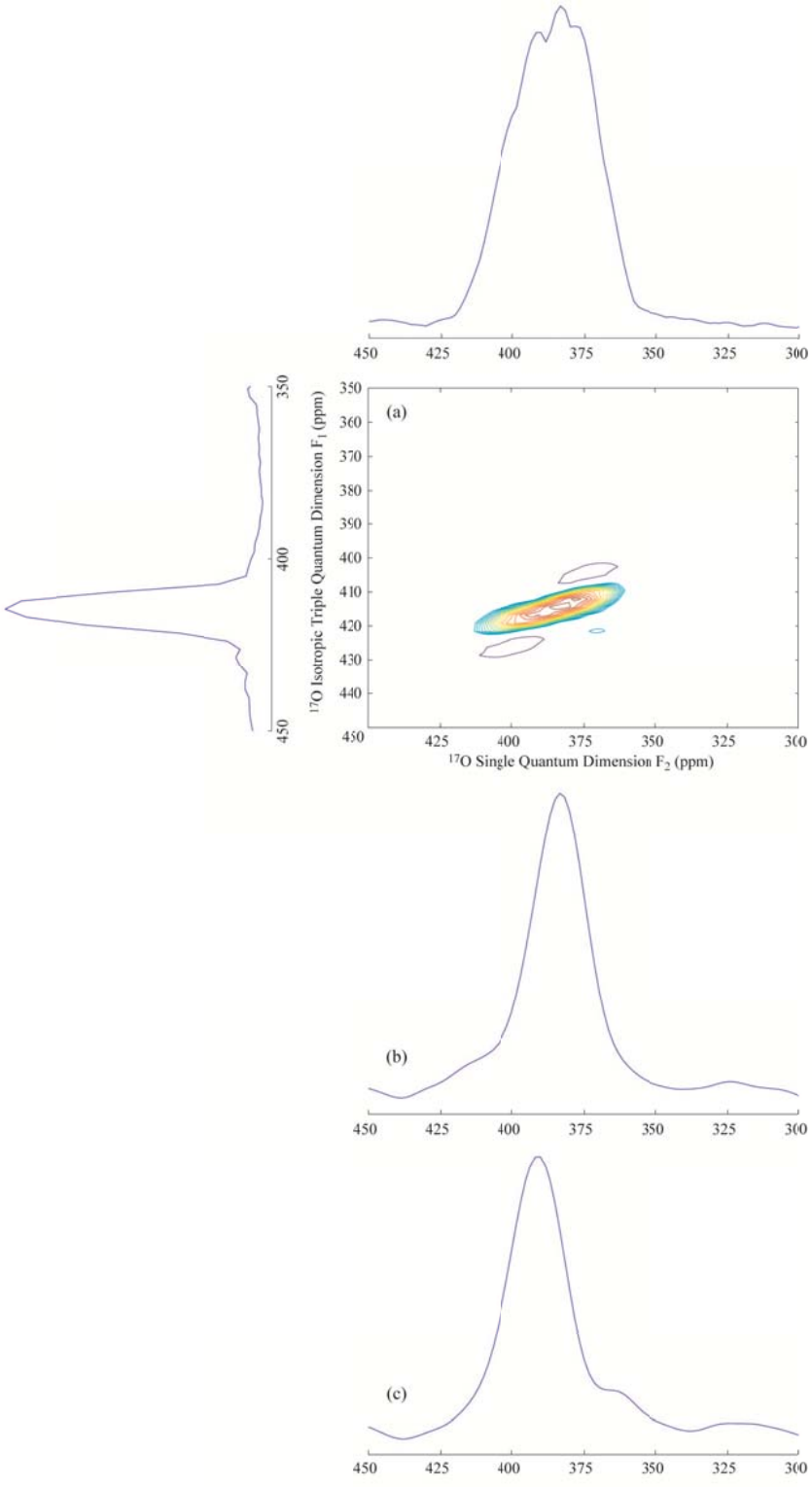

Figure 3.6. ^{17}O MQMAS of dry $BaZr_{0.50}Y_{0.50}O_{2.75}$ at room temperature. (a) Triple quantum MAS spectrum. On top is the skyline projection along the F_2 dimension and on the left the isotropic projection along the F_1 dimension. Cross sections extracted along the F2 dimension at (b) 414 ppm and (c) 417 ppm.

The high temperature ^{17}O NMR spectra of $BaZr_{0.70}Y_{0.30}O_{2.85}$ are presented in *Figure 3.7*. The resonances are not as well resolved as in the previous spectra simply because the spinning speeds that can be reached with the DOTY high temperature probe are much more limited (4 kHz at room temperature and 6 kHz for 200°C and above) than with a 4 mm HX probe (typically 15 kHz). Starting at 400°C we observe the coalescence of the two oxygen environments due to the motion of the oxygen ions in the structure; the oxygen atoms are hopping from Zr-O-Zr to Zr-□-Y and from Zr-O-Y to Zr-□-Zr averaging out the two resonances. This confirms the existence of oxygen conduction at high temperatures which starts at about 400°C in this material, the coalescence requiring a jump frequency k greater than the frequency separation Δν between the two resonances and given by:[32]

$$k = \frac{\pi \Delta \nu}{\sqrt{2}}$$

which yields approximately k = 4 kHz. We can also note the loss of spinning sidebands at 700°C. Very slow motion of the ions on the order of the spinning frequency (15 kHz) prevents the refocusing of some of the interactions at the end of the echo that gives rise to the spinning sidebands.[33-34] The loss of the spinning sideband at higher temperatures indicates the increased motion of the oxygen ions from about 4 kHz at 400°C to 15 kHz and faster at 550°C and above.

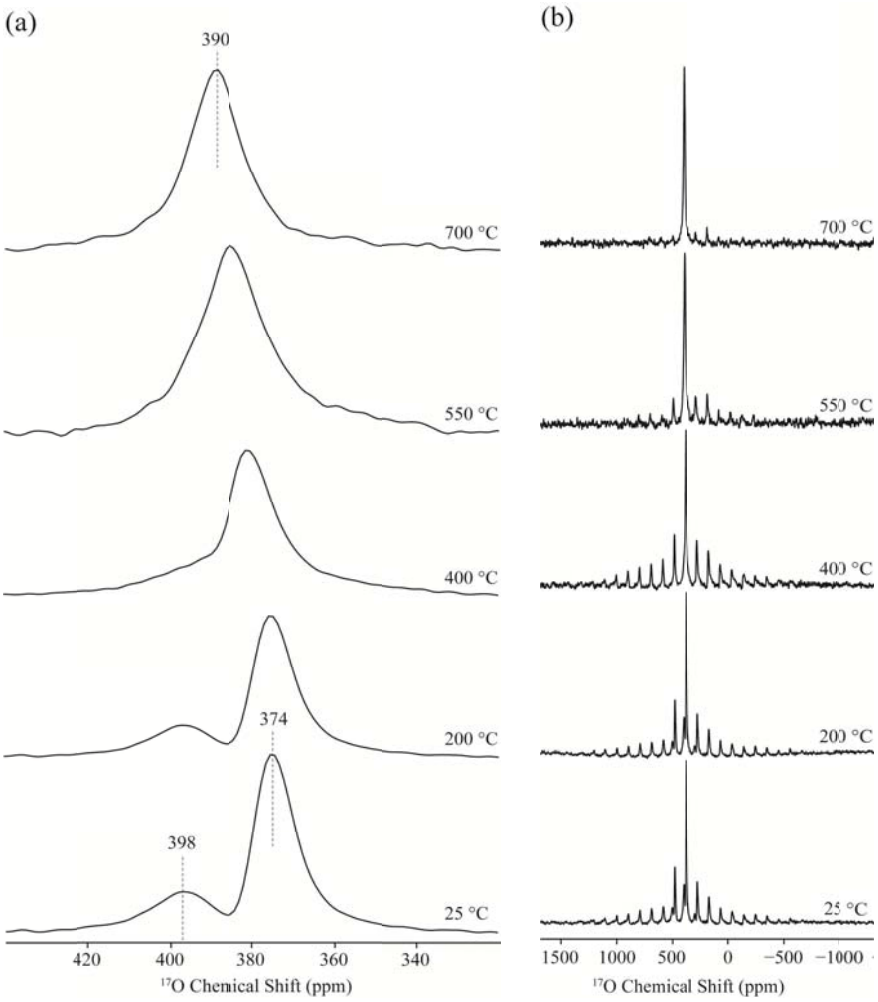

Figure 3.7. Effect of high temperature on the ^{17}O NMR spectrum of dry $BaZr_{0.70}Y_{0.30}O_{2.85}$.

C. ^{89}Y NMR

Figure 3.8 shows the ^{89}Y NMR of dry $BaZr_{1-x}Y_xO_{3-\delta}$. We can observe approximately three different resonances: a very broad one in the range of 100 - 300 ppm present for x = 0.10 and 0.50, one at around 407 ppm seen for all samples and finally one at 500 ppm only observed for x = 0.30. The resonance at 407 ppm grows consistently with yttrium concentration and always constitutes the main environment; we can therefore assign this resonance to 6-coordinated Y cations, i.e. $Y\text{-}(OB)_6$ where B = Zr or Y. The chemical shift of this site is in agreement with other 6-coordinated Y environments reported in the literature.[35-46] In order to assign the other two resonances, we need to compare our chemical shifts with the range of ^{89}Y chemical shifts observed for a variety of Y local environments reported in the literature (*Figure 3.9*).[35-46] The shift ranges observed for different coordination numbers tend to overlap; however there is a clear overall trend for an increase in shift with decreasing coordination number. Therefore we can assign the resonance at 500 ppm observed in $BaZr_{0.70}Y_{0.30}O_{2.85}$ to 5-coordinated Y cations. While one would expect to observe the highest concentration of 5-coordinated Y cations in $BaZr_{0.50}Y_{0.50}O_{2.75}$, we actually resolve none in this sample. The third resonance is observed in the range of 100 - 300 ppm. The chemical shift of this resonance matches the one of the only nominally 12-coordinated Y environment reported in the literature for $YAlO_3$;[37] while $YAlO_3$ crystallizes in a perovskite structure, it is somewhat distorted leading to a A (Y) site coordination number of 8 rather than 12. We can therefore assign this resonance to a 12-coordinated Y cation substituting Ba on the A site, in agreement with the small cell parameter observed by XRD. The substitution of yttrium on the A site of our materials must distort the local structure of the A site due to the large difference in ionic radius between Y^{3+} and Ba^{2+}, 0.90 and 1.35 Å respectively. The distortion of the site may lead to the presence of yttrium cations coordinated to slightly fewer oxygen ions than the theoretical value of 12 for a symmetric A site, nevertheless it does confirm the substitution of yttrium on both the A and B sites. The broad resonance at around 150 ppm observed in $BaZr_{0.90}Y_{0.10}O_{2.95}$ is also due to A site substitution of yttrium.

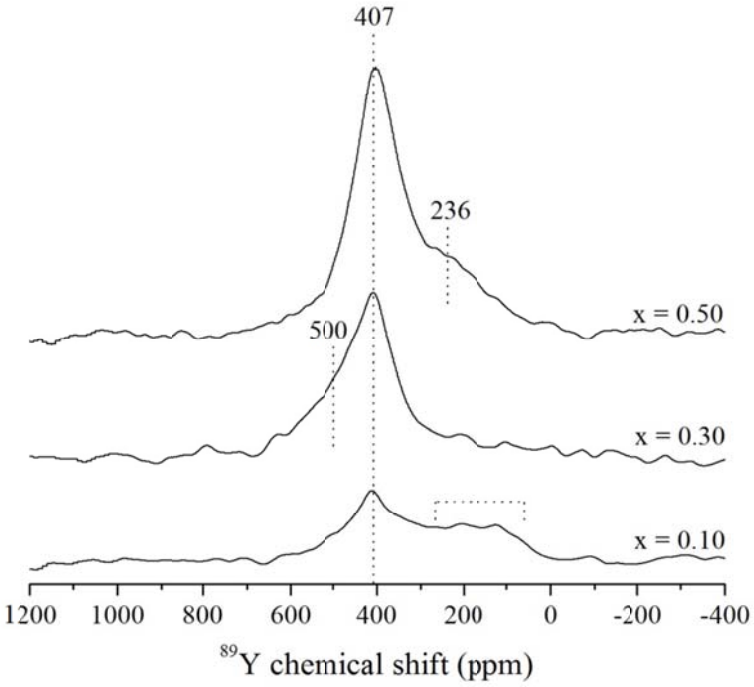

Figure 3.8. ^{89}Y NMR of dry $BaZr_{1-x}Y_xO_{3-\delta}$.

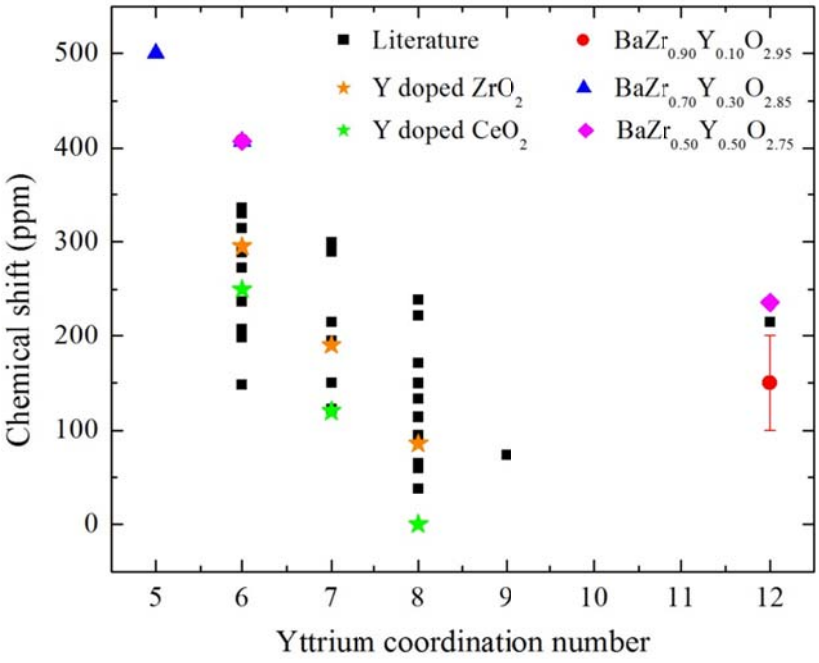

Figure 3.9. A comparison of the experimental shifts observed in $BaZr_{1-x}Y_xO_{3-x/2}$, x = 0.10 (red circle), 0.30 (blue triangle) and 0.50 (purple star), and the ^{89}Y chemical shifts reported for stoichiometric materials in the literature (black squares).[35-46] The shifts for the different yttrium coordination environments in yttrium substituted ZrO_2 and CeO_2 respectively, are shown as orange and green stars, respectively.

The ratios of the different Y environments are gathered in *Table 3.4*. For $BaZr_{0.70}Y_{0.30}O_{2.85}$ the proportion of 5 to 6 coordinated Y sites (0.30:0.70) is very close to the one expected in the case of a random distribution of the oxygen vacancies in the structure (0.26:0.74); therefore we can assume that the vacancies are not preferentially located next to the Y cations in this sample. In the case of $BaZr_{0.90}Y_{0.10}O_{2.95}$ and $BaZr_{0.50}Y_{0.50}O_{2.75}$ the A site substitution of yttrium will lead to the following stoichiometry: $(Ba_{1-2b}Y_{2b})(Sn_{1-a+b}Y_{a-b})O_{3-a/2+1.5b}$. According to the ratio of Y-O_6 to Y-O_{12} environments displayed in *Table 3.4*, we can calculate the amount of A site substitution for x = 0.10 and 0.50. The actual formulae for those two samples are: $(Ba_{0.954}Y_{0.0456})(Sn_{0.946}Y_{0.054})O_{2.996}$ and $(Ba_{0.83}Y_{0.17})(Sn_{0.67}Y_{0.33})O_{3.00}$ respectively. There is close to no oxygen vacancies left in those samples due to the presence of A site substitution; it is therefore not surprising not to observe 5-coordinated Y cations in these two samples.

A-site substitution of yttrium in these materials leads to a smaller concentration of Y on the B site and therefore a smaller lattice parameter; the replacement of the large Ba^{2+} cations by the smaller Y^{3+} cations does not result in cell expansion but rather contributes to cell contraction. The amounts of A site substitution estimated from the ^{89}Y ratio for "$BaZr_{0.90}Y_{0.10}O_{2.95}$" and "$BaZr_{0.50}Y_{0.50}O_{2.75}$" lead to B site substitution levels of 5 and 33% respectively. According to the literature,[35-46] the expected lattice parameters for such substitution levels are in good agreement with our cell parameters: a = 4.1995 and 4.2338 Å for "$BaZr_{0.90}Y_{0.10}O_{2.95}$" and "$BaZr_{0.50}Y_{0.50}O_{2.75}$" respectively (*Figure 3.2*), confirming the presence of A site substitution.

For x = 0.50 which led to the $(Ba_{0.83}Y_{0.17})(Sn_{0.67}Y_{0.33})O_{3.00}$ composition, the lattice parameter (a = 4.2338 Å) is very close to the one of our $BaZr_{0.70}Y_{0.30}O_{2.85}$ sample (a = 4.2307 Å) consistent with an approximate Y substitution of 30% on the B site of the former. Even though all samples were prepared following the same route, "$BaZr_{0.90}Y_{0.10}O_{2.95}$" and "$BaZr_{0.50}Y_{0.50}O_{2.75}$" were sintered at the same time while $BaZr_{0.70}Y_{0.30}O_{2.85}$ had been sintered on a different day which may explain why no A site substitution took place in the latter.

Table 3.4. Distribution of the yttrium cations in the dry $BaZr_{1-x}Y_xO_{3-\delta}$ structure.			
x	B site		A site
	□-Y-O_5	Y-O_6	Y-O_{12}
0.10	-	0.54(2)	0.46(3)
0.30	0.30(2)	0.70(2)	-
0.50	-	0.66(1)	0.34(2)

D. ^{91}Zr NMR

The $Zr(OZr)_6$ octahedral unit in $BaZrO_3$ is characterized by a very sharp resonance at 317 ppm confirming the cubic symmetry of the pure material (*Figure 3.10*). Upon yttrium substitution, the local distortion around zirconium is clearly observed by the increasing broadening of the sharp resonance at 317 ppm. For $BaZr_{0.90}Y_{0.10}O_{2.95-\delta}$ and $BaZr_{0.70}Y_{0.30}O_{2.85-\delta}$ the broadening is still fairly reasonable leaving the structure symmetric. In $BaZr_{0.50}Y_{0.50}O_{2.75-\delta}$ the extent of the broadening is a lot more significant, reflecting the larger amount of structural distortions in this material. The samples were not packed in a glovebox for these experiments; therefore it is possible that the samples were not fully dry since the powders pick up water readily. Even if the structures still contain some 5-coordinated Zr cations, it is possible that this site could be too broad to be detected.

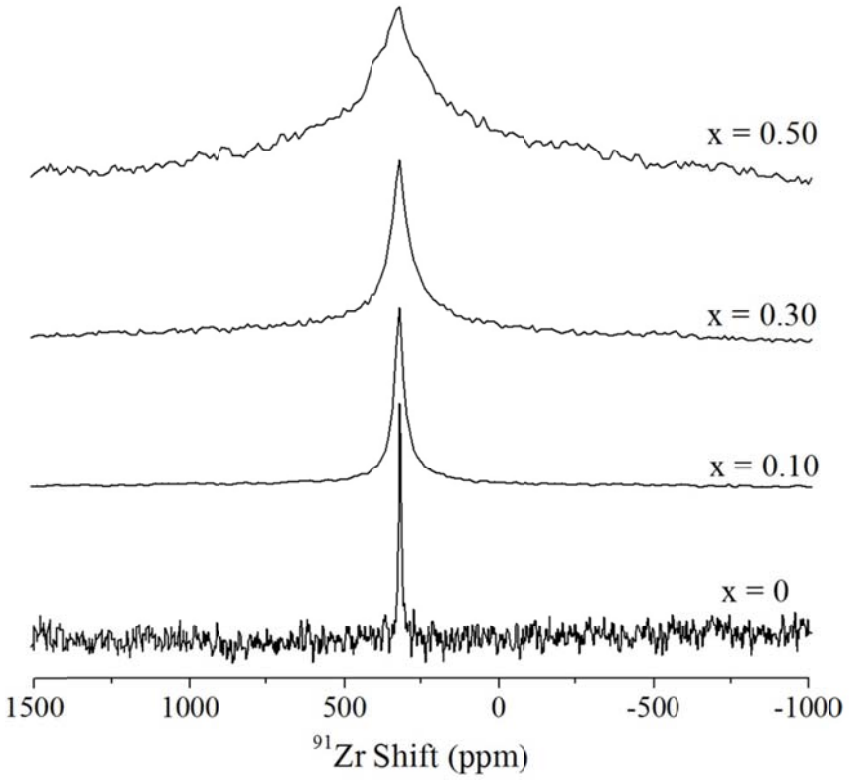

Figure 3.10 Static ^{91}Zr NMR of dry $BaZr_{1-x}Y_xO_{3-x/2}$. Number of transients recorded for x = 0, 0.10, 0.30 and 0.50 are 128, 93173, 350196 and 753809 respectively.

IV. Discussion

The sintering process of $BaZr_{1-x}Y_xO_{3-\delta}$ has a critical influence on the substitution of yttrium in the structure. Depending on the amount of BaO loss resulting from sintering the materials at high temperature (above 1250°C), yttrium will readily occupy the A site of the perovskite, in addition to occupying the B site, strongly affecting the number of oxygen vacancies available in the samples; all substitution levels are subject to this phenomenon. The ionic radius of Y^{3+} (0.90 Å) lies in between the ionic radii of Zr^{4+} (0.70 Å) and Ba^{2+} (1.35 Å),[19] leading to two possible substitution scenarios : yttrium is small enough to replace Zr^{4+} but also big enough to substitute for Ba^{2+} without bringing major overall structural distortions. While it is possible to predict a double site substitution from the XRD patterns, the observation in the ^{89}Y NMR spectra of yttrium resonances with coordination number higher than 6 for some of the samples constitutes a direct proof. The absence of Y-O-Y environments as seen by ^{17}O NMR

spectroscopy indicates the instability of such oxygen environments. The presence of Y-O-Y sites is also prevented by A site substitution of yttrium for barium. Unfortunately the A site substitution significantly decreases the concentration of oxygen vacancies in the materials; it then becomes difficult to incorporate protonic defects in the structure. Care has to be taken in the preparation of those materials in order to ensure the highest possible protonic conduction; the absence of oxygen vacancies limits the concentration of protons, *i.e.,* of charge carriers.

V. Conclusions

XRD and ^{89}Y NMR showed the presence of A site substitution of yttrium, compensating for the BaO loss occurring during sintering. 5-coordinated yttrium will only be present if all the yttrium cations are available on the B site. We did not observed particular arrangements of oxygen vacancies and yttrium cations in the sample free of A site substitution. Additionally Y-O-Y environments were not seen, indicating the random distribution of yttrium in the structure.

VI. References

1. H. Iwahara, T. Yajima, T. Hibino, K. Ozaki and H. Suzuki, *Solid State Ionics*, 1993, **61**, 65.

2. R. C. T. Slade, S. D. Flint and N. Singh, *Solid State Ionics*, 1995, **82**, 135.

3. K. D. Kreuer, *Solid State Ionics*, 1997, **97**, 1.

4. K. D. Kreuer, *Solid State Ionics*, 1999, **125**, 285.

5. H. G. Bohn and T. Schober, *Journal of the American Ceramic Society*, 2000, **83**, 768.

6. K. D. Kreuer, S. Adams, W. Münch, A. Fuchs, U. Klock and J. Maier, *Solid State Ionics*, 2001, **145**, 295.

7. K. D. Kreuer, *Annual Review of Materials Research*, 2003, **33**, 333.

8. F. M. M. Snijkers, A. Buekenhoudt, J. Cooymans and J. J. Luyten, *Scripta Materialia*, 2004, **50**, 655.

9. F. Iguchi, N. Sata, T. Tsurui and H. Yugami, *Solid State Ionics*, 2007, **178**, 691.

10. S. B. C. Duval, P. Holtappels, U. F. Vogt, E. Pomjakushina, K. Conder, U. Stimming and T. Graule, *Solid State Ionics*, 2007, **178**, 1437.

11. S. Tao and J. T. S. Irvine, *Journal of Solid State Chemistry*, 2007, **180**, 3493.

12. Y. Yamazaki, R. Hernandez-Sanchez and S. M. Haile, *Chemistry of Materials*, 2009, **21**, 2755.

13. Y. Yamazaki, R. Hernandez-Sanchez and S. M. Haile, *Journal of Materials Chemistry,* 2010, **20**, 8158.

14. P. Babilo and S. M. Haile, *Journal of the American Ceramic Society*, 2005, **88**, 2362.

15. J.-P. Amoureux, C. Fernandez and S. Steuernagel, *Journal of Magnetic Resonance, Series A*, 1996, **123**, 116.

16. A. Bielecki and D. P. Burum, *Journal of Magnetic Resonance, Series A*, 1995, **116**, 215.

17. J. B. Grutzner, K. W. Stewart, R. E. Wasylishen, M. D. Lumsden, C. Dybowski and P. A. Beckmann, *Journal of the American Chemical Society*, 2001, **123**, 7094.

18. G.-J. M. P. van Moorsel, E. R. H. Van Eck and C. P. Grey, *Journal of Magnetic Resonance, Series A*, 1995, **113**, 159.

19. R. D. Shannon, *Acta Crystallographica, Section A Crystal Physics, Diffraction, Theoretical and General Crystallography*, 1976, **A32**, 751.

20. A. Magrez and T. Schober, *Solid State Ionics*, 2004, **175**, 585.

21. Y. Yamazaki, C.-K. Yang and S. M. Haile, *Scripta Materialia*, 2011, **65**, 102.

22. T. Schober and H. G. Bohn, *Solid State Ionics*, 2000, **127**, 351.

23. Y. Yamazaki, P. Babilo and S. M. Haile, *Chemistry of Materials*, 2008, **20**, 6352.

24. E. Fabbri, D. Pergolesi, S. Licoccia and E. Traversa, *Solid State Ionics*, 2010, **181**, 1043.

25. P. Babilo, T. Uda and S. M. Haile, *Journal of Materials Research*, 2007, **22**, 1322.

26. R. B. Cervera, Y. Oyama, S. Miyoshi, K. Kobayashi, T. Yagi and S. Yamaguchi, *Solid State Ionics*, 2008, **179**, 236.

27. A. K. Azad, C. Savaniu, S. Tao, S. Duval, P. Holtappels, R. M. Ibberson and J. T. S. Irvine, *Journal of Materials Chemistry,* 2008, **18**, 3414.

28. F. Iguchi, T. Tsurui, N. Sata, Y. Nagao and H. Yugami, *Solid State Ionics*, 2009, **180**, 563.

29. T. Omata, M. Takagi and S. Otsuka-Yao-Matsuo, *Solid State Ionics*, 2004, **168**, 99.

30. S. Imashuku, T. Uda, Y. Nose, G. Taniguchi, Y. Ito and Y. Awakura, *Journal of the Electrochemical Society,* 2009, **156**, B1.

31. F. Iguchi, N. Sata and H. Yugami, *Journal of Materials Chemistry,* 2010, **20**, 6265.

32. T. J. Bastow, P. J. Dirken, M. E. Smith and H. J. Whitfield, *Journal of Physical Chemistry*, 1996, **100**, 18539.

33. M. H. Levitt, *Spin Dynamics: Basics of Nuclear Magnetic Resonance*, John Wiley & Sons, 2001.

34. M. M. Maricq and J. S. Waugh, *Journal of Chemical Physics*, 1979, **70**, 3300.

35. L. Holmes, L. Peng, I. Heinmaa, L. A. O'Dell, M. E. Smith, R.-N. Vannier and C. P. Grey, *Chemistry of Materials*, 2008, **20**, 3638.

36. S. E. Ashbrook, K. R. Whittle, G. R. Lumpkin and I. Farnan, *Journal of Physical Chemistry B,* 2006, **110**, 10358.

37. R. Dupree and M. E. Smith, *Chemical Physics Letters*, 1988, **148**, 41.

38. A. I. Becerro, A. Escudero, P. Florian, D. Massiot and M. D. Alba, *Journal of Solid State Chemistry*, 2004, **177**, 2783.

39. T. Harazono and T. Watanabe, *Bulletin of the Chemical Society of Japan,* 1997, **70**, 2383.

40. C. P. Grey, M. E. Smith, A. K. Cheetham, C. M. Dobson and R. Dupree, *Journal of the American Chemical Society*, 1990, **112**, 4670.

41. P. Florian, D. Massiot, G. Humbert and J.-P. Coutures, *Comptes Rendus de l'Académie des Sciences, Série IIb: Mécanique,Physique, Chimie, Astronomie,* 1995, **320**, 99.

42. K. Kawata, H. Maekawa, T. Nemoto and T. Yamamura, *Solid State Ionics*, 2006, **177**, 1687.

43. P. Jain, H. J. Avila-Paredes, C. Gapuz, S. Sen and S. Kim, *Journal of Physical Chemistry C*, 2009, **113**, 6553.

44. N. Kim and J. F. Stebbins, *Chemistry of Materials*, 2007, **19**, 5742.

45. S. W. Reader, M. R. Mitchell, K. E. Johnston, C. J. Pickard, K. R. Whittle and S. E. Ashbrook, *Journal of Physical Chemistry C*, 2009, **113**, 18874.

46. E. J. Harvey, S. E. Ashbrook, G. R. Lumpkin and S. A. T. Redfern, *Journal of Materials Chemistry,* 2006, **16**, 4665.

47. K. J. D. MacKenzie and M. E. Smith, *Multinuclear Solid-State Nuclear Magnetic Resonance of Inorganic Materials*, Pergamon Oxford, 2002.

Chapter 4:

Probing Cation and Vacancy Ordering in the Perovskite $BaSn_{1-x}Y_xO_{3-\delta}$ by NMR Spectroscopy: Implications for Proton Mobility

Hydrated $BaSn_{1-x}Y_xO_{3-x/2}$ is a protonic conductor that, and unlike many other related perovskites, shows high conductivity even at the highest substitution level of x = 0.50. (Kreuer, K. D. *Annu. Rev. Mater. Res.* **2003**, *33*, 333 and Murugaraj, P. *et al. Solid State Ionics* **1997**, *98*, 1) A structural investigation of $BaSn_{1-x}Y_xO_{3-x/2}$ ($0.10 \leq x \leq 0.50$) using multinuclear NMR spectroscopy has been performed to investigate cation ordering and the location of the oxygen vacancies in the dry material. The ^{119}Sn NMR spectra illustrate that Y substitution on the Sn (B) site is close to random up to x = 0.20. At higher substitution levels, clear evidence for the avoidance Y-O-Y linkages is seen, leading to strict Y-O-Sn alternation of the cations in the B site of the perovskite structure when x = 0.50. These results are confirmed by the absence of the Y-O-Y oxygen environment, as shown by ^{17}O NMR. Five coordinate Sn and Y sites are seen by ^{119}Sn and ^{89}Y NMR, respectively, which disappear on hydration. The concentration of 5 coordinated Sn sites is higher than the 5 coordinated Y sites, even when x = 0.50. This is ascribed to the presence of residual Sn-O-Sn defects in the cation-ordered material, which can accommodate oxygen vacancies. Very high temperature ^{119}Sn NMR (up to 700 ºC) reveals that the oxygen ions are mobile above 400 ºC, oxygen mobility being required in order to hydrate these materials. The high protonic mobility in these systems is ascribed to the Y-O-Sn cation ordering in the high Y-content materials, the predominance of single oxygen site preventing proton trapping on more basic sites such as those nearby two Y atoms.

I. Introduction

One approach to lowering the operation temperature of a solid oxide fuel cell (SOFC) involves the use of ceramic electrolytes that rely on protonic conduction to transfer charges between electrodes. To date, the most stable materials include perovskite based protonic conductors such as $BaZr_{1-x}M_xO_{3-\delta}$, $BaCe_{1-x}M_xO_{3-\delta}$, $SrCe_{1-x}M_xO_{3-\delta}$ where M is a large trivalent ion.[1] Generally, the best conductivity values are obtained for low M^{3+} substitution levels, usually between 5 and 20%. The case of $BaSn_{0.50}Y_{0.50}O_{2.75}$ is more unusual as very high conductivities have been obtained for an exceptionally high substitution level of 50%.[1-2] $BaSn_{0.50}Y_{0.50}O_{2.75}$ has been much less studied as a protonic conductor, although it reaches conductivity values comparable to $BaZr_{1-x}Y_xO_{3-\delta}$[1-2] and shows good stability under CO_2 and H_2O atmospheres. In all of these potential protonic conductors, substituting the +4 cation by M^{3+} creates oxygen vacancies in the structure, of up to 8% (of all O sites) in the case of $BaSn_{0.50}Y_{0.50}O_{2.75}$. Incorporation of protons occurs by reaction of the oxygen vacancies with water molecules leading to the formation of hydroxyl groups.

The unsubstituted member, $BaSnO_3$, crystallizes in a cubic perovskite (ABO_3) structure with space group *Pm-3m*.[3] Yttrium can substitute for tin on the B site, the end-member $BaSn_{0.50}Y_{0.50}O_{2.75}$ again adopting a cubic perovskite structure (*Figure 4.1a*). Additional weak reflections were, however, observed in the X-ray diffraction patterns reported in some studies; these have been ascribed to Y^{3+} and Sn^{4+} ordering on the B site, forming a $A_2BB'O_6$ superstructure (a double perovskite) involving a doubling of the ABO_3 unit cell.[2, 4-6] The local structures found in these materials remain unclear since the intensities of the superlattice reflections are noticeably weaker than predicted for the fully ordered structure indicating only partial ordering. Furthermore, no structural studies have been reported on materials with intermediate yttrium contents. On hydration, the oxygen vacancies formed as a result of the yttrium substitution are filled by hydroxyl groups, but the underlying cation sublattice presumably remains unchanged (*Figure 4.1a*).

In this study, we investigate the local structure of $BaSn_{1-x}Y_xO_{3-x/2}$ in order to understand why high conductivities are seen at high substitution levels. NMR spectroscopy is an ideal technique with which to investigate local structure in this material, since it is sensitive to local

environments, coordination numbers and site symmetry. Additionally, the local environments surrounding the different atoms can be probed individually by acquiring NMR spectra of the different NMR active nuclei present in the solid, *i.e.* ^{119}Sn, ^{17}O and ^{89}Y, for $BaSn_{1-x}Y_xO_{3-x/2}$. ^{119}Sn is a (8.6% abundant) spin I = ½ nucleus and is used to identify the distribution of yttrium in the materials as the ^{119}Sn nucleus is very sensitive to the nature of the nearby cations.[7-8] Furthermore, the location of oxygen vacancies nearby Sn should also be readily observed, as the presence of a vacancy reduces the coordination number of Sn, resulting in a change of chemical shift.[7] The spectra of both the dry and hydrated samples are acquired in this work to assign the resonances and to help determine the location of the oxygen vacancies. ^{17}O (spin I = 5/2, 0.037% natural abundance) NMR is then used to confirm the cation ordering observed by ^{119}Sn NMR, as its shift is sensitive to the chemical nature of the surrounding cations. ^{89}Y (spin I = ½, 100% natural abundance) NMR spectra are acquired to determine whether any substitution on the A site occurs; this is particularly important because substitution on this site will decrease the concentration of vacancies. For example, equal substitution on the A and B sites, represented by the formula $(Ba_{1-y}Y_y)_A(Sn_{1-y}Y_y)_BO_3$ results in a stoichiometric oxygen sub-lattice. Finally, very high temperature ^{119}Sn MAS NMR spectra are used to explore the mobility of the vacancies in the lattice, mobility of the vacancies being required for water incorporation in the solid.

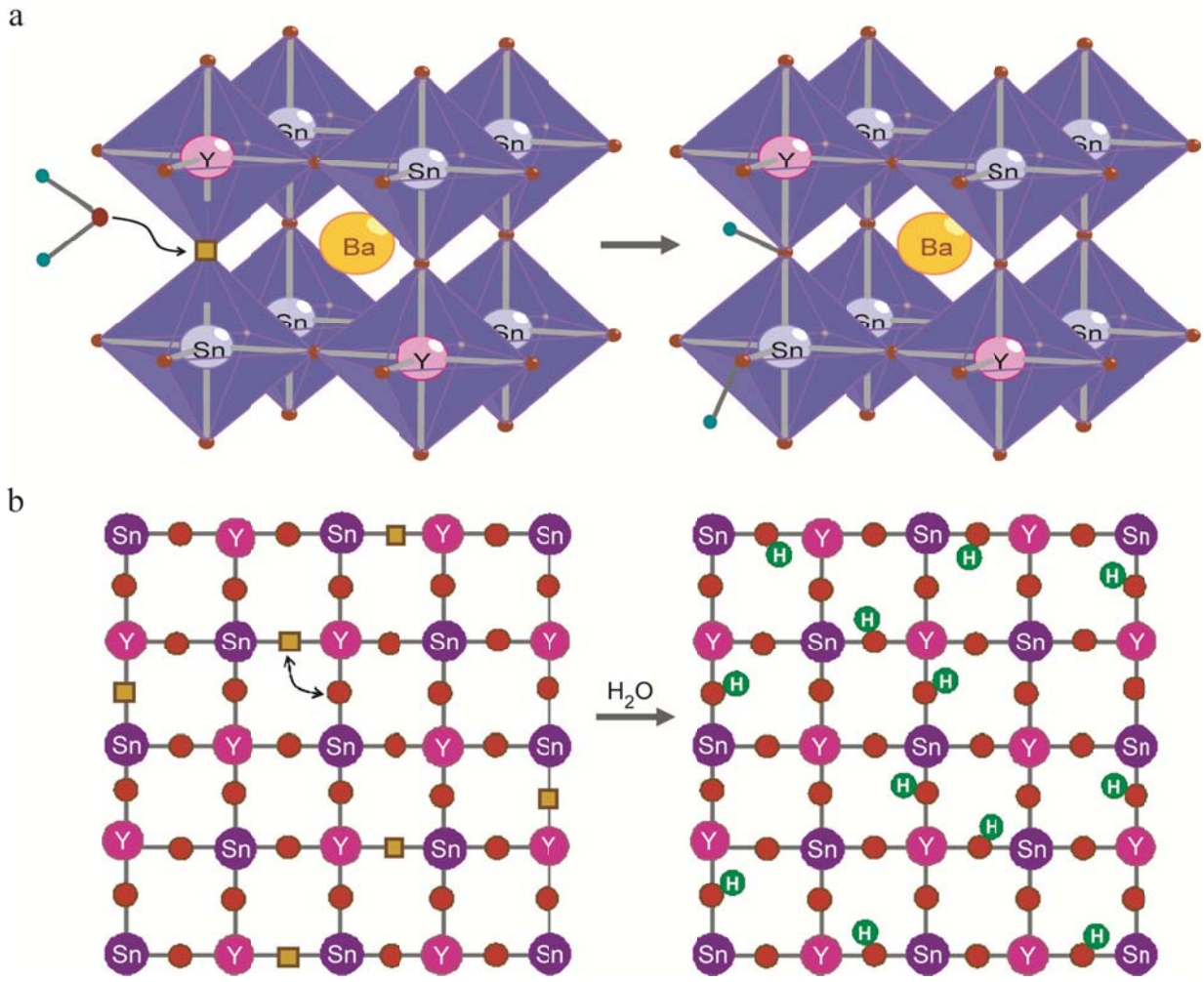

Figure 4.1. Structure of $BaSn_{1-x}Y_xO_{3-x/2}$. (a) Schematic representation of the hydration process by reaction of a molecule of water with an oxygen site from the lattice and an oxygen vacancy leading to the formation of two hydroxyl groups, *i.e.*, protonic defects. (b) Proposed structure for dry and hydrated $BaSn_{0.50}Y_{0.50}O_{2.75}$ with complete ordering of the B site cations. Barium atoms have been omitted for clarity. Yellow, blue, purple, red and green spheres represent Ba, Sn, Y, O and H atoms, respectively; yellow squares represent the oxygen vacancies. The double arrow indicates the oxygen migration from a 6 to a 5 coordinate Sn cation at high temperature, leading to a Sn atom with an average coordination number of 5.5 on the timescale of the migration.

II. Experimental section

A. Sample Preparation

$BaSn_{1-x}Y_xO_{3-x/2}$ (x = 0.10, 0.20, 0.30, 0.40 and 0.50) samples were synthesized through a glycine-nitrate combustion route[9] using $Ba(NO_3)_2$ (Alfa Aesar, 99.999%), SnO_2 (Fisher Scientific, 99.40%), $Y(NO_3)_3$. 6 H_2O (Alfa Aesar, 99.9%) and glycine (Alfa Aesar, 99.7%) as starting materials. Stoichiometric ratios of the reactants were mixed in a small amount of deionized water with a nitrate to glycine ratio of 2:1. Mixtures were then dehydrated on a hot plate and auto-ignition followed. Powders were then ground and fired at 1200 °C for 10 h, pressed into pellets, buried in $BaZrO_3$ powder to prevent barium evaporation and sintered at 1600 °C for another 10 h. Hydration of the powders was carried out in a tube furnace. The powders were first dried at 1000 °C for 2 h and then cooled down by steps of 100 °C every 2 h until the temperature reached 200 °C with wet N_2 flowing over the samples at a rate of 60 $mL.min^{-1}$. The previous cycle was repeated once from 800 to 200 °C to increase the hydration level of the powders. ^{17}O enrichment was performed by heating the dried samples (1 h at 950 °C under vacuum) in 50% ^{17}O enriched $^{17}O_2$ gas (Isotec, 99%, used as received) for 2 days at 950 °C. The purity of the different compounds was checked by X-Ray diffraction (XRD) by using a Scintag diffractometer with CuKα radiation and by comparison to diffraction patterns in the JCPDS (Joint Committee on Powder Diffraction Standards) database. Levels of hydration were obtained by thermogravimetric (TGA) analysis using a Q500 TA instrument under dry N_2 atmosphere.

B. ^{119}Sn NMR spectroscopy

^{119}Sn NMR experiments were acquired at 11.7 T on a wide bore Oxford 500 MHz Varian Infinity Plus spectrometer using a 3.2 mm HX Chemagnetics probehead tuned to 186.26 MHz. The samples were dried, prior to the experiments, at 950°C overnight and then packed under an N_2 atmosphere in 3.2 mm zirconia rotors which were then spun at a spinning frequency ω_r of 20 kHz. ^{119}Sn single pulse experiments were carried out using a $\pi/2$ pulse width of 2 μs (*i.e.* at an rf field amplitude of ω_1^{Sn} = 125 kHz) and recycle delays of 70 s allowing full relaxation of the ^{119}Sn spins for the dry samples. Similar experimental conditions were used for the hydrated samples *albeit* with a shorter recycle delay of 30 s. High temperature ^{119}Sn MAS NMR

experiments of $BaSn_{0.50}Y_{0.50}O_{2.75}$ were performed on a 8.45 T wide bore Varian Oxford Infinity Plus 360 MHz spectrometer equipped with a 7 mm HX high temperature MAS probe from Doty Scientific, Inc tuned to 134.18 MHz. The sample was packed in a boron nitride BN insert which was then placed in a 7 mm silicon nitride Si_3N_4 rotor. Spinning was performed under nitrogen at 4 kHz at room temperature and at 6 kHz above 200 °C. Temperature calibration of the probe was carefully performed by using the ^{207}Pb resonance of $Pb(NO_3)_3$[10-11] below 400 °C and ^{119}Sn resonance of $Pr_2Sn_2O_7$[12] above 400 °C. The temperatures given in the text are actual sample temperatures and are given with an accuracy of ± 4 °C. One-pulse spectra were recorded with a $\pi/2$ pulse width of 5 μs at ω_1^{Sn} = 50 kHz and a recycle delay of 3 s was used. Chemical shifts were externally referenced to SnO_2 at -604.3 ppm.

C. ^{17}O NMR spectroscopy

^{17}O NMR experiments were carried out on a 14.1 T wide bore Bruker Avance 600 MHz spectrometer equipped with a 4 mm HX probehead operating at 81.36 MHz. All samples were packed inside 4 mm MAS zirconia rotors and spun at a spinning frequency ω_r of 15 kHz. ^{17}O one-dimensional spectra were recorded by using rotor synchronized Hahn echo experiments with an evolution period τ_r of one rotor period to avoid probe ringing. Small $\pi/6$ pulses were used corresponding to an rf field amplitude of ω_1^O = 100 kHz. Two-dimensional triple-quantum MAS NMR experiments were performed using the *z-filtered* pulse sequence.[13] Hard and soft pulses were applied at ω_1^O = 100 kHz and approximately 15 kHz, respectively. The multiple-quantum transfer was optimized on every sample to increase the excitation sensitivity of the MQ coherences. The t_1 increment was rotor synchronized to one rotor period ω_r of 15 kHz, *i.e.* 66.67 μs. The recycle delay was set to 5 s for all the experiments. The chemical shift was externally referenced to water at 0.0 ppm The signal observed at approximately 380 ppm corresponds to either ^{17}O enrichment of the ZrO_2 rotor or some remaining $BaZrO_3$ powder that was used during sintering.

D. ^{89}Y NMR Spectroscopy

^{89}Y NMR experiments for the dry samples were performed at 11.7 T on a wide bore Oxford 500 MHz Varian Infinity Plus spectrometer equipped with a 7 mm HX Chemagnetics

probehead tuned to 24.50 MHz. The samples were prepared as described above, and were packed in 7 mm silicon nitride Si_3N_4 rotors and spun at a spinning frequency of 4 kHz. ^{89}Y single pulse experiments were carried out using a $\pi/6$ pulse width of 4 μs at an r.f. field amplitude of ω_1^Y = 20 kHz and recycle delays of 250 s. High field ^{89}Y NMR experiments on the hydrated materials were performed at 19.6 T on a ultra narrow bore Bruker DRX 830 MHz spectrometer at the National High Magnetic Field Laboratory, Tallahassee, Florida, USA using a 7 mm single channel probe tuned to 40.84 MHz. All samples were packed inside 7 mm ZrO_2 rotors and spun at a spinning frequency ω_r of 8 kHz. The chemical shift was externally referenced to the most intense resonance of solid Y_2O_3 at 330 ppm.

E. NMR analyses

MatLab and MatNMR[14] were used to process the data and perform the deconvolutions. ^{119}Sn deconvolutions were accomplished with fixed chemical shifts across the whole series for the different peaks after a first refinement. Simulations were performed using SIMPSON[15] and standard numerical techniques.[16]

III. Results

A. XRD

In order to understand cation and vacancy ordering, we have studied both dry and hydrated solid solutions of $BaSn_{1-x}Y_xO_{3-x/2}$ with x values ranging from 0.10 to 0.50. *Figure 4.2* shows the diffraction pattern for nominally dry $BaSn_{1-x}Y_xO_{3-x/2}$ ($0.10 \leq x \leq 0.50$). For the whole range of compositions, the powders adopt a cubic perovskite structure, space group *Pm3m*, the cell parameter increasing with the yttrium substitution level. No yttria Y_2O_3 impurity, the most common impurity for this system, was detected for these samples. Additionally, no extra reflections are observed at low angles due to long range cation ordering, which, if present, should give rise to a superstructure appropriate to a doubling of the perovskite unit cell, and a space group *Fm3m*.[17] The x = 0.1 phase contains a small fraction of the unsubstituted $BaSnO_3$ phase present as an impurity (as indicated by arrows).

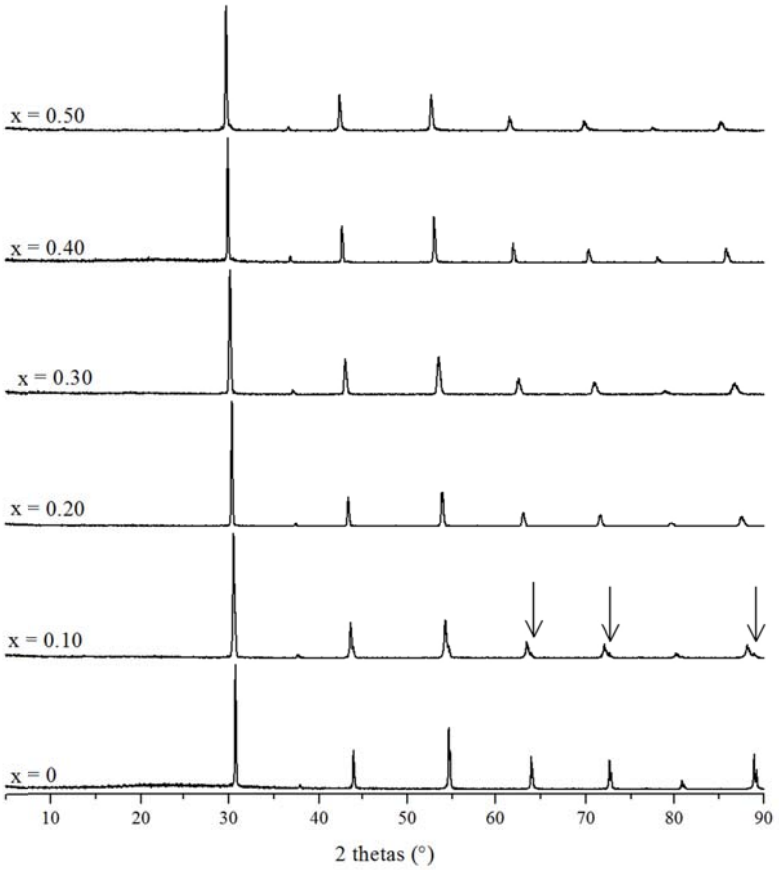

Figure 4.2. Powder X-ray diffraction patterns of $BaSn_{1-x}Y_xO_{3-x/2}$ for $0 \leq x \leq 0.50$. Shoulders (peaks) due to the Cu $K\alpha_2$ radiation are visible at high angles. Arrows indicate small fraction of unsubstituted $BaSnO_3$.

B. TGA

Figure 4.3 shows the thermogravimetric analysis (TGA) of the hydrated samples, $BaSn_{1-x}Y_xO_{3-x/2-y}(OH)_{2y}$ (where $2y \leq x$), from which the hydroxyl content associated with water loss can be readily extracted. The concentration of protonic defects increases in the hydrated samples along with the yttrium substitution as expected. All samples show a hydration level close to maximum, *i.e.* two hydroxyl groups for one oxygen vacancy ($2y \leq x$), except for $BaSn_{0.60}Y_{0.40}O_{2.80}$ where a lower hydration content could only be achieved. We have repeated the hydration process a number of times for this sample, and the total update was always noticeably lower than the theoretical maximum value. The small weight loss seen below 200 ºC for the x = 0.1 and 0.5 samples is ascribed to the loss of surface water.

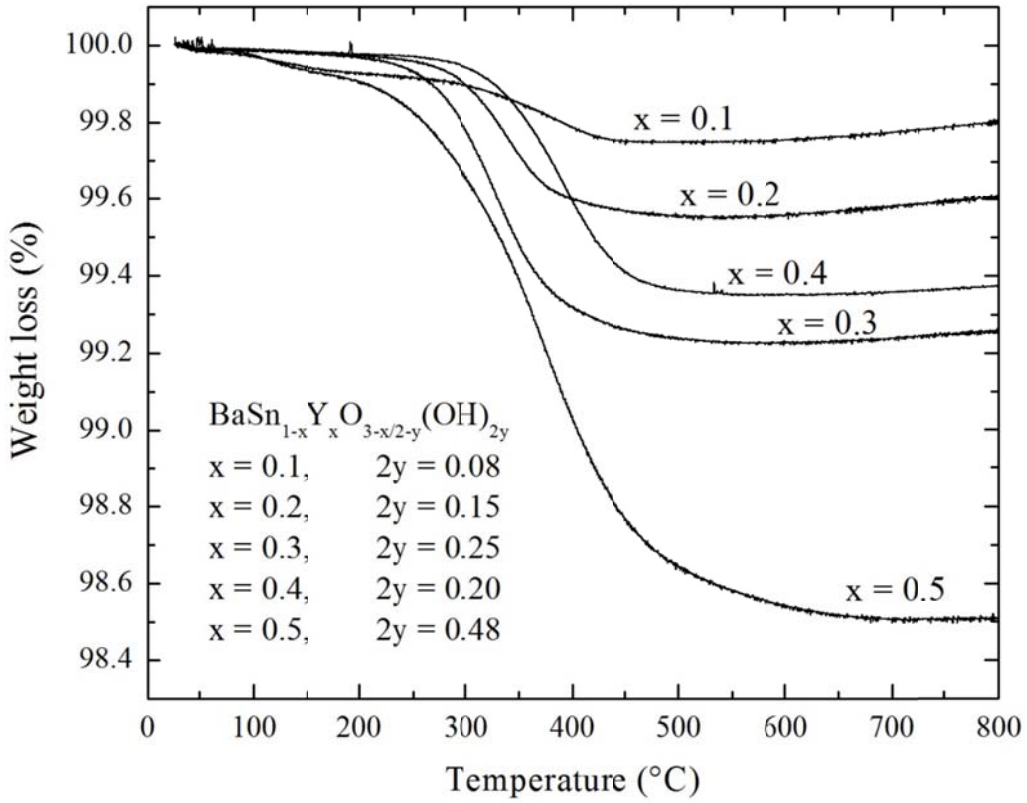

Figure 4.3. TGA of $BaSn_{1-x}Y_xO_{3-x/2-y}(OH)_{2y}$ ($2y \leq x$) for $0.10 \leq x \leq 0.50$. The protonic defect concentrations were calculated from the mass of water lost from room temperature to 800°C.

C. ^{119}Sn NMR

The ^{119}Sn magic angle spinning (MAS) NMR spectrum of unsubstituted $BaSnO_3$ (*Figure 4.4a*) contains a single, sharp resonance at -679 ppm from tin in an octahedral environment. This environment is surrounded by 6 tin atoms in its 1st B-site cation coordination shell,[7] giving rise to a $Sn(OSn)_6$ local environment, where the nearby A (Ba^{2+}) cations have been omitted for simplicity. Two very different chemical shift regions are seen in the spectra of the dry yttrium substituted materials (*Figure 4.4a*). The first region, between -550 and -700 ppm, contains a series of resonances, whose number and intensities depend strongly on the yttrium substitution level. In this region in addition to the resonance due to $Sn(OSn)_6$, two other resonances at -645 and -618 ppm are seen for $BaSn_{0.90}Y_{0.10}O_{2.95}$ and $BaSn_{0.80}Y_{0.20}O_{2.90}$ that can be assigned to tin octahedra containing respectively 1 and 2 yttrium atoms in the 1st cation coordination shell, *i.e.*, $Sn(OSn)_5(OY)_1$ and $Sn(OSn)_4(OY)_2$, the substitution of one yttrium ion in the tin local

coordination shell causing a shift of approximately 30 ppm. Further resonances from environments with higher numbers of nearby yttrium ions are observed at higher frequencies as the yttrium substitution increases ($x \geq 0.30$), but it becomes more difficult to assign specific local environments to these additional resonances as they increasingly overlap, the shift observed per yttrium substitution becoming smaller. The tin local environments are radically different in $BaSn_{0.60}Y_{0.40}O_{2.80}$, as compared to the lower substituted compounds, and segregate into environments rich in yttrium (resonance at around -570 ppm) and environments poor in yttrium (resonance at around -645 ppm) : phase separation is occurring in this sample which contains a low substituted phase ($x < 0.30$) and a partially ordered phase ($x > 0.40$). At an yttrium substitution level of 50%, *i.e.* for the composition of the reported protonic conductor $BaSn_{0.50}Y_{0.50}O_{2.75}$, only one broad resonance at -564 ppm is seen in this first region, indicating that one local environment, tentatively assigned to $Sn(OY)_6$, dominates. The second region, which becomes clearly visible at higher substitution levels ($x \geq 0.20$), contains only one broad resonance at -423 ppm. Prior ^{119}Sn NMR studies of M_2SnO_3 (M = Li, Na or K) by Clayden *et al.*[7] showed that the change from 6 to 5 coordinate tin sites in this class of compounds resulted in a shift of 140 ppm to higher frequencies (*i.e.* less negative). This observation is general, a shift to higher frequencies on decreasing the coordination number being well established for ^{27}Al, ^{25}Mg and ^{71}Ga, for example.[18] On this basis we assign the resonance in the 2nd region to the 5 coordinate Sn environments that are associated with the oxygen vacancies, *i.e.* $Sn(OX)_5(\square X)$ where $\square$ is the oxygen vacancy and X = Sn or Y.

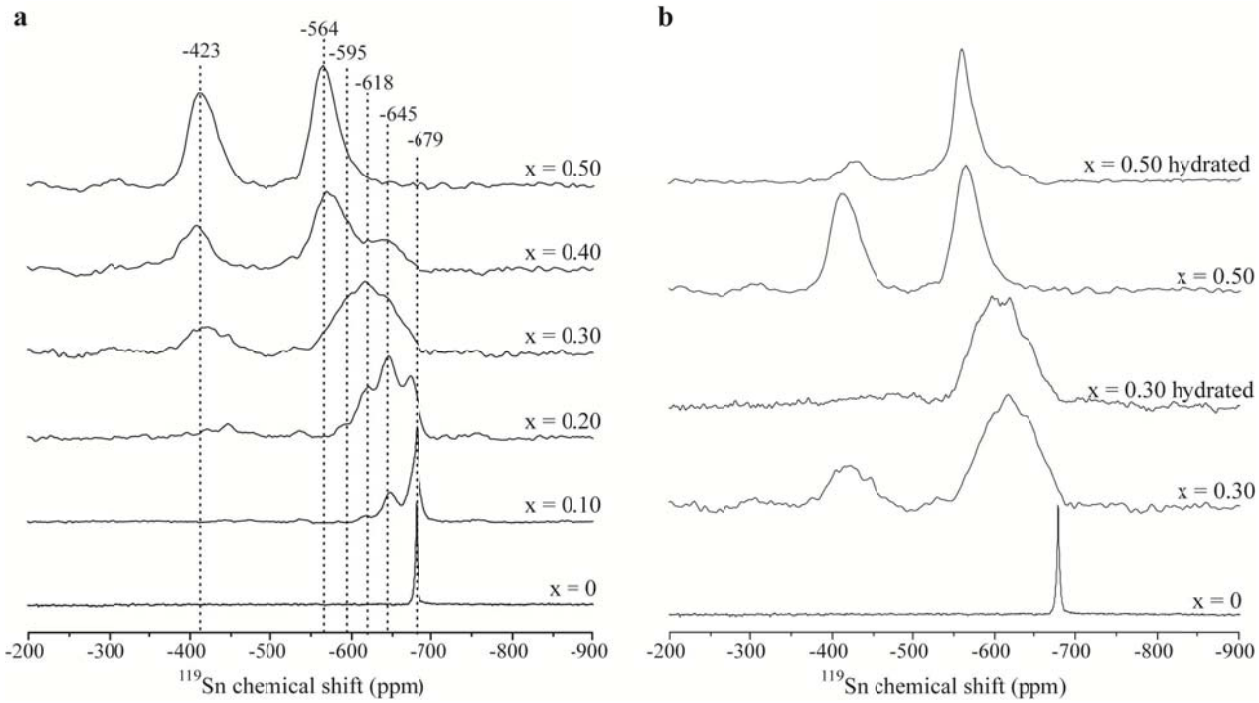

Figure 4.4. ^{119}Sn MAS NMR single pulse spectra of $BaSn_{1-x}Y_xO_{3-\delta}$ samples. (a) Dry $BaSn_{1-x}Y_xO_{3-x/2}$. (b) Comparison between dry and hydrated samples for $BaSn_{0.30}Y_{0.70}O_{2.85}$ and $BaSn_{0.50}Y_{0.50}O_{2.75}$. The major resonances have been labelled with their isotropic chemical shifts.

In order to confirm the assignment of these resonances, we compared the spectra of the dry and hydrated samples (*Figure 4.4b*). On hydration, the resonance at -423 ppm disappears for $BaSn_{0.70}Y_{0.30}O_{2.85}$ while it is greatly reduced in the case of $BaSn_{0.50}Y_{0.50}O_{2.75}$, consistent with its assignment to a 5 coordinate tin site, $Sn(OX)_5(\square X)$, the tin atom being nearby an oxygen vacancy. During the hydration process, the oxygen vacancies are filled by hydroxyl groups or oxide ions (*Figure 4.1b*), reducing the proportion of 5 coordinate tin cations present in the structure in favor of the 6 coordinate tin sites. The residual resonance at -423 ppm in the hydrated $BaSn_{0.50}Y_{0.50}O_{2.75}$ is due to incomplete hydration of the material in agreement with TGA data (*Figure 4.3*). The remaining signal from the 5 coordinated Sn is more pronounced for $BaSn_{0.50}Y_{0.50}O_{2.75}$ than for $BaSn_{0.70}Y_{0.30}O_{2.85}$, even though almost complete hydration is nominally achieved as determined by TGA for the former, while 17% vacant sites remain for the latter. This suggests that some of the water in $BaSn_{0.50}Y_{0.50}O_{2.75}$ is present as surface water rather than occupying sites in the bulk of the sample; this water presumably gives rise to the loss of

water seen between room temperature and approximately 200 ºC in the TGA experiment (*Figure 4.3*).

The concentration of the different local environments expected for random substitution of yttrium and vacancies in the lattice can be readily calculated and compared with the experimental data[14-16] (*Figure 4.5 and Table 4.1*) to determine if there is any evidence for clustering. We focus on the six coordinate sites since many of the different environments are resolved. To overcome the difficulty of extracting intensities from overlapping resonances and to provide a simpler and more reliable analysis, the ratio of the $Sn(OSn)_6$ resonance is compared with the intensity of the z = 1, 2 and 3 $Sn(OSn)_{6-z}(OY)_z$ resonances and the sum of the z = 4, 5 and 6 resonances. For substitution levels below 30%, the concentration of tin local environments is close to the predicted values for a randomly substituted lattice (*Figures 4.5a-e*). In contrast, for substitution levels of 30% and above, there is a clear tendency to form more tin octahedral units with 4, 5 and 6 yttrium atoms nearby, *i.e.* $Sn(OSn)_2(OY)_4$, $Sn(OSn)_1(OY)_5$ and $Sn(OY)_6$, over that predicted for a randomly substituted lattice (*Figure 4.5e*). This provides clear evidence for cation clustering or ordering. The simplest ordering in this system consists of tin and yttrium atoms alternating on the B site of the lattice, as shown in *Figure 4.1b*, resulting in a single environment for tin, $Sn(OY)_6$, when the substitution level reaches 50%. This is consistent with the NMR spectrum of $BaSn_{0.50}Y_{0.50}O_{2.75}$, which is dominated by the $Sn(OY)_6$ resonance at -564 ppm, indicating that at least locally, the material is ordered. This ordering, if long-range, should give rise to superlattice reflections in the XRD pattern, indexable to the space group *Fm-3m*. Although our XRD measurements (*Figure 4.2*) did not show the presence of the additional reflections, they have been observed by previous workers, *albeit* with intensities that are significantly weaker than predicted for full ordering.[4-5, 17] For $BaSn_{0.60}Y_{0.40}O_{2.80}$, the $Sn(OY)_6$ resonance again dominates, but now a clear shoulder at more negative frequencies due to environments such as $Sn(OSn)(OY)_5$ is seen along with a broad resonance at lower frequencies due to environments such as $Sn(OSn)_{6-x}(OY)_x$ (x = 0 - 2). This suggests that this material comprises Sn-rich clusters within an overwhelmingly Y-Sn ordered network. The presence of the Sn-rich clusters, which will not contain many vacancies, may represent one reason why this material is difficult to fully hydrate: domains or regions containing few vacancies (and thus

poorer oxygen transport) preventing or blocking diffusion of the water into all parts of the sample.

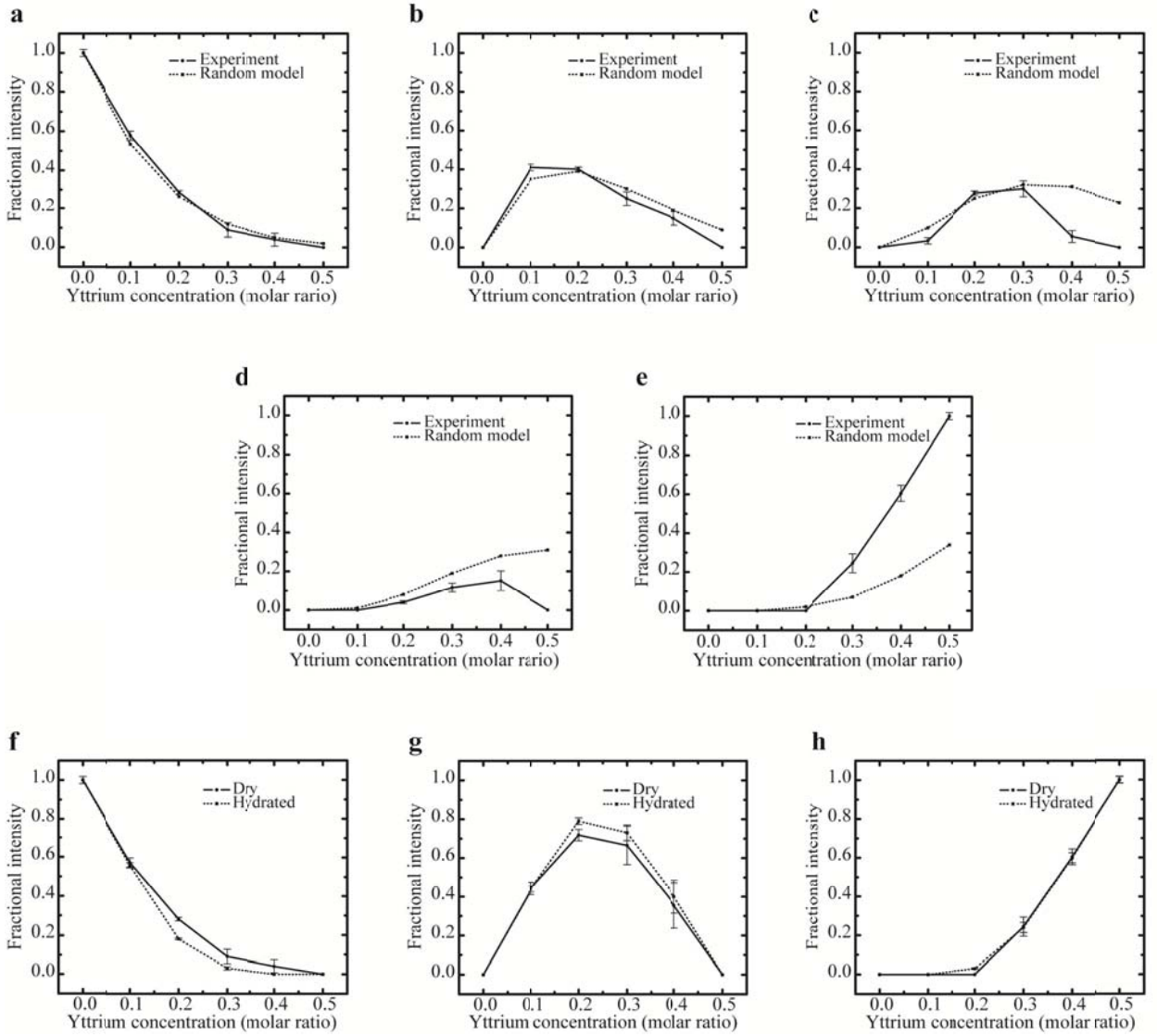

Figure 4.5. A comparison between the experimental intensity ratios of the different $Sn(OSn)_{6-z}(OY)_z$ local environments and those calculated by assuming a random distribution of Y on the Sn sublattice, as a function of Y content. Dry samples: (a) $Sn(OSn)_6$, (b) $Sn(OSn)_5(OY)_1$, (c) $Sn(OSn)_4(OY)_2$, (d) $Sn(OSn)_3(OY)_3$, (e) $Sn(OSn)_2(OY)_4$, $Sn(OSn)_1(OY)_5$ and $Sn(OY)_6$ tin environments. Comparison between the dry and hydrated samples: (f) $Sn(OSn)_6$, (g) $Sn(OSn)_5(OY)_1$, $Sn(OSn)_4(OY)_2$, $Sn(OSn)_3(OY)_3$, (h) $Sn(OSn)_2(OY)_4$, $Sn(OSn)_1(OY)_5$ and $Sn(OY)_6$ tin environments.

Table 4.1. Ratios and isotropic chemical shifts of the different six coordinate Sn environments in the dry samples obtained from deconvolution of the experimental spectra.

$Sn(OSn)_{6-x}(OY)_x$	x						δ_{iso} (ppm)
	0	0.10	0.20	0.30	0.40	0.50	
0	1.00(2)	0.57(3)	0.28(1)	0.09(4)	0.04(3)		-674
1		0.41(2)	0.40(1)	0.25(4)	0.15(4)		-645
2		0.03(2)	0.28(1)	0.30(4)	0.05(3)		-618
3			0.04(1)	0.12(2)	0.15(5)		-595
				0.24(5)			-579
4/5/6[a]					0.61(4)		-571
						1.00(2)	-564

[a] Only one peak is used to deconvolute this region; however its shift gradually increases upon yttrium substitution due to a higher number of yttrium surrounding this particular tin environment.

Table 4.2. Ratios and isotropic chemical shifts of the different six coordinate Sn environments in the hydrated samples obtained from deconvolution of the experimental spectra.

$Sn(OSn)_{6-x}(OY)_x$	x						δ_{iso} (ppm)
	0	0.10	0.20	0.30	0.40	0.50	
0	1.00(2)	0.56(2)	0.18(1)	0.03(1)			-674
1		0.30(1)	0.31(1)	0.16(1)	0.07(2)		-647
2		0.14(1)	0.38(1)	0.28(2)	0.10(3)		-622
3			0.10(1)	0.29(1)	0.23(3)		-591
				0.16(2)			-579
4/5/6[a]			0.03(1)				-570
				0.08(1)	0.60(3)	1.00(2)	-563

[a] Only one peak is used to deconvolute this region; however its shift gradually increases upon yttrium substitution due to a higher number of yttrium surrounding this particular tin environment.

Analysis of the changes in intensity of the various six coordinate tin units after hydration (*Figure 4.5f-h*, *Tables 4.1 and 4.2*) suggests that the distribution has changed. For x = 0.20 to 0.40, the relative fraction of the $Sn(OSn)_6$ environment decreases slightly on hydration (*Figure 4.5f*), and is compensated by an increase in relative fraction of tin environments surrounded by 1, 2 or 3 yttrium atoms (*Figure 4.5g*). Since the new environments must originate from sites that were originally nearby a vacancy, these results suggest that the oxygen vacancies do not reside in the tin-rich region of these samples. (The total concentration of six-coordinate sites increases on hydration, and thus the relative intensity of the $Sn(OSn)_6$ site decreases since no new $Sn(OSn)_6$ sites are created on hydration.) In the case of $BaSn_{0.50}Y_{0.50}O_{2.75}$, we observe the presence of some $Sn(OSn)_{6-x}(OY)_x$ ($x > 0$) sites after hydration (*Figure 4.4b*) whose ratio is difficult to estimate by spectral deconvolution since it is in the level of spectral noise. This suggests that there are some residual Sn-O-Sn defects in the lattice which can accommodate oxygen vacancies (forming environments such as $Sn(OSn)_{5-x}(OY)_x(\square Sn)$) in the dry material. The presence of the defects may explain the lack of long range cationic ordering as seen by XRD in this sample. This suggestion will be further explored by ^{17}O and ^{89}Y NMR.

D. ^{17}O NMR

In order to confirm the local ordering proposed above, it is important to show that no clustering of the yttrium ions occurs, something that is more difficult to definitely rule out based on the ^{119}Sn NMR data alone. One straightforward approach is to use ^{17}O solid state NMR spectroscopy since this quadrupolar nucleus is very sensitive to the chemical nature of the nearby cations.[19-20] $BaSnO_3$ gives rise to a single resonance centered at 120 ppm with a distinctive second order quadrupolar lineshape (*Figure 4.6a*). Upon substitution of tin by yttrium, a second resonance appears, at 236 ppm for $BaSn_{0.90}Y_{0.10}O_{2.95}$, whose intensity is proportional to the yttrium content and is therefore assigned to oxygen in a Sn-O-Y linkage, Y substitution in the O local environment producing a large shift of 51 ppm. An additional sharp resonance is seen at 186 ppm for $BaSn_{0.70}Y_{0.30}O_{2.85}$, $BaSn_{0.60}Y_{0.40}O_{2.80}$ and $BaSn_{0.50}Y_{0.50}O_{2.75}$, which is tentatively assigned to water bound to the surface of the particles. The shift of the Sn-O-Sn environment gradually increases upon substitution as more yttrium substitutes for tin in the second cation coordination shell of oxygen. The change is more sudden for the Sn-O-Y environment where a

10 ppm shift is observed at a substitution level of 30% and above, *i.e.* at about the same point where the B site cation clustering/ordering is observed by ^{119}Sn NMR.

Two-dimensional (2D) multiple-quantum magic angle spinning (MQMAS) experiments,[13, 21-22] from which high resolution one dimensional spectra can be extracted, were recorded for each sample to ensure that no other resonances are hidden under the Y-O-Sn and Sn-O-Sn signals. The Y-O-Sn and Sn-O-Sn environments are clearly resolved for $BaSn_{0.90}Y_{0.10}O_{2.95}$ as illustrated in *Figure 4.6b*. Even in the highly yttrium substituted samples, no additional resonances at a frequency greater than 246 ppm, *i.e.* in the chemical shift region expected for a Y-O-Y environment, are observed (*Figure 4.7*). This corroborates the tendency for strict cation ordering at high substitution levels, and further suggests that yttrium substitutions above 50% on the B site of the perovskite structure will not be thermodynamically stable.

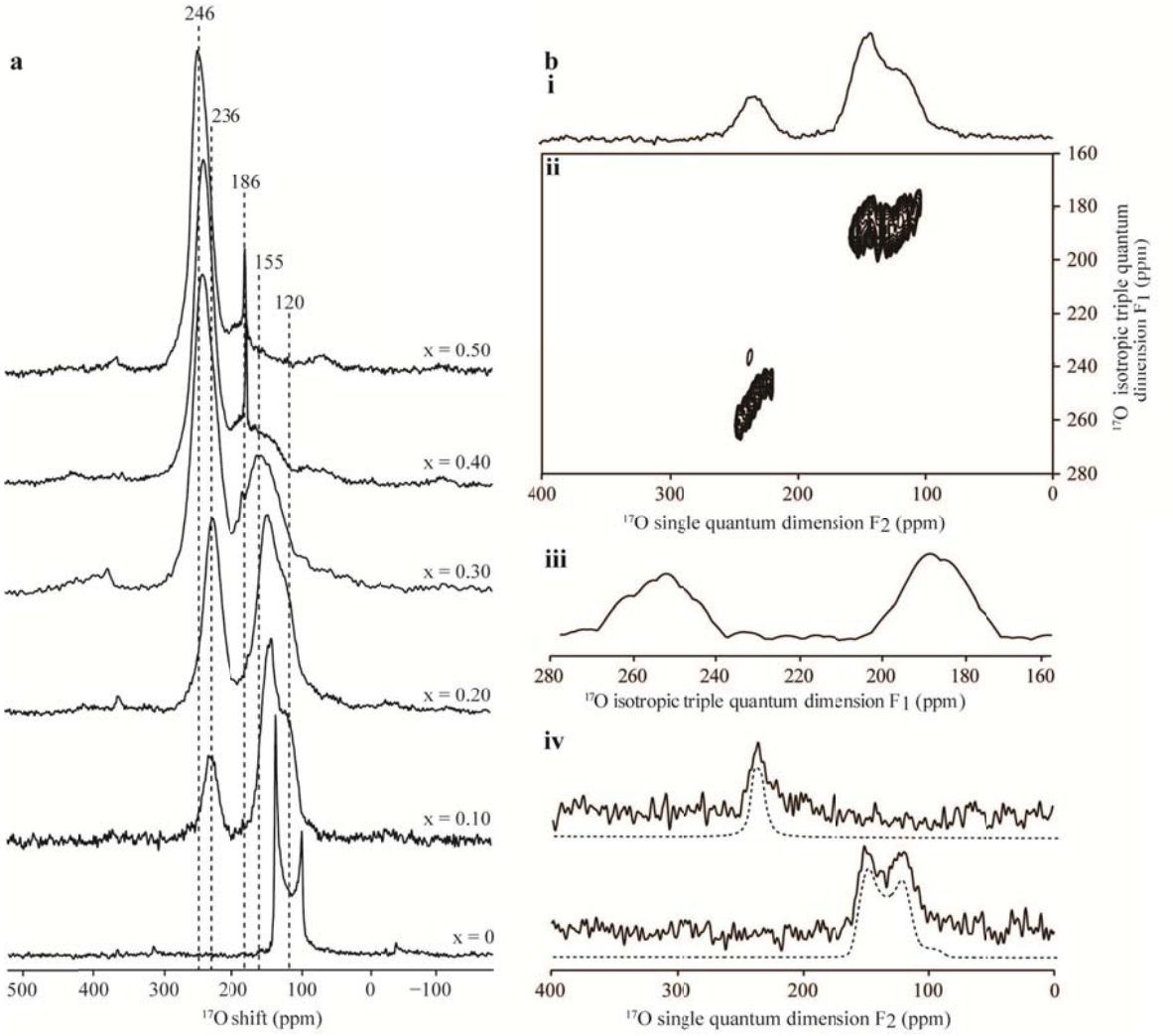

Figure 4.6. ^{17}O MAS NMR spectra of $BaSn_{1-x}Y_xO_{3-x/2}$. (a) Dry $BaSn_{1-x}Y_xO_{3-x/2}$, (b) Triple quantum MAS data of $BaSn_{0.90}Y_{0.10}O_{2.95}$. Peaks have been labeled with their center of gravity (or peak positions). (i) Hahn echo spectrum. (ii) Two-dimensional triple-quantum MAS spectrum. 1320 transients were accumulated for each of the 16 t_1 increments. (iii) Isotropic projection of the 2D MQMAS spectra. (iv) Cross sections (full lines) extracted parallel to F_2 of the 2D MQMAS at δ_1 values of 254 (top) and 187 (bottom) ppm for Sn-O-Y and Sn-O-Sn respectively along with the best fit simulations (dashed lines) using the following parameters: δ_{iso} = 247 p.p.m., C_Q = 3.8 MHz and η_Q = 0.02 (top) and δ_{iso} = 168 p.p.m., C_Q = 5.5 MHz and η_Q = 0.02 (bottom).

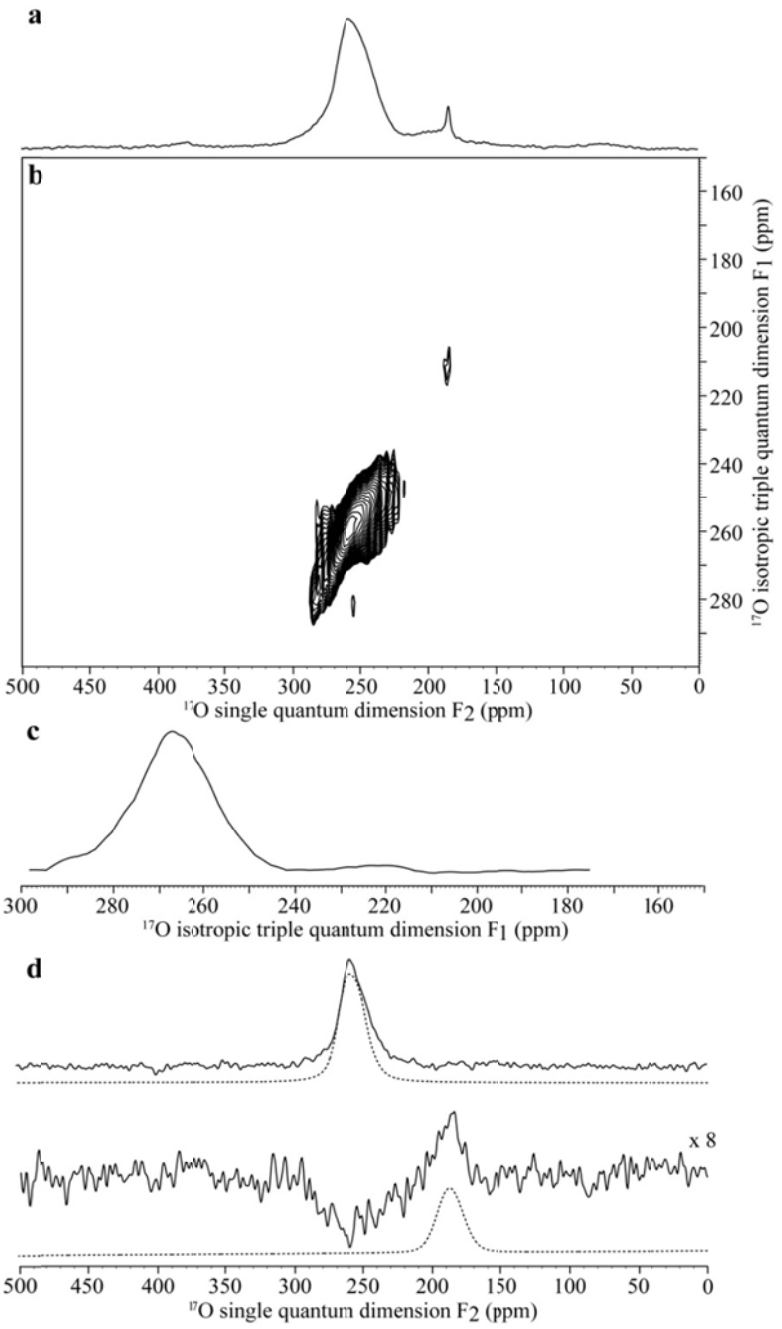

Figure 4.7. ^{17}O MAS NMR spectra of $BaSn_{0.50}Y_{0.50}O_{2.75}$. (a) Rotor synchronized Hahn echo spectrum. (b) Two-dimensional triple-quantum MAS spectrum. 876 transients were accumulated for each of the 32 t_1 increments. (c) Isotropic projection of the 2D MQMAS. (d) Cross sections (full lines) extracted parallel to F_2 of the 2D MQMAS at δ_1 of 262 (top) and 213 (bottom) ppm for Sn-O-Y and Sn-O-Sn respectively along with the best fit (dashed lines) using the following parameters: δ_{iso} = 261 p.p.m., C_Q = 3.4 MHz and η_Q = 0.15 (top) and δ_{iso} = 203 p.p.m., C_Q = 2.6 MHz and η_Q = 0.02 (bottom).

E. ^{89}Y NMR

Due to the long acquisition time required to perform ^{89}Y NMR particularly in systems with very long ^{89}Y T_1 relaxation time (around 250 s) and low Y substitution levels, we recorded the ^{89}Y NMR spectra of $BaSn_{1-x}Y_xO_{3-x/2}$ for only three substitution levels: x = 0.1, 0.3 and 0.5. In the dry compounds (*Figure 4.8a*), the main environment which ranges from 300 to 343 ppm is assigned to 6 coordinated Y environments in agreement with previously published results for other samples containing 6 coordinate Y environments.[18, 23-33] Its shift is presumably affected by the increasing number of yttrium atoms in the second (B-site) cation coordination shell with increasing yttrium substitution level, since, on the basis of the ^{17}O NMR, the first cation coordination shell is fully occupied by the tin atoms. In the case of $BaSn_{0.90}Y_{0.10}O_{2.95}$ the second cation coordination shell is mostly occupied by Sn atoms while for $BaSn_{0.70}Y_{0.30}O_{2.85}$ it is occupied by both Sn and Y, consistent with the broader lineshape of the 6 coordinated Y environments observed in $BaSn_{0.70}Y_{0.30}O_{2.85}$. The sharper lineshape observed for $BaSn_{0.50}Y_{0.50}O_{2.75}$ provides further support for the presence of yttrium and tin ordering in the structure, the ordering limiting the number of possible arrangements for Y and Sn in the second (B-) cation coordination shell surrounding the $Y(OSn)_6$ atoms. This second cation coordination shell is mostly occupied by yttrium in the case of $BaSn_{0.50}Y_{0.50}O_{2.75}$.

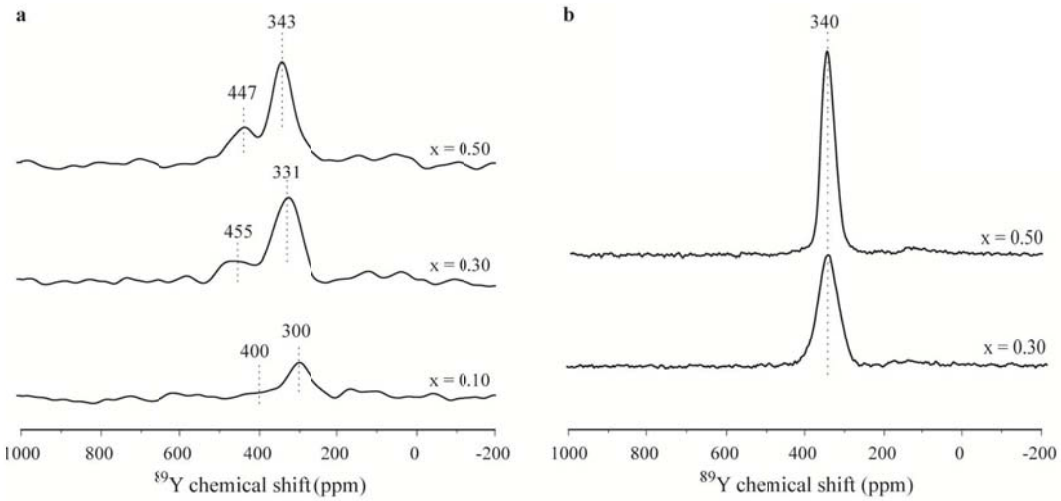

Figure 4.8. ^{89}Y MAS NMR spectra of $BaSn_{1-x}Y_xO_{3-x/2.}$ (a) dry materials acquired at 11.7 T and (b) hydrated materials acquired at 19.6 T.

A second resonance is clearly observed for $BaSn_{0.70}Y_{0.30}O_{2.85}$ and $BaSn_{0.50}Y_{0.50}O_{2.75}$ at higher field in the range of 455 – 447 ppm. To help assign this resonance, the ^{89}Y chemical shifts observed for a variety of different Y local environments have been plotted as a function of Y coordination number (*Figure 4.9*); although there is an overlap between the shift ranges observed for the different coordination numbers, there is a clear overall trend for an increase in shift with decreasing coordination number. This observation suggests that this second resonance arises from a lower coordinated yttrium site. We can therefore confidently assign this resonance to a 5 coordinated yttrium environment, which represents, to our knowledge, the first spectrum of a 5 coordinated yttrium environment reported in the literature. $BaSn_{0.90}Y_{0.10}O_{2.95}$ gives rise to a weaker 5-coordinated Y resonance at 400 ppm, which is seen more clearly in the deconvoluted spectrum (*Figure 4.10a*). After hydration (*Figure 4.8b*), the 5 coordinated Y resonances disappear as the oxygen vacancies are now filled with OH groups confirming the previous assignment.

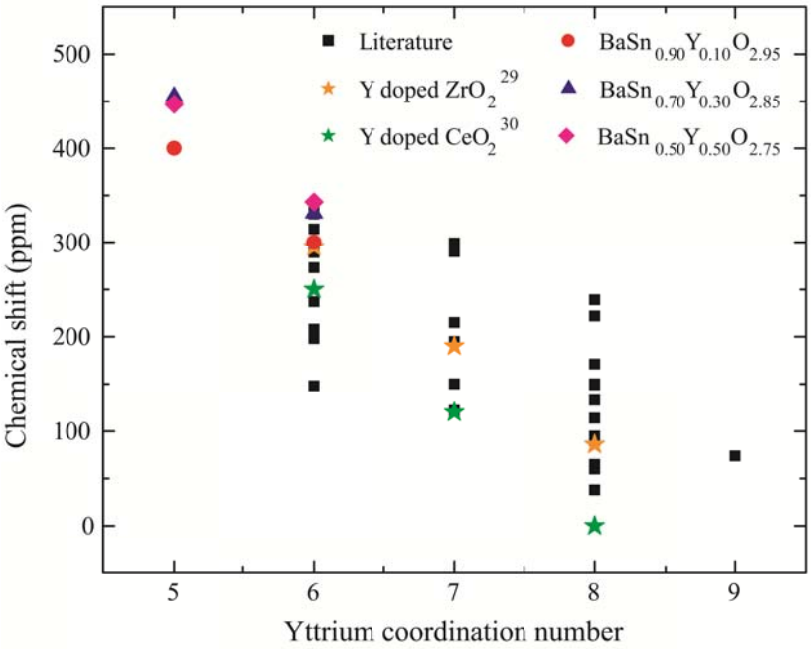

Figure 4.9. A comparison of the experimental shifts for 5 and 6 coordinated Y environments in $BaSn_{1-x}Y_xO_{3-x/2}$, x = 0.10 (red circle), 0.30 (blue triangle) and 0.50 (purple star), and the ^{89}Y chemical shifts reported for stoichiometric materials in the literature (black squares).[18, 23-33] The shifts for the different yttrium coordination environments in yttrium substituted ZrO_2 and CeO_2 respectively, are shown as orange and green stars, respectively.

The ratios of 5 to 6 coordinated Y environments for all three substitution levels were extracted by spectral deconvolution (*Figure 4.10*) and are compared to the ratios obtained for 5 and 6 coordinated Sn environments in *Table 4.3*. For $BaSn_{0.90}Y_{0.10}O_{2.95}$ and $BaSn_{0.70}Y_{0.30}O_{2.85}$ the ratios of 5 to 6 coordinated environments are very similar for both Sn and Y showing that the vacancies seem to order randomly at low substitution levels. For $BaSn_{0.50}Y_{0.50}O_{2.75}$ the ratio of 5:6 coordinated Y environments (0.34:0.66) is noticeably smaller than the one observed earlier for 5:6 coordinated Sn environments (0.44:0.56), while for strict Y – Sn cationic ordering, these ratios should be identical. This discrepancy is ascribed to a number of factors. First, ^{89}Y relaxation times are extremely long and although we have measured spectra with different recycle delays than those reported here (250 s), where no change in relative intensity was observed, it is difficult to completely exclude the possibility that the relaxation time for the 5-coordinated Y environment is longer than that of the 6-coordinate environment, leading to a reduction of its intensity. Second, it is possible that some of the yttrium atoms substituted on the A site rather than on the B site as a result of BaO loss during sintering, as reported by *Haile et al.* for the Y substituted $BaZrO_3$ system.[34] This gives rise to the stoichiometry $Ba_{1-2b}Y_{2b}(Sn_{0.5+b}Y_{0.5-b})O_{2.75+1.5b}$, Y substitution on the B site reducing the oxygen vacancy content, and thus the 5:6 ratio, for both Y and Sn. Furthermore, Sn-O-Sn environments are created (consistent with the ^{17}O NMR). Assuming that there is a tendency for the vacancies to be located between two Sn ions (, *i.e.* there would a considerable amount of Sn-□-Sn), reflecting the preference for Sn over Y for a 5 –coordinate environment, this would account for the larger amount of 5 coordinated Sn environments observed in the dry structures. This is consistent with the observation of some $Sn(OSn)_{6-x}(OY)_x$ ($x > 0$) environments after hydration by ^{119}Sn NMR. These Sn rich clusters must be much smaller in size and be nearer more yttrium ions (required for vacancy formation), since unlike those seen in the $x = 0.4$ sample, they are more readily hydrated. A 12 coordinate yttrium A site should, in principle, be visible in the ^{89}Y NMR spectrum as a resonance at lower frequencies than the 6 coordinate yttrium resonance according to the trends shown in *Figure 4.8*. Such an environment may be quite disordered as there are many different cationic arrangements on the nearby B site, rendering the number of possible 12 coordinated yttrium environments quite large. This would result in a very broad signal which, combined with only a small amount of A site substitution, very long T_1 may prevent the observation of this particular 12 coordinate yttrium resonance. The presence of A site substitution by Y may be another factor that hinders

long range ordering of the Y – Sn sublattice. Finally, it is also possible that not all of the yttrium is actually accommodated into the structure, and that the Y_2O_3 impurity phase is either too low in concentration or too small in size (XRD) to be detected by NMR and XRD.

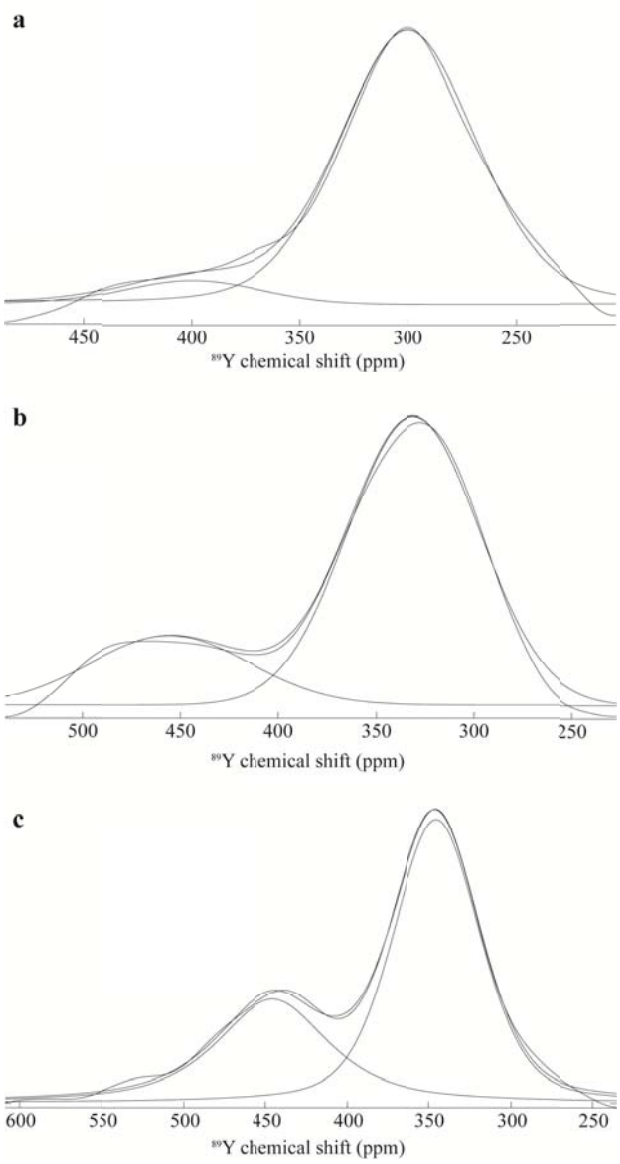

Figure 4.10. Decovonlution of the 89Y NMR spectra of dry $BaSn_{1-x}Y_xO_{3-x/2}$. (a) $BaSn_{0.90}Y_{0.10}O_{2.95}$, (b) $BaSn_{0.70}Y_{0.30}O_{2.85}$ and (c) $BaSn_{0.50}Y_{0.50}O_{2.75}$.

Table 4.3. Experimental ratios of the intensities of the 5 and 6 coordinated Y and Sn environments extracted from deconvolution of the ^{89}Y and ^{119}Sn NMR spectra of $BaSn_{1-x}Y_xO_{3-x/2}$, respectively.

x	^{89}Y NMR		^{119}Sn NMR	
	5 coord. Y	6 coord. Y	5 coord. Sn	6 coord. Sn
0.10	0.08(2)	0.92(2)	0.00(4)	1.00(4)
0.30	0.22(2)	0.78(2)	0.21(3)	0.79(3)
0.50	0.34(2)	0.66(2)	0.44(1)	0.56(1)

F. ^{119}Sn NMR at high temperature

Although little discussed in the literature, hydration of the material requires that the oxygen vacancies are mobile, so that they can move to the surface to react with the water molecules. For this reason, hydration of these materials is generally performed at high temperatures (between 200 and 800 °C), which is a trade-off since higher temperature will lead to increased desorption of the water. In order to investigate the oxygen vacancy transport in this system, we have recorded high temperature ^{119}Sn MAS NMR spectra of $BaSn_{0.50}Y_{0.50}O_{2.75}$ (*Figure 4.11*). At room temperature, the 5 and 6 coordinate tin environments are clearly resolved at -423 and -564 ppm respectively. As the temperature increases, a broad component appears at 400 °C in between these two environments at around -497 ppm. Upon additional heating, the intensity of this resonance increases and its linewidth narrows. This new resonance is ascribed to a Sn atom with an average coordination of 5.5 on the NMR timescale, which results from oxygen ion hopping between a tin octahedron into a vacant site nearby a 5 coordinate cation, the former becoming a 5 coordinate tin atom and the latter a 6 coordinate tin atom (*Figure 4.1b*). This process starts above 200 °C, the coalescence requiring a jump frequency k greater than the frequency separation Δν between the two resonances and given by[35]

$$k = \frac{\pi \Delta \nu}{\sqrt{2}}$$

which yields approximately k = 58 kHz. This motional process is in agreement with the previously reported hydration behaviour, where significant water uptake starts at around 300 °C.[1] This is also the temperature at which the loss of structural water is seen in the TGA experiments. The observation of residual (5 and 6- coordinated Sn) resonances at -423 and -564 ppm at the

highest temperature indicates that there is a distribution of correlation times for this system. Studies are in progress to investigate the role that water plays in altering the activation energy of the oxygen-ion migration, a phenomenon that has also been explored by using computer simulations.[36-37]

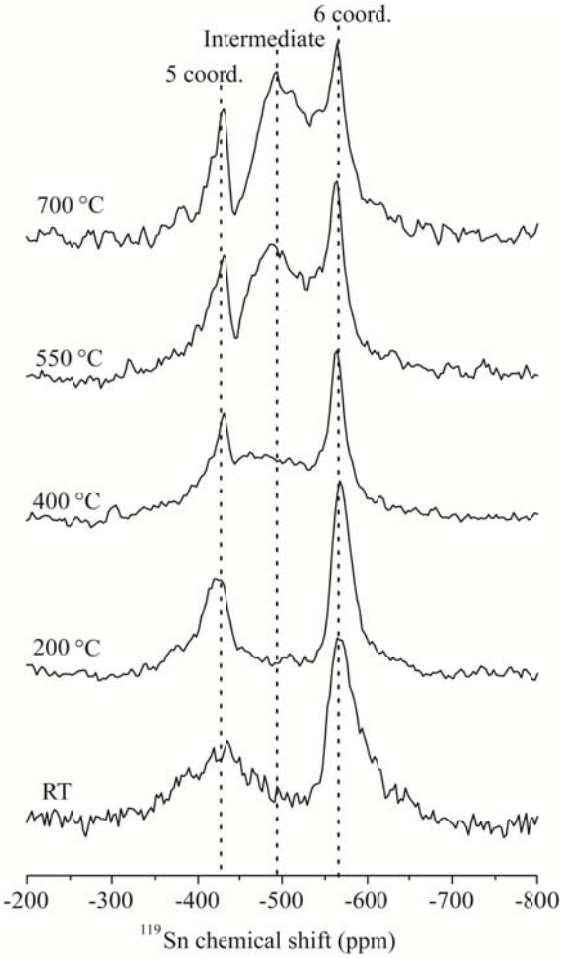

Figure 4.11. High temperature ^{119}Sn MAS NMR spectra of the dry $BaSn_{0.50}Y_{0.50}O_{2.75}$ sample.

IV. Conclusion

In summary, this multinuclear NMR study reveals strong evidence for random yttrium distributions at low substitution levels, and short-range Y-O-Sn ordering at high substitution levels in $BaSn_{1-x}Y_xO_{3-x/2}$. The tendency for yttrium and tin to alternate on the B site of the perovskite structure was observed by ^{119}Sn NMR, with all the tin environments being surrounded by at least 4 yttrium atoms in the 1st B-site cation coordinate shell in $BaSn_{0.50}Y_{0.50}O_{2.75}$. This ordering is in agreement with the ^{17}O NMR spectra, which for $BaSn_{0.50}Y_{0.50}O_{2.75}$ is dominated by a Y-O-Sn, ^{17}O resonance. No Y-O-Y local environments were observed; this cannot be explained by the preferential location of the vacancies in between two yttrium atoms, since no preference for 5 coordinate over 6 coordinate environments was seen by ^{89}Y NMR. Indeed, the intensity ratio of the 5:6-coordinate environments in $BaSn_{0.50}Y_{0.50}O_{2.75}$ is actually higher in the ^{119}Sn spectrum, than in the ^{89}Y spectrum.

Even $BaSn_{0.50}Y_{0.50}O_{2.75}$ contains some residual Sn-O-Sn environments, consistent with the lack of long-range cation ordering observed in our study, as probed by XRD. This is ascribed to either incomplete Y substitution, and/or the presence of some Y^{3+} cations on the A site as has been reported for the yttrium substituted $BaZrO_3$ system.[34] A-site substitution of yttrium is driven or is coupled with BaO loss during sintering and leads to the stoichiometry, $Ba_{1-2b}Y_{2b}(Sn_{0.5+b}Y_{0.5-b})O_{2.75+1.5b}$, and the formation of Sn-O-Sn groups. Preferential location of the oxygen vacancies in between two tin atoms, accounts for the different 5:6 ratios for Sn and Y. The difficulty in achieving long-range cation ordering, especially with systems containing Y^{3+} and Sn^{4+} ions, which will show very low diffusivities even at very high temperatures, and in a system that will not tolerate Y-O-Y linkages, is likely to be one cause of the differences between the extent of ordering observed in different studies; further, it may also be associated with the observation, in one report,[2] of an amorphous component on the particles or between grain boundaries.

Finally, these results have significant implications for proton conductivity because they indicate that the majority of the protons in the hydrated material will be coordinated to the same type of oxygen linkage (Y-O-Sn) for locally-ordered $BaSn_{0.50}Y_{0.50}O_{2.75}$ (the residual protons being Sn-O-Sn oxygen ions). The ability of the structure to accommodate Y-O-Sn ordering

allows very high levels of yttrium, and thus vacancies (and protons on hydration) to be incorporated into the structure, without forming basic oxygen sites such as the Y-O-Y environments. The high concentration of Y-O-Sn and lack of Y-O-Y environments allows hops to occur via jumps involving similar local environments, without being trapped on the more basic Y – O –Y environments. Such cation ordering has not been seen in the yttrium substituted $BaZrO_3$ and $BaCeO_3$ systems, which show higher conductivity at lower yttrium substitution levels.[1] Thus, we believe that the high conductivity of $BaSn_{0.50}Y_{0.50}O_{2.75}$ is due to the predominance of a single O site, the lack of basic Y-O-Y sites, combined with the large number of protons in the material due to the high substitution level. Finally, the oxygen conduction required for hydration of such a protonic conductor was observed via the exchange of the 5 and 6 coordinated Sn environments in $BaSn_{0.50}Y_{0.50}O_{2.75}$ at 400°C and above.

V. References

1. K. D. Kreuer, *Annual Review of Materials Research*, 2003, **33**, 333.

2. P. Murugaraj, K. D. Kreuer, T. He, T. Schober and J. Maier, *Solid State Ionics*, 1997, **98**, 1.

3. I. Naray-Szabo, *Naturwissenschaften*, 1943, **31**, 202.

4. K. V. Paulose, P. Murugaraj, J. Koshy and A. D. Damodaran, *Japanese Journal of Applied Physics, Part 1 Regular Papers, Short Notes & Review Papers*, 1992, **31**, 1323.

5. J. Koshy, K. S. Kumar, J. Kurian, Y. P. Yadava and A. D. Damodaran, *Bulletin of Materials Science*, 1994, **17**, 577.

6. H. D. Megaw, *Proceedings of the Physical Society,* 1946, **58**, 133.

7. N. J. Clayden, C. M. Dobson and A. Fern, *Journal of the Chemical Society, Dalton Transactions Inorganic Chemistry*, 1989, 843.

8. M. R. Mitchell, S. W. Reader, K. E. Johnston, C. J. Pickard, K. R. Whittle and S. E. Ashbrook, *Physical Chemistry Chemical Physics*, 2011, **13**, 488.

9. P. Babilo and S. M. Haile, *Journal of the American Ceramic Society*, 2005, **88**, 2362.

10. A. Bielecki and D. P. Burum, *Journal of Magnetic Resonance, Series A*, 1995, **116**, 215.

11. J. B. Grutzner, K. W. Stewart, R. E. Wasylishen, M. D. Lumsden, C. Dybowski and P. A. Beckmann, *Journal of the American Chemical Society*, 2001, **123**, 7094.

12. G.-J. M. P. van Moorsel, E. R. H. Van Eck and C. P. Grey, *Journal of Magnetic Resonance, Series A*, 1995, **113**, 159.

13. J.-P. Amoureux, C. Fernandez and S. Steuernagel, *Journal of Magnetic Resonance, Series A*, 1996, **123**, 116.

14. J. D. van Beek, *Journal of Magnetic Resonance*, 2007, **187**, 19.

15. M. Bak, J. T. Rasmussen and N. C. Nielsen, *Journal of Magnetic Resonance*, 2000, **147**, 296.

16. P. Hodgkinson and L. Emsley, *Progress in Nuclear Magnetic Resonance Spectroscopy*, 2000, **36**, 201.

17. M. A. Subramanian, *Journal of Solid State Chemistry*, 1994, **111**, 134.

18. K. J. D. MacKenzie and M. E. Smith, *Multinuclear Solid-State Nuclear Magnetic Resonance of Inorganic Materials*, Pergamon Oxford, 2002.

19. S. E. Ashbrook and M. E. Smith, *Chemical Society Reviews*, 2006, **35**, 718.

20. T. J. Bastow, P. J. Dirken, M. E. Smith and H. J. Whitfield, *Journal of Physical Chemistry*, 1996, **100**, 18539.

21. L. Frydman and J. S. Harwood, *Journal of the American Chemical Society*, 1995, **117**, 5367.

22. A. Medek, J. S. Harwood and L. Frydman, *Journal of the American Chemical Society*, 1995, **117**, 12779.

23. S. E. Ashbrook, K. R. Whittle, G. R. Lumpkin and I. Farnan, *Journal of Physical Chemistry B*, 2006, **110**, 10358.

24. R. Dupree and M. E. Smith, *Chemical Physics Letters*, 1988, **148**, 41.

25. A. I. Becerro, A. Escudero, P. Florian, D. Massiot and M. D. Alba, *Journal of Solid State Chemistry*, 2004, **177**, 2783.

26. T. Harazono and T. Watanabe, *Bulletin of the Chemical Society of Japan*, 1997, **70**, 2383.

27. C. P. Grey, M. E. Smith, A. K. Cheetham, C. M. Dobson and R. Dupree, *Journal of the American Chemical Society*, 1990, **112**, 4670.

28. P. Florian, D. Massiot, G. Humbert and J.-P. Coutures, *Comptes Rendus de l'Académie des Sciences, Série IIb: Mécanique,Physique, Chimie, Astronomie*, 1995, **320**, 99.

29. K. Kawata, H. Maekawa, T. Nemoto and T. Yamamura, *Solid State Ionics*, 2006, **177**, 1687.

30. P. Jain, H. J. Avila-Paredes, C. Gapuz, S. Sen and S. Kim, *Journal of Physical Chemistry C*, 2009, **113**, 6553.

31. N. Kim and J. F. Stebbins, *Chemistry of Materials*, 2007, **19**, 5742.

32. S. W. Reader, M. R. Mitchell, K. E. Johnston, C. J. Pickard, K. R. Whittle and S. E. Ashbrook, *Journal of Physical Chemistry C*, 2009, **113**, 18874.

33. E. J. Harvey, S. E. Ashbrook, G. R. Lumpkin and S. A. T. Redfern, *Journal of Materials Chemistry*, 2006, **16**, 4665.

34. Y. Yamazaki, R. Hernandez-Sanchez and S. M. Haile, *Journal of Materials Chemistry*, 2010, **20**, 8158.

35. M. H. Levitt, *Spin Dynamics: Basics of Nuclear Magnetic Resonance*, John Wiley & Sons, 2001.

36. M. S. Islam, *Journal of Materials Chemistry*, 2000, **10**, 1027.

37. M. S. Islam, P. R. Slater, J. R. Tolchard and T. Dinges, *Dalton Transactions*, 2004, 3061.

Chapter 5:

Understanding the protonic organization and motion in protonic conductors by ^{1}H NMR

This chapter reports the use of ^{1}H solid-state NMR to identify the different interactions and processes involved in protonic conduction and how they affect the conductivity of the various perovskite-based materials. The protonic distribution becomes accessible at low temperatures after freezing of the motion. In $BaZr_{1-x}Sc_xO_{3-\delta}$, $^{1}H/^{45}Sc$ TRAPDOR experiments at -120°C allow identification of the different proton environments. In this material the protons are strongly attracted to Sc-O-Sc environments where they can compensate for the extra negative charge present on the oxygen site, even at low substitution levels. This preferential location and the short Sc…Sc distance creates a secluded environment for proton from which it requires a high activation energy to escape, hereby limiting the protonic conduction in this material. In $BaZr_{1-x}Y_xO_{3-\delta}$ the larger ionic size of Y^{3+} vs. Sc^{3+} minimizes the trapping of protons on Y-O-Y environments, the disparities in B…B (B = Zr or Y) being less pronounced than in $BaZr_{1-x}Sc_xO_{3-\delta}$. For low substitution levels, the protons are found predominantly on Zr-O-Zr sites but above 20% substitution a consequent concentration of proton is present on Y-O-Y sites, which explains why the conduction in $BaZr_{1-x}Y_xO_{3-\delta}$ is better at lower substitution levels (10 to 20%). For $BaSn_{0.50}Y_{0.50}O_{2.75}$ even though the B site cationic ordering described in Chapter 4 is expected to considerably enhance the protonic motion, the conductivity is limited by the presence of small Sn-rich clusters throughout the structure, creating Sn-O-Sn environments where the protons reside for a longer time compared to Sn-O-Y. High temperature experiments show that $BaZrO_3$ holds protons longer than $BaSnO_3$.

I. Introduction

Most of the protonic migration studies in $A^{2+}B^{4+}O_3$ perovskites have been performed by impedance spectroscopy.[1-21] This technique efficiently discriminates between good and bad candidates based on activation energies and conductivity; however it does not provide a clear understanding of the mechanism involved during the conduction process. Based on these observations, it is difficult to explain why a particular substituting element gives better results than another. A lot of interactions have to be taken into account: the size of the substituting element, its distribution in the structure, its effect on the location of oxygen vacancies which will impact the distribution of protons in the hydrated structure; none of this is accessible via impedance spectroscopy. In this context, an increasing number of computational studies[22-31] have been performed to help understand the mechanism underlying the protonic conduction; however only the overall effect can be compared to actual experimental results (since impedance spectroscopy is limited to overall conduction analysis). There is a real lack of knowledge of the ongoing processes occurring at the atomic level and techniques that can access local structure will be of great use to investigate such detailed mechanism. A few reports based on structural refinements[32-34] and vibrational spectroscopy[35-36] aimed at explaining the microscopic processes; however limited information is accessible from each technique and there is a need to extend our knowledge on local structure and protonic behavior to validate the current hypotheses. In this context, solid-state NMR is one of the best techniques to clarify some of the uncertainty related to the local processes since it gives access to both structural and motional details of a particular structure. In this chapter, we will explore the differences underlying the protonic conduction mechanism in the three systems reported in Chapters 2, 3 and 4: $BaZr_{1-x}Sc_xO_{3-\delta}$, $BaZr_{1-x}Y_xO_{3-\delta}$ and $BaSn_{1-x}Y_xO_{3-\delta}$. I would like to acknowledge numerous discussions between our group, Professor Sossina Haile and Dr. Yoshihiro Yamazaki from Caltech which have helped draw some of our conclusions. I would like to specially thank Dr. Yamazaki for providing some of the $BaZr_{1-x}Y_xO_{3-\delta}$ samples.

The first key problem to overcome, which may be responsible for the disparities in protonic conduction reported in the literature, involves controlling the amount of water dissolved in the structure.[37] Hydration of the perovskite materials requires the migration of the oxygen vacancies from the bulk to the surface where they can react with water. Elevated temperatures

are required for the mobility of the oxide vacancies; however high temperatures are also associated with dehydration. The dissolution of water can result in the presence of bulk protons, successfully incorporated in the structure, but also hydroxide species covering the surface area. While the former actively participate in the conduction mechanism, the latter will prevent further hydration of the material; therefore it is important to have a good control over the hydration process. Thus it is not always straightforward to fully hydrate these materials without covering the surface with hydroxide species. The community is fairly divided between the idea that the protons can be strongly associated with the substituting element[38-39] and that the energy barrier for proton migration is only related to the basicity of the oxygen site. [40] ^{1}H NMR experiments performed at low temperature will provide a lot of information on the distribution of protons in the three different systems and we will analyze the reasons behind such a particular protonic distribution in Sections III.B and III.C. Another key point widely discussed in the literature is the protonic migration process. The most commonly thought behavior involves a two-step process:[25, 30, 41] the first step consists of the rotation of the proton around the hosting oxygen and the second involves the jump of the proton to the next oxygen, the latter being considered the rate-limiting step in the conduction mechanism.[22-23] We will observe proofs of protonic motion at temperature as low as -120°C in some of the systems in Section III.C. Finally, since water is generated *in situ* in a fuel cell, it is important to determine the extent of hydration/dehydration of these materials to understand the relevant conduction mechanisms of potential SOFC electrolytes – protonic vs. anionic – under hydrated conditions at elevated temperatures. We will report the differences of behaviour in $BaZrO_3$ and $BaSnO_3$ in Section III.D based on our analysis of high temperature ^{1}H NMR spectra.

First we will explore the effect of sample preparation and hydration scheme on the proton distribution in $BaZr_{0.70}Y_{0.30}O_{2.85-y}(OH)_{2y}$. Our results will clearly illustrate the need of a rigorous hydration method to maximize reproducibility. Second, we will observe the different proton resonances in $BaZr_{1-x}Sc_xO_{3-x/2-y}(OH)_{2y}$ depending on substitution level and temperature. Definite assignments of the various resonances will be made possible by analysis of ^{1}H/^{45}Sc TRAPDOR experiments at -120°C. Based on this assignment, a similar analysis of the proton environments present in $BaZr_{1-x}Y_xO_{3-x/2-y}(OH)_{2y}$ and $BaSn_{1-x}Y_xO_{3-x/2-y}(OH)_{2y}$ will be performed. Finally the

change in proton distribution at high temperatures will be identified in $BaZr_{1-x}Y_xO_{3-x/2-y}(OH)_{2y}$ and $BaSn_{1-x}Y_xO_{3-x/2-y}(OH)_{2y}$.

II. Experimental section

The synthesis of all materials has been described in the previous chapters and will not be covered in this chapter. Please refer to the previous chapters for more information about the synthesis procedures.

A. Hydration method

In order to understand the impact of sample preparation and hydration method, we studied the ^1H NMR spectra of two sets of $BaZr_{0.70}Y_{0.30}O_{2.85-y}(OH)_{2y}$ samples. One batch of $BaZr_{0.70}Y_{0.30}O_{2.85-y}(OH)_{2y}$ pellets was prepared by combustion synthesis and then separated into two sets: the first set was crushed manually and the second set was attritor milled at 500 rpm for 4 hours with yttria stabilized zirconia 3 mm balls leading to a higher surface area. Different hydration schemes were then tested on the two sets of powders in order to identify the best hydration method by ^1H NMR. The hand crushed samples were hydrated in a tube furnace. First the powder was dried at 1000°C for 2 h and then cooled down by steps of 100°C every 2 h with wet N_2 flowing over the samples at a rate of 60 $mL.min^{-1}$. Half of the hand crushed powder was hydrated from 1000°C down to 350°C and the second half from 1000°C down to 200°C. Half of the attritor milled powder was hydrated following the same method, from 1000°C down to 50°C. The second half of the attritor milled sample was hydrated by exposure to ambient atmosphere for several days.

B. Low temperature ^1H NMR

$BaZr_{1-x}Sc_xO_{3-\delta}$ (x = 0.05, 0.15 and 0.30) $BaZr_{1-x}Y_xO_{3-\delta}$ (x = 0.10, 0.20, 0.30 and 0.50) and $BaSn_{1-x}Y_xO_{3-\delta}$ (x = 0.10, 0.30 and 0.50) were hydrated in a tube furnace under moist N_2 gas down to 350°C to limit the presence of surface hydroxide species. At the end of the hydration scheme all powders were rapidly transferred to a N_2 glove box in order to pack the samples into the rotors with limited exposure to ambient air, hereby preventing formation of hydroxide species. Low temperature ^1H NMR experiments were performed on a 8.5 T wide bore Varian Oxford Infinity Plus spectrometer with a 4 mm Varian probehead tuned to 360.0 MHz. Single pulse experiments were performed for all samples at 25°C, -20°C, -60°C and -120°C using 100

transients. Pulse delays were determined using an inversion recovery pulse sequence before acquisition of the one pulse experiment. All spectra have been normalized by weight for comparison of hydration levels. Additional Hahn echo experiments with increasing delay time between pulses were recorded to evaluate the T_2 value for each proton sites. ^{1}H chemical shifts were externally referenced to TMS at 0 ppm.

C. ^{1}H/^{45}Sc TRAPDOR

All ^{1}H/^{45}Sc TRAPDOR were performed on a 17.6 T Bruker wide bore magnet at the NYSBC facility in NYC with a 4 mm Bruker probehead tuned to 750.2 MHz. Rotors were packed quickly under ambient atmosphere with $BaZr_{1-x}Sc_xO_{3-x/2-y}(OH)_{2y}$ (x = 0.05, 0.15 and 0.30) and spun at 12.5 kHz. Recycle delays of 2 s and 10 s were used at room temperature and -120°C respectively. The ^{1}H shift was externally referenced to chloroform at 0 ppm respectively.

D. High temperature ^{1}H NMR

High temperature ^{1}H MAS NMR were acquired on a 8.5 T wide bore Varian Oxford Infinity Plus spectrometer using a 7 mm HX high temperature MAS probe from Doty Scientific, Inc tuned to 360 MHz. Samples were packed in a boron nitride BN insert and placed in a 7 mm silicon nitride Si_3N_4 rotor. One pulse, T_1 inversion recovery and T_2 spin-spin lattice relaxation experiments were performed using 128, 4 and 4 transients respectively. Spinning was performed under nitrogen at 4 kHz at room temperature and at 6 kHz above 200°C. ^{1}H chemical shifts were externally referenced to H_2O at 4.2 ppm.

III. Results

For the ^{1}H NMR experiments, different references have been used on different magnets (chloroform *vs.* TMS *vs.* H_2O), although they should in principle lead to identical chemical shifts for one material, it appears that the referencing introduces translational shift, therefore the chemical shift value from one field to the next may be slightly different but the chemical shift difference between resonances will not be affected by the referencing. For this reason, the reference used for each experiment will be mentioned in the figure caption.

A. Effect of the hydration method on the proton distribution

The ^{1}H NMR spectra of $BaZr_{0.70}Y_{0.30}O_{2.85-y}(OH)_{2y}$ sample resulting from the four different hydration schemes are reported in *Figure 5.1*. The lower the final hydration temperature is, the more resonances we can observe. The ^{1}H NMR spectrum of the hand crushed sample hydrated down to 350°C shows two broad resonances at 5.4 and 2.6 ppm. When the final hydration temperature is lowered down to 200°C, an additional sharper resonance at 1.6 ppm is observed. For the attritor milled samples, the 5.4 ppm resonance is a lot broader than for the previous two hydration schemes and is accompanied by sharper resonances at smaller shifts, at 1.9 ppm for the attritor milled sample hydrated down to 50°C and at both 2 and 1.2 ppm for the sample left under ambient atmosphere. Since the 5.4 ppm resonance is observed for all samples and accounts for a majority of the protons, we can assign this signal to the bulk protons in our materials. The resonances from 2 to 1.2 ppm, which are sharper, are a signature for more mobile protons and can be assigned to the presence of hydroxide species on the surface of the particles. Due to the higher surface area resulting from mechanical crushing, the attritor milled samples are more subject to the formation of hydroxide species.

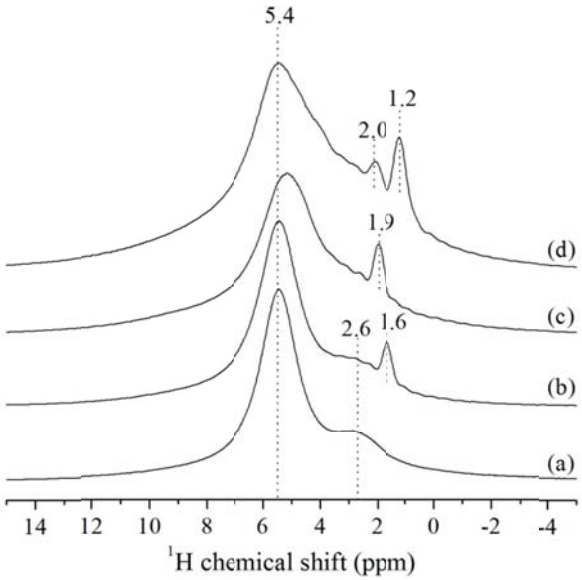

Figure 5.1. ^{1}H NMR of $BaZr_{0.70}Y_{0.30}O_{2.85-y}(OH)_{2y}$ after different grinding and hydration methods. Hand crushed powders hydrated from 1000°C down to (a) 350°C and (b) 200°C. Attritor milled powders hydrated (c) from 1000°C down to 50°C and (d) by exposure to ambient atmosphere for several days. Spectra referenced to TMS.

Attritor milling of the powders induces the creation of cracks in the particles. We can indeed observe higher proton contents for the powders that were attritor milled (*Figure 5.1*). The bulk hydration seems to be more important than for the hand crushed samples: the 5.4 ppm resonance is broader in case of attritor milling; however it also introduces the presence of surface hydroxides that will inhibit any additional hydration. The presence of these hydroxides will certainly complicate the understanding of the NMR spectra and will also fail to reproduce the conditions encountered by the material in the real fuel cell. We will therefore limit our study to materials that have been hydrated down to 350°C and exposed to ambient atmosphere for a limited amount of time whenever it is feasible, *i.e.* when the experiments were run at Stony Brook.

B. Low temperature ^{1}H NMR of $BaZr_{1-x}Sc_xO_{3-x/2-y}(OH)_{2y}$

The single pulse ^{1}H NMR spectra for $BaZr_{1-x}Sc_xO_{3-x/2-y}(OH)_{2y}$ at 25°C and -120°C are reported in *Figure 5.2*. At room temperature we observed an average resonance due to the proton transfer between different oxygen sites. At -120°C we can resolve the various proton environments observed in Chapter 2 but shifted by approximately 1.7 ppm. The resonances at 4.5 and 2.9 ppm correspond either to Zr-OH-Zr and Zr-OH-Sc or to Zr-OH-Sc and Sc-OH-Sc environments respectively. The environment at 4.1 ppm results from unfrozen proton exchange still occurring at -120°C. For $BaZr_{0.85}Sc_{0.15}O_{2.925-y}(OH)_{2y}$ not all the protons of the environment at 2.8 ppm are taking part in the hopping mechanism at 25°C, hereby showing the higher immobility of those protons.

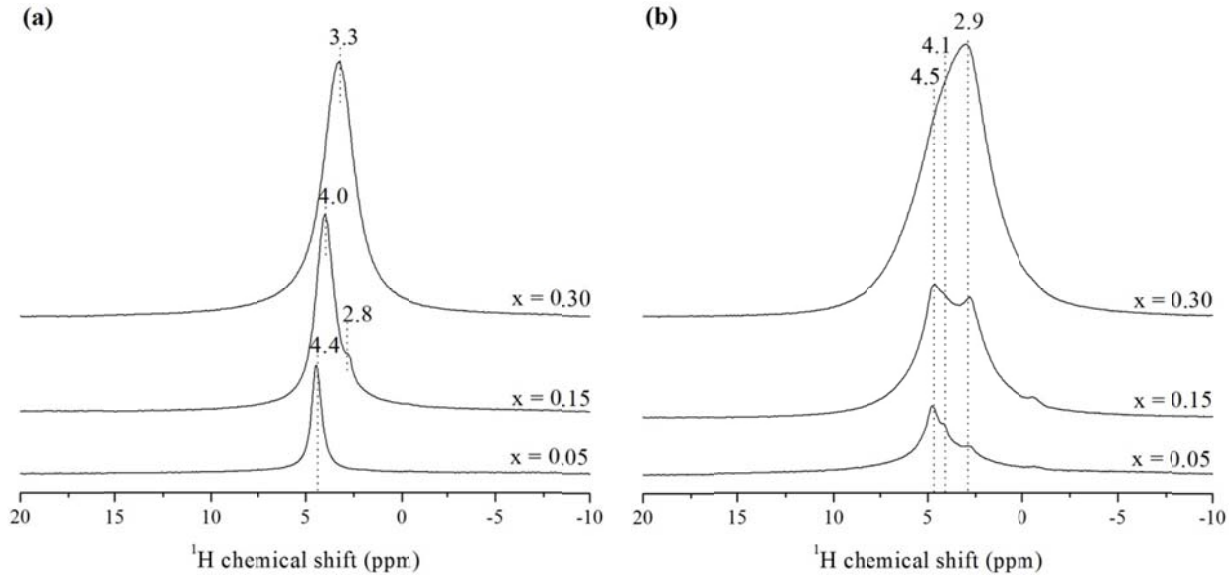

Figure 5.2. Comparison of single pulse ^{1}H NMR of $BaZr_{1-x}Sc_xO_{3-x/2-y}(OH)_{2y}$ at (a) 25°C and (b) -120°C. Spectra referenced to TMS.

In order to definitively assign the various proton environments, we performed ^{1}H/^{45}Sc TRAPDOR of $BaZr_{1-x}Sc_xO_{3-x/2-y}(OH)_{2y}$ (x = 0.05, 0.15 and 0.30) at 25°C and -120°C (*Figure 5.3*). For all samples, the shifts observed by TRAPDOR are at lower frequency than the one seen by single pulse experiments, by approximately 1.6 ppm. At room temperature, we observe a single resonance at 2.2 - 3.0 ppm that is not altered by the TRAPDOR effect, no matter how long Sc is irradiated, at least up to a value of 800 μs. For $BaZr_{0.85}Sc_{0.15}O_{2.925-y}(OH)_{2y}$ at -120°C we now observe the three different proton resonances at approximately 2.9, 2.4 and 1.0 ppm which all show a TRAPDOR effect, the impact on the one at 1.0 ppm being the most dramatic. From these results it seems that all sites are directly bonded to Sc atoms, the site at 1.0 ppm being bonded to a higher number of Sc atoms. We can therefore tentatively assign the sites at 2.9 and 1.0 ppm to protons residing on Zr-O-Sc and Sc-O-Sc oxygen sites respectively. The resonance at 2.4 ppm whose shift is almost identical to the one of the resonance observed at 25°C results from some remaining local protonic exchange[30] in between Zr-O-Sc and Sc-O-Sc, in other words not all of the protonic motion has been frozen out at this temperature.

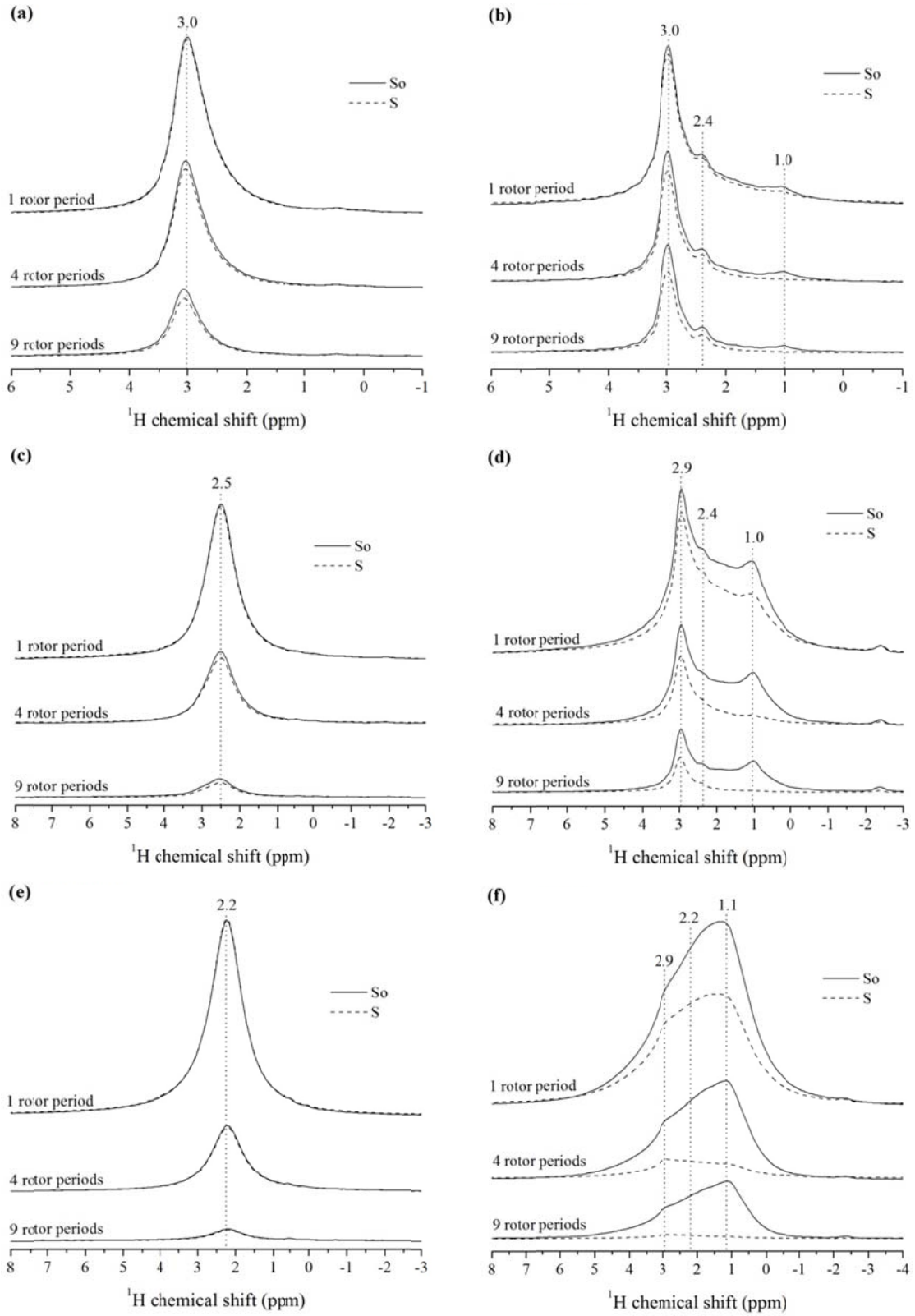

Figure 5.3. $^{1}H/^{45}Sc$ TRAPDOR effect on $BaZr_{1-x}Sc_xO_{3-x/2-y}(OH)_{2y}$. For x = 0.05 at (a) 25°C and (b) -120°C, for x = 0.15 at (c) 25°C and (d) -120°C and for x = 0.30 at (e) 25°C and (f) -120°C. Spectra referenced to chloroform.

A comparison of the TRAPDOR effect at -120°C throughout the $BaZr_{1-x}Sc_xO_{3-x/2-y}(OH)_{2y}$ solid solution shows a similar trend for all samples (*Figure 5.3*). The resonance at 1.0 ppm is always more affected than the one at 2.9 ppm. However the effect of the Sc irradiation seems to be more pronounced for the 2.9 ppm resonance at higher Sc substitution levels. Presumably the nearest oxygen atoms, to which the protons at 2.9 ppm are hydrogen bonded, are surrounded by a higher ratio of Sc, hereby increasing the TRAPDOR effect for the Zr-OH-Sc site through hydrogen bonding. This tendency is not as clearly observed for the Sc-OH-Sc site since such protons are already surrounded by two Sc cations and the TRAPDOR outcome is already maximized. According to our current proton assignment, we are observing a high ratio of Sc-OH-Sc while we were barely able to detect a resonance for Sc-O-Sc by ^{17}O NMR in Chapter 2, even for $BaZr_{0.70}Sc_{0.30}O_{2.85-y}(OH)_{2y}$. Why did we not detect more Sc-O-Sc environments? In the quantification of the different oxygen sites in Chapter 2, we seemed to be missing some Sc from the structure, which was ascribed to incomplete substitution of scandium. One possibility is that a significant proportion of the oxygen vacancies are actually located in between two Sc cations. After hydration the Sc-□-Sc environments lead to a non-negligible amount of available Sc-O-Sc oxygen sites, which could be the preferential location for protons. This would account for such a high concentration of protons observed on Sc-O-Sc sites, particularly in $BaZr_{0.70}Sc_{0.30}O_{2.85-y}(OH)_{2y}$. Additionally we qualitatively reported quite a significant amount of 5 (*vs.* 6) coordinate Sc environments, which supports our latest assignment. A comparison to the other hydrated systems presented in this chapter will further test this new assignment. The ratios of the different proton sites were extracted by deconvolution of the single pulse spectra obtained at -120°C (*Table 5.1*). The Sc-OH-Sc to Zr-OH-Sc ratios observed, *i.e.* the areas of the resonances at 2.9 *vs.* 4.5 ppm, are quite different from the ones obtained in Chapter 2: 0.2:1, 0.9:1 and 2.1:1 here *vs.* 0.3:1, 0.5:1 and 1:1 in Chapter 2 for $BaZr_{0.95}Sc_{0.05}O_{2.975-y}(OH)_{2y}$, $BaZr_{0.85}Sc_{0.15}O_{2.925-y}(OH)_{2y}$ and $BaZr_{0.70}Sc_{0.30}O_{2.85-y}(OH)_{2y}$ respectively. As was discussed in section III.A, the hydration used in the current scenario is far from leading to complete hydration of the samples; therefore the distribution of the protons over the different oxygen sites clearly demonstrates which sites are the first to be occupied and which ones are less likely to be occupied. From the previous results we can conclude that the Sc-O-Sc oxygen sites present the smallest binding energy. In turn, if a higher degree of hydration is reached, the entropy factor has a much greater impact on the distribution of the proton atoms and it becomes more difficult to evaluate the strength of the O-H

bond. The different conclusions drawn from Chapter 2 compared to the ones deduced from this set of results clearly illustrates the sensitivity of the hydration method used for qualitative analysis of the NMR spectra.

Table 5.1. Ratios of the different proton sites in $BaZr_{1-x}Sc_xO_{3-x/2-y}(OH)_{2y}$ at -120°C.

x	Sites (ppm)		Weight average (ppm)
	4.5	2.9	
0.05	0.86(3)	0.14(4)	4.3
0.15	0.53(1)	0.47(2)	3.8
0.30	0.32(2)	0.68(6)	3.4
Assignment	Zr-OH-Sc	Sc-OH-Sc	

Figure 5.4 illustrates the protonic motion being slowed down with decrease of the temperature in $BaZr_{1-x}S_xO_{3-x/2-y}(OH)_{2y}$. For $BaZr_{0.85}Sc_{0.15}O_{2.925-y}(OH)_{2y}$ some of the protons hosted by Sc-O-Sc do not take part in the local motion occurring at room temperature, hereby showing the higher immobility of Sc-OH-Sc environments restricting the overall protonic conduction. The motion observed at room temperature is limited to the hop of the proton in between the different oxygen sites surrounding its initial location, with a tendency to jump to oxygen atoms bonded to the nearest available Sc cation; however this motion does not extend throughout the structure at 25°C. Until we reach a temperature where most of the exchange has been stopped (-120°C in our case), the spectrum will give a good picture of how the different proton environments are involved in the exchange. In the case of a Zr-OH-Sc environment, if we assume that the Sc cation is surrounded by 6 Zr cations, then the proton can hop around the 6 different oxygen atoms connecting Sc to the next 5 Zr cations. In the case of a Sc-OH-Sc environment with each scandium cation surrounded by 5 Zr atoms, the proton will most likely be hoping in between the 10 oxygen atoms connecting the two Sc cations to the rest of the $BaZr_{0.85}Sc_{0.15}O_{2.925-y}$ structure plus the oxygen atom common to the two Sc cations, with a preference for the Zr-O-Sc environments the closest to the Sc-O-Sc hosting site, i.e. 8 of the 10 Zr-O-Sc sites. Therefore no matter what the identity of the initial hosting oxygen site was, unless most of the motion has been frozen out, the proton will more likely be found on a Zr-O-Sc site, which is what is observed when the temperature is reduced.

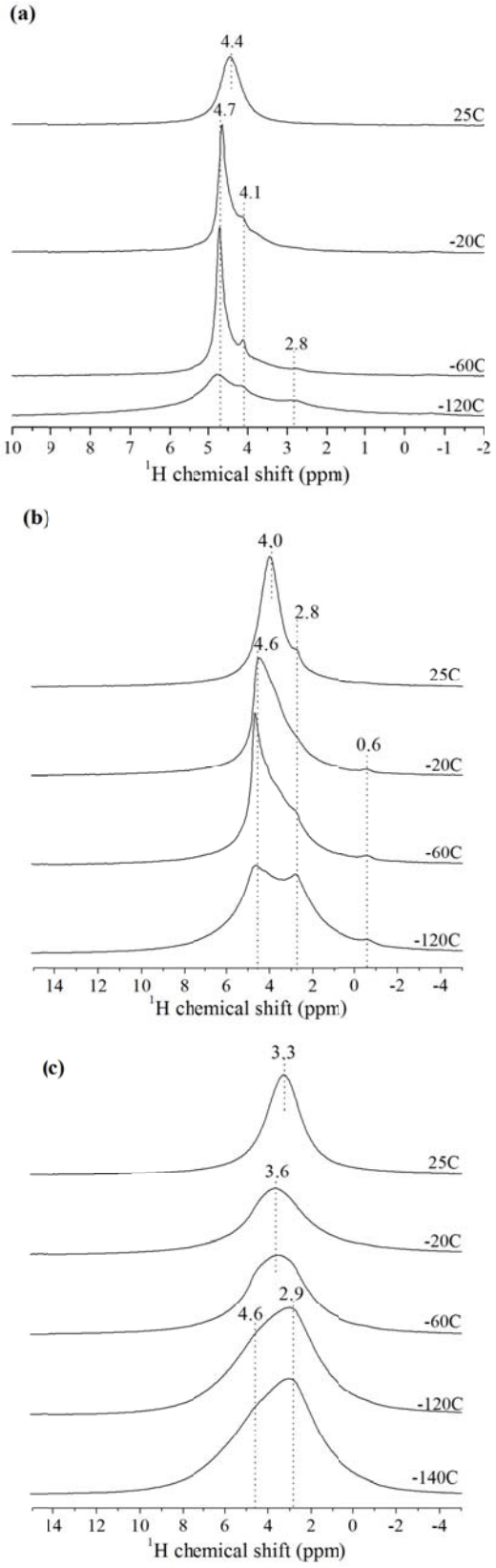

Figure 5.4. ^{1}H NMR of $BaZr_{1-x}Sc_xO_{3-x/2-y}(OH)_{2y}$ at low temperatures. (a) x = 0.05, (b) x = 0.15, (c) x = 0.30. Spectra referenced to TMS.

The resonance at 2.9 ppm corresponding to Sc-OH-Sc is only clearly resolved at -120°C. The hop of the proton over a larger part of the structure requires the presence of another Sc cation in the third cationic coordination shell of the hosting oxygen atom or implies the brief stay of the proton on a Zr-O-Zr site. The second scenario will only happen at higher temperature since the protons are not first attracted to Zr-O-Zr and will require more energy to travel through one of those oxygen environments. On the other hand, the protonic repulsion towards such an oxygen site limits the time the proton spends on this site which in turn increases the conductivity. One can easily understand the complexity of the interactions involved during protonic conduction in this type of materials. Finally we can also observe the presence of some surface hydroxide species at 0.6 ppm, the motion of these species is also frozen out while decreasing the temperature.

Figure 5.5 shows the ^{1}H Hahn echo spectra recorded to extract the spin-spin relaxation times T_2 of the different proton environments. The signal at 4.5 ppm is lost first, confirming the higher mobility of the protons hosted on the Zr-O-Sc sites.

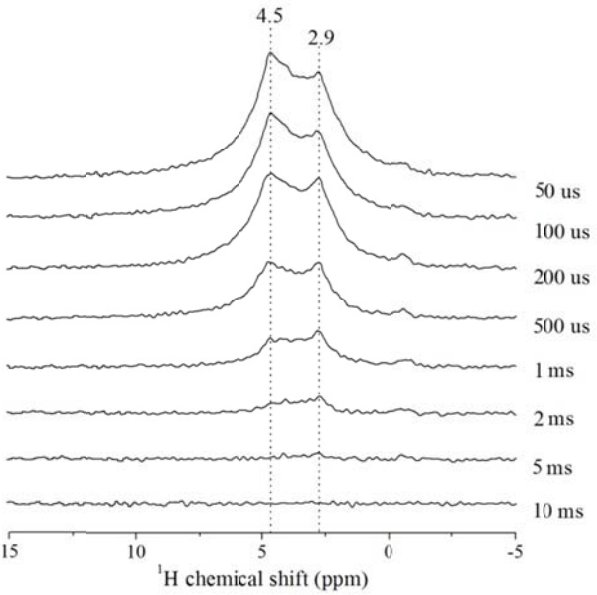

Figure 5.5. ^{1}H spectra recorded with different Hahn echo delays to determine the T_2 relaxation rates for the different proton environments in $BaZr_{0.85}Sc_{0.15}O_{2.925-y}(OH)_{2y}$ at -120°C. The values on the right correspond to the delay time between the 90° and the 180° pulses. Spectra referenced to TMS.

C. Low temperature ^{1}H NMR of $BaZr_{1-x}Y_xO_{3-x/2-y}(OH)_{2y}$

Figure 5.6 shows the ^{1}H NMR of $BaZr_{1-x}Y_xO_{3-x/2-y}(OH)_{2y}$ (x = 0.10, 0.20, 0.30 and 0.50) at 25°C and -120°C. There is a noticeable difference between this set of samples compared to the previous system. At room temperature we only observe one resonance at 5.7 ppm for $BaZr_{0.80}Y_{0.20}O_{2.90-y}(OH)_{2y}$. For $BaZr_{0.70}Y_{0.30}O_{2.85-y}(OH)_{2y}$ and $BaZr_{0.50}Y_{0.50}O_{2.75-y}(OH)_{2y}$ we can clearly separate a second resonance at 2.8 ppm. In the case of $BaZr_{0.50}Y_{0.50}O_{2.75-y}(OH)_{2y}$ based on the ^{1}H intensity, the hydration level seems to be much lower than for $BaZr_{0.80}Y_{0.20}O_{2.90-y}(OH)_{2y}$ and $BaZr_{0.70}Y_{0.30}O_{2.85-y}(OH)_{2y}$. This corroborates our conclusions in Chapter 3 where we observed amphoteric substitution of yttrium on both A and B sites in $BaZr_{0.50}Y_{0.50}O_{2.75}$. This A/B site substitution pattern leads to an actual sample formula of $(Ba_{0.83}Y_{0.17})(Sn_{0.67}Y_{0.33})O_{3.00}$ where no oxygen vacancies are left. It is therefore not surprising to find such a low hydration level in this sample. The resonances observed for this substitution level are much broader than for the 20% and 30% samples due to the higher disorder in the structure. Additionally the proton level in $BaZr_{0.90}Y_{0.10}O_{2.95-y}(OH)_{2y}$ is extremely limited compared to all other samples which is once again in agreement with our findings of Chapter 3 where the actual sample formula was reported to be $(Ba_{0.954}Y_{0.0456})(Sn_{0.946}Y_{0.054})O_{2.996}$ leaving very few oxygen vacancies for hydration.

At -120°C the different resonances are not as well resolved as for $BaZr_{1-x}Sc_xO_{3--x/2-y}(OH)_{2y}$. This makes it more difficult to evaluate with confidence the number of proton environments encountered in the structure. After deconvolution it appears that all spectra can be well fitted by using three sites with chemical shifts of 7.3, 5.2 and 2.7 ppm. The resonance at 2.7 ppm is clearly not taking part into the proton hopping observed at room temperature, or at least not all the protons in this environment are participating in the local motion. The ratio of this site is also increasing with yttrium substitution; therefore we can assign this resonance to the more immobile Y-OH-Y environments while the resonances at 5.2 and 7.3 ppm can be attributed to Zr-OH-Y and Zr-OH-Zr environments respectively. These shifts are closely related to the ones observed in $BaZr_{1-x}Sc_xO_{3-x/2-y}(OH)_{2y}$ where Zr-OH-Sc and Sc-OH-Sc were reported at 4.5 and 2.9 ppm respectively.

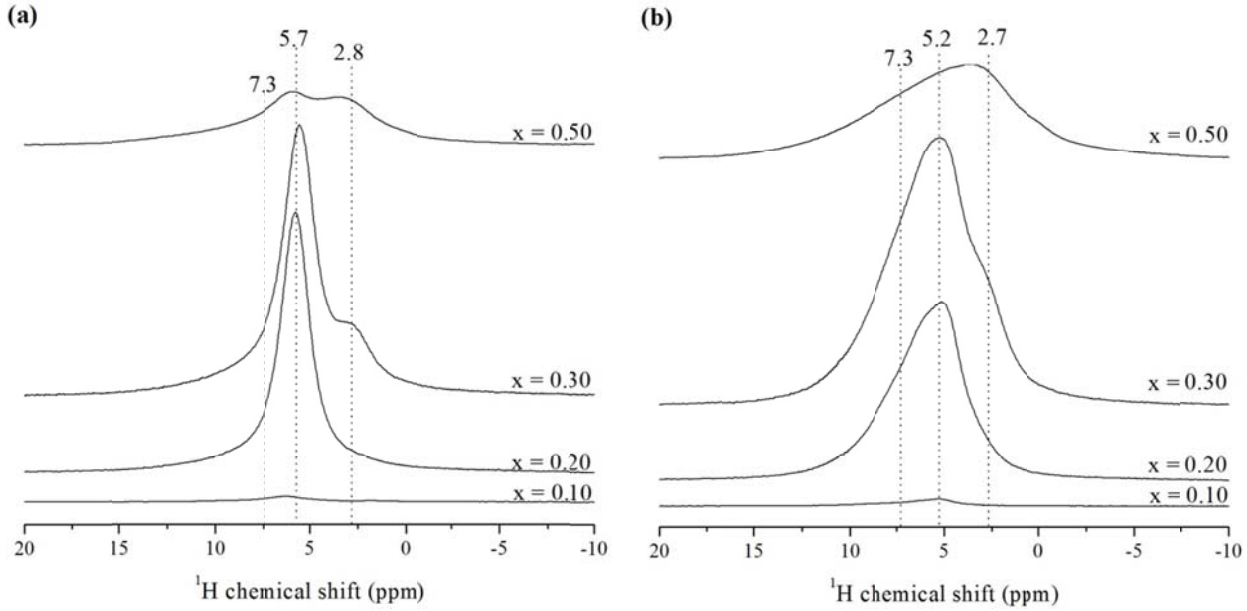

Figure 5.6. ^{1}H NMR of $BaZr_{1-x}Y_xO_{3-x/2-y}(OH)_{2y}$ at (a) 25°C and (b) -120°C. Spectra referenced to TMS.

The ratios of the different sites extracted by spectral deconvolution are gathered in *Table 5.2*. According to Chapter 3, the cations seemed to be randomly distributed over the B site with a possible ordering of the oxygen vacancies in between Y atoms preventing us from observing Y-O-Y environment in higher substituted samples as observed by ^{17}O NMR. Our ^{1}H NMR results suggest preferential ordering of proton next to yttrium. Indeed we observe a higher number of Zr-OH-Y sites in both $BaZr_{0.90}Y_{0.10}O_{2.95-y}(OH)_{2y}$ and $BaZr_{0.80}Y_{0.20}O_{2.90-y}(OH)_{2y}$ and a higher number of Y-OH-Y environments for all substitution levels expect the 10% sample. What is more surprising is that the protons tend to distribute over the Y-O-Y and Zr-O-Zr sites preferentially, leaving the Zr-O-Y sites under populated in $BaZr_{0.70}Y_{0.30}O_{2.85-y}(OH)_{2y}$ and $BaZr_{0.50}Y_{0.50}O_{2.75-y}(OH)_{2y}$ by comparison to a random distribution model. However caution has to be taken for two reasons. First not all the motion is being frozen out at -120°C; therefore the extracted ratios do not correspond to a purely enthalpic distribution. Secondly the resonance at 5.2 ppm could very well be remaining from the coalescence of the resonances at 7.3 and 2.7 ppm due to strong residual protonic exchange at -120°C. At low substitution levels, 20% and below, there are almost no Y-OY environments available in the structure (about 7% in $BaZr_{0.80}Y_{0.20}O_{2.90-y}(OH)_{2y}$); therefore the protons will be distributed only over Zr-O-Zr and Zr-O-Y sites and the conduction mechanism will be maximized as the time for the protons spent in the

vicinity of yttrium cations is limited. Above 20% substitution, there are enough Y-O-Y sites to host a large amount of the proton population: 20% and 61% in the case of $BaZr_{0.70}Y_{0.30}O_{2.85-y}(OH)_{2y}$ and $BaZr_{0.50}Y_{0.50}O_{2.75-y}(OH)_{2y}$ respectively as estimated from deconvolution. This tendency for protons to occupy Y-O-Y sites at higher substitution levels considerably decreases the protonic conductivity of the materials. If we assume that the rest of the protons, Zr-OH-Y and Zr-OH-Zr, have the same mobility throughout the solid-solution, the ones in $BaZr_{0.70}Y_{0.30}O_{2.85-y}(OH)_{2y}$ and $BaZr_{0.50}Y_{0.50}O_{2.75-y}(OH)_{2y}$ will soon encounter a Y-O-Y environment where they will be residing for a much longer time than on Zr-O-Zr or Zr-O-Y, thereby reducing the conductivity in those two materials. Our proton assignment and the observed ratios nicely explain the conductivity results reported in the literature,[10-11, 20-21] hereby supporting our assignment and the minimal effect of the residual protonic exchange at -120°C. The proton distribution observed in $BaZr_{1-x}Y_xO_{3-\delta}$ clearly explains the conductive behavior reported for this material, the best conductivities being obtained for substitution levels between 10 and 20%.

Table 5.2. Ratios of the different proton sites in $BaZr_{1-x}Y_xO_{3-x/2-y}(OH)_{2y}$ at -120°C.

x	Deconvolution results by site (ppm)			Random distribution model		
	7.3	5.2	2.6	Zr-OH-Zr	Zr-OH-Y	Y-OH-Y
0.10	0.68(2)	0.32(3)	0.0(0)	0.81	0.18	0.01
0.20	0.53(3)	0.40(8)	0.07(2)	0.64	0.32	0.04
0.30	0.48(4)	0.32(5)	0.20(1)	0.49	0.42	0.09
0.50	0.24(3)	0.16(6)	0.61(4)	0.25	0.50	0.25
Assignment	Zr-OH-Zr	Zr-OH-Y	Y-OH-Y			

Figure 5.7 illustrates the change in protonic distribution as the temperature of $BaZr_{1-x}Y_xO_{3x/2-y}(OH)_{2y}$ is decreased. For $BaZr_{0.70}Y_{0.30}O_{2.85-y}(OH)_{2y}$ we see the growth of the site at 2.6 ppm as the temperature is reduced along with the appearance of a broad resonance at 7.3 ppm. The resonance at 5.2 ppm gets broader with cooling; however its intensity does not vary much supporting the fact that this resonance is more likely due to Zr-OH-Y environments than the result of coalescence of the 7.3 and 2.6 ppm resonances. In addition if the resonance observed at 5.5 ppm at room temperature were only due to coalescence of the 7.3 and 2.6 ppm sites, it should occur at the weight ratio of these two resonances, therefore at a shift of approximately 4.0 ppm

based on the deconvolution results for both $BaZr_{0.80}Y_{0.20}O_{2.90-y}(OH)_{2y}$ and $BaZr_{0.70}Y_{0.30}O_{2.85-y}(OH)_{2y}$. This once again corroborates the observation of Zr-OH-Y environments at 5.2 ppm.

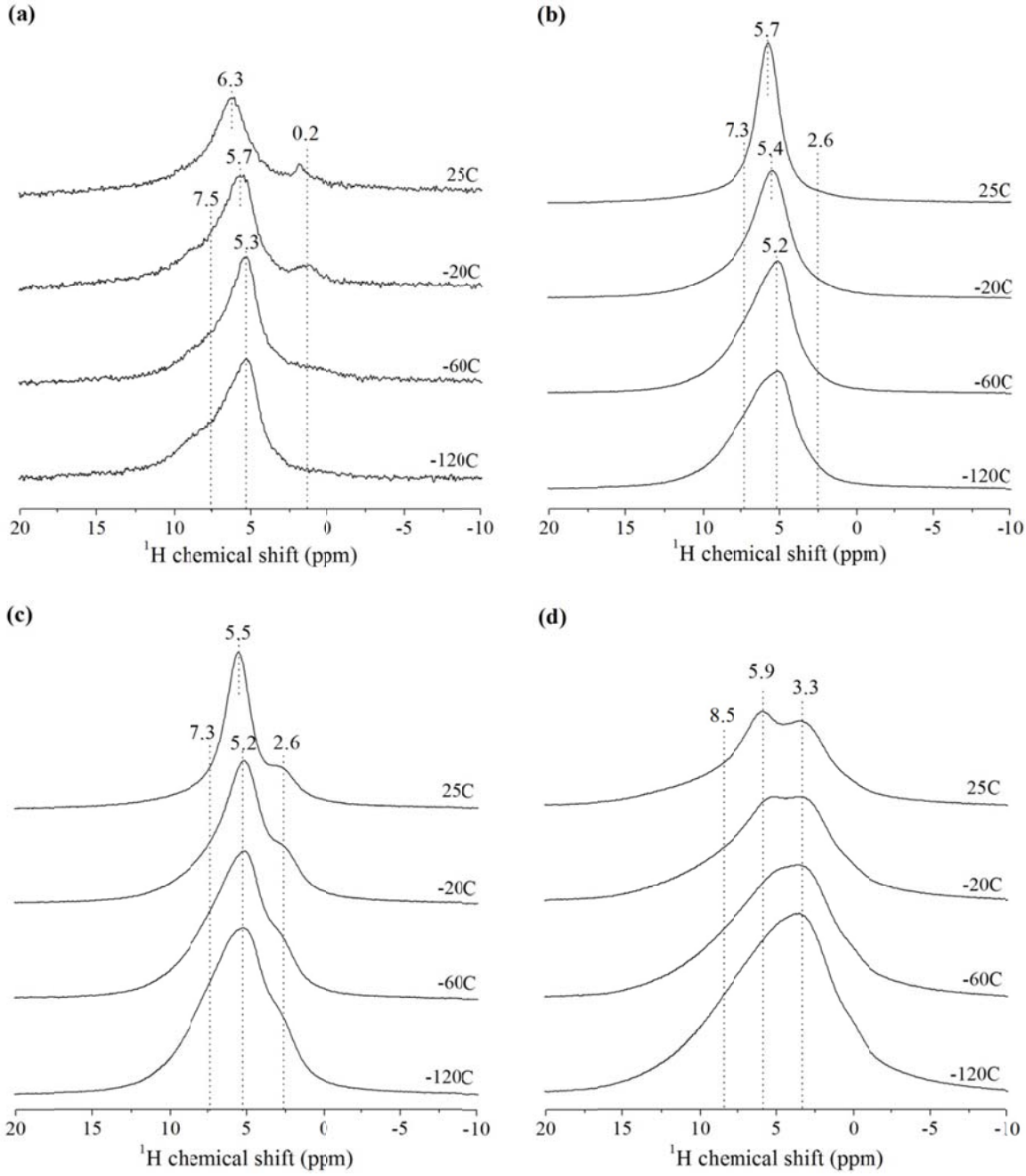

Figure 5.7. ^{1}H NMR of $BaZr_{1-x}Y_xO_{3-x/2-y}(OH)_{2y}$ at low temperatures. (a) x = 0.10, (b) x = 0.20, (c) x = 0.30 and (d) x = 0.50. Spectra referenced to TMS.

The spin-spin relaxation behavior T_2 of the different proton environments is shown in *Figure 5.8*. Similarly to $BaZr_{0.85}Sc_{0.15}O_{2.925-y}(OH)_{2y}$ the resonance at 2.8 ppm is the last to fully relax, confirming the higher immobility of the Y-OH-Y protons that are not participating in the motion at 25°C.

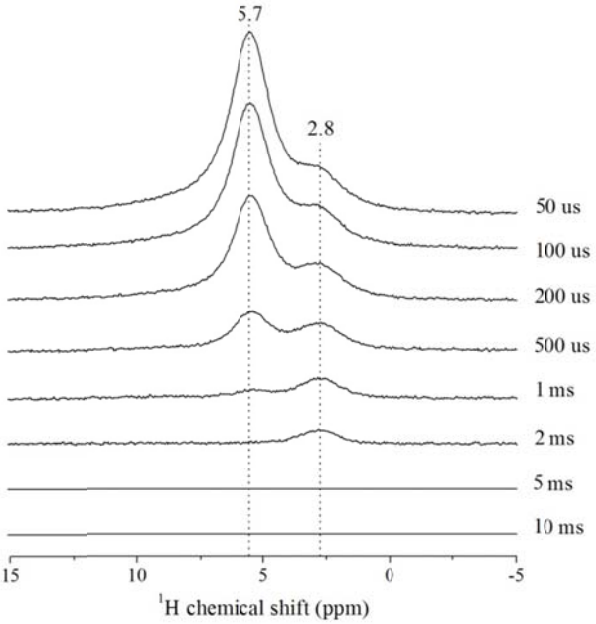

Figure 5.8. ^1H spectra recorded with different Hahn echo delays to determine the T_2 relaxation rates for the different proton environments in $BaZr_{0.70}Y_{0.30}O_{2.85-y}(OH)_{2y}$ at 25°C. The values on the right correspond to the delay time between the 90° and the 180° pulses. Spectra referenced to TMS.

Tables 5.3 and 5.4 present detailed ratios and relaxation times for all temperatures in $BaZr_{0.80}Y_{0.20}O_{2.90-y}(OH)_{2y}$ and $BaZr_{0.70}Y_{0.30}O_{2.85-y}(OH)_{2y}$ respectively. All relaxation times, T_1, T_2 and $T_{1\rho}$, show the higher rigidity of protons on the Y-O-Y site at 25°C. As the temperature decreases, the motion is frozen out and the relaxation times for all three proton sites become similar. There is no clear evidence of a higher rigidity of protons on Zr-O-Y *vs.* Zr-O-Zr; however the distribution of protons over these two sites is strongly influenced by the temperature.

Table 5.3. Ratios and T_1, T_2, $T_{1\rho}$ relaxation times at low temperatures for $BaZr_{0.80}Y_{0.20}O_{2.90-y}(OH)_{2y}$.

Temperature (°C)	Site (ppm)	Ratio	T_1 (s) [(a)]	T_2 (ms)	$T_{1\rho}$ (ms)
-120	7.3	0.53(3)	23.70	3.1(4)	21(4)
	5.1	0.40(8)	24.67	3.1(3)	26(5)
	2.7	0.07(2)	19.42	- [(b)]	- [(b)]
-60	7.3	0.50(2)	6.22	1.07(9)	13(2)
	5.1	0.45(6)	6.38	0.89(7)	12(2)
	2.7	0.05(2)	5.67	0.10(2)	12(2)
-20	7.0	0.43(2)	0.79	0.32(3)	3.0(3)
	5.4	0.53(4)	0.81	0.26(2)	3.1(3)
	2.7	0.03(1)	0.81	0.16(2)	2.7(5)
25	7.3	0.14(0)	0.12	0.16(2)	1.4(1)
	5.7	0.86(1)	0.13	0.30(2)	1.4(0)
	2.7	0	-	-	-

[(a)] T_1 value estimated from the τ time for the zero intensity point, [(b)] Intensity too small to allow estimation of T_2.

Table 5.4. Ratios and T_1, T_2, $T_{1\rho}$ relaxation times at low temperatures for $BaZr_{0.70}Y_{0.30}O_{2.85-y}(OH)_{2y}$.

Temperature (°C)	Site (ppm)	Ratio	T_1 (s) [(a)]	T_2 (ms)	$T_{1\rho}$ (ms)
-120	7.3	0.48(0)	13.13	2.3(5)	20(4)
	5.1	0.32(0)	13.03	1.8(3)	22(4)
	2.7	0.20(0)	11.01	1.1(3)	22(6)
-60	7.3	0.49(1)	4.24	1.1(1)	14(3)
	5.1	0.34(0)	4.20	0.8(1)	12(1)
	2.7	0.17(0)	4.10	0.9(2)	18(2)
-20	7.1	0.36(1)	0.58	0.4(1)	5.1(6)
	5.1	0.44(0)	0.59	0.3(0)	4.2(3)
	2.5	0.20(0)	0.71	0.7(2)	13(2)
25	7.2	0.17(1)	0.07	0.3(0)	1.4(1)
	5.5	0.66(0)	0.08	0.3(0)	1.5(1)
	2.7	0.18(0)	0.14	0.8(4)	5.5(10)

[(a)] T_1 value estimated from the τ time for the zero intensity point.

For $BaZr_{0.70}Y_{0.30}O_{2.85-y}(OH)_{2y}$ at -120°C, we observe 48% of protons on Zr-O-Zr and 32% on Zr-O-Y, this distribution being dominated by the entropy factor. At 25°C we now observe 17% of protons on Zr-O-Zr and 66% on Zr-O-Y. At this temperature, the protons have enough energy to reorganize over the oxygen sites and tend to get trapped on the Zr-O-Y environments for charge balance reasons. Throughout the whole set of temperatures, the number of protons on Y-O-Y does not seem to vary; these protons are strongly bonded to their oxygen site. For $BaZr_{0.80}Y_{0.20}O_{2.90-y}(OH)_{2y}$ the distribution of protons over Zr-O-Zr and Zr-O-Y follows the same pattern, going from 0.53:0.40 to 0.14:0.86 at -120°C and 25°C respectively.

D. Low temperature ^{1}H NMR of $BaSn_{1-x}Y_xO_{3-x/2-y}(OH)_{2y}$

The ^{1}H NMR results of $BaSn_{1-x}Y_xO_{3-x/2-y}(OH)_{2y}$ (x = 0.10, 0.30 and 0.50) at room temperature and -120°C are plotted in *Figure 5.9*. The spectra at room temperature show one resonance at 4.2 – 4.5 ppm throughout the solid solution with a clear increase of the proton concentration with yttrium substitution level. At low temperature we can observe two resonances for all substitution levels, the first one at 3.7 ppm and the second at 7.3 ppm. In comparison to the two previous systems, the resonance at 7.3 ppm can be assigned to Sn-OH-Sn environment and the one at 3.7 ppm to Sn-OH-Y environments.

In Chapter 3, the structural analysis of $BaSn_{1-x}Y_xO_{3-\delta}$ revealed the cation ordering of Sn and Y at higher substitution levels. Under such circumstances, one would expect to only observe one proton environment, Sn-OH-Y, for $BaSn_{0.50}Y_{0.50}O_{2.75-y}(OH)_{2y}$. However, it was apparent by ^{17}O NMR that the structure was not fully ordered as some Sn-O-Sn environments were still observed in $BaSn_{0.50}Y_{0.50}O_{2.75}$. Additionally the ^{89}Y NMR revealed that some of the oxygen vacancies seemed to be located in between Sn atoms forming Sn-□-Sn environments, in agreement with one computational study.[29] After hydration these Sn-□-Sn environments become Sn-O-Sn sites, additional potential hosts for protons. When those new Sn-O-Sn environments are added to the Sn-O-Sn sites present before hydration, the ratio of Sn-O-Sn environments turns out to represent a considerable amount of the overall oxygen sites as is observed in *Figure 5.9*.

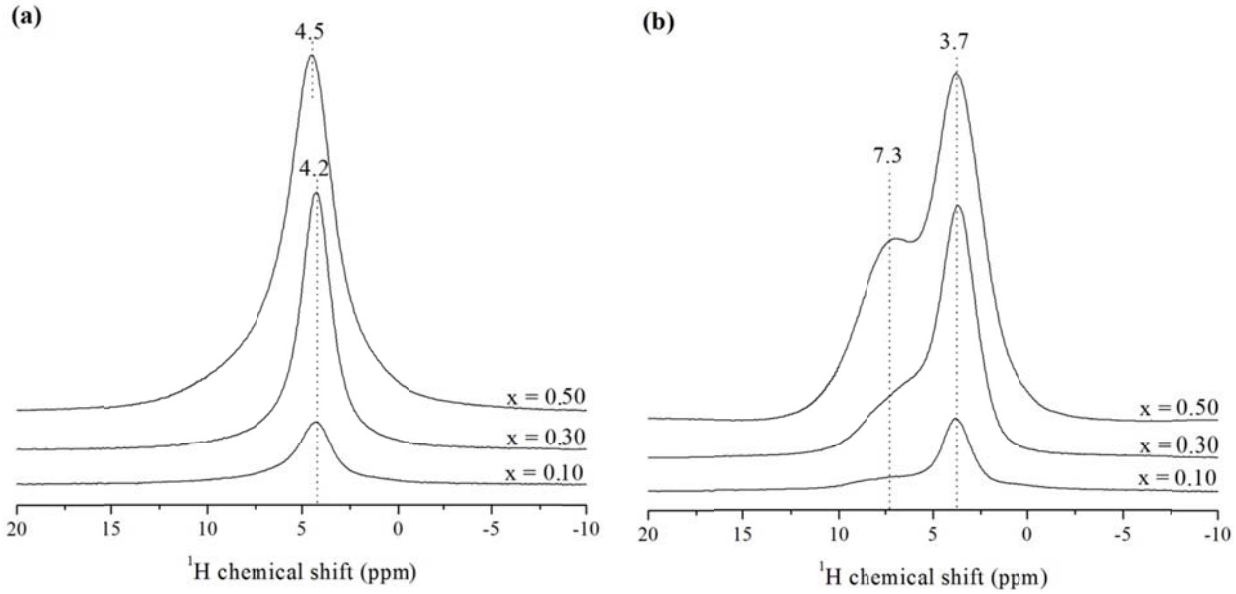

Figure 5.9. ^{1}H NMR of $BaSn_{1-x}Y_xO_{3-x/2-y}(OH)_{2y}$ at (a) 25°C and (b) -120°C. Spectra referenced to TMS.

After deconvolution of the low temperature ^{1}H spectra (*Table 5.5*), it appears that the ratio of Sn-OH-Sn to Sn-OH-Y varies only slightly throughout the series, the amount of Sn-OH-Y only increasing by 2% from $BaSn_{0.70}Y_{0.30}O_{2.85-y}(OH)_{2y}$ to $BaSn_{0.50}Y_{0.50}O_{2.75-y}(OH)_{2y}$. Since yttrium prefers being 6 coordinate rather than 5, the vacancies tend to order in between Sn atoms and limit the amount of ordering that can actually exist in $BaSn_{0.50}Y_{0.50}O_{2.75-\delta}$. This corroborates the difficulty in preparing long range ordered $BaSn_{0.50}Y_{0.50}O_{2.75-\delta}$; there will always be a tendency for some Sn to cluster hereby preventing the yttrium cations from becoming 5-coordinate.

Table 5.5. Ratios of the different proton sites in $BaSn_{1-x}Y_xO_{3-x/2-y}(OH)_{2y}$ at -120°C.

x	Sites (ppm)	
	7.3	3.7
0.10	0.21(1)	0.76(1)
0.30	0.32(1)	0.68(1)
0.50	0.34(2)	0.66(2)
Assignment	Sn-OH-Sn	Sn-OH-Y

Figure 5.10 shows the ^{1}H NMR distribution for $BaSn_{1-x}Y_xO_{3-x/2-y}(OH)_{2y}$ when decreasing the temperature. The motion is frozen more quickly than for $BaZr_{1-x}Y_xO_{3-x/2-y}(OH)_{2y}$ where even at -120°C some exchange was still observed. The clustered Sn cations certainly prevent the $BaSn_{1-x}Y_xO_{3-\delta}$ system from conducting protons as well as in $BaZr_{0.80}Y_{0.20}O_{2.90-\delta}$. Once again the motion observed at room temperature is limited to nearby oxygen sites, the Sn clusters must therefore be small enough to participate in this exchange with Sn-O-Y environments. This would result in a distribution of Sn clusters throughout the structure, an additional barrier for the protons to conduct: the higher the number of Sn clusters, the more the protonic conduction will be slowed down.

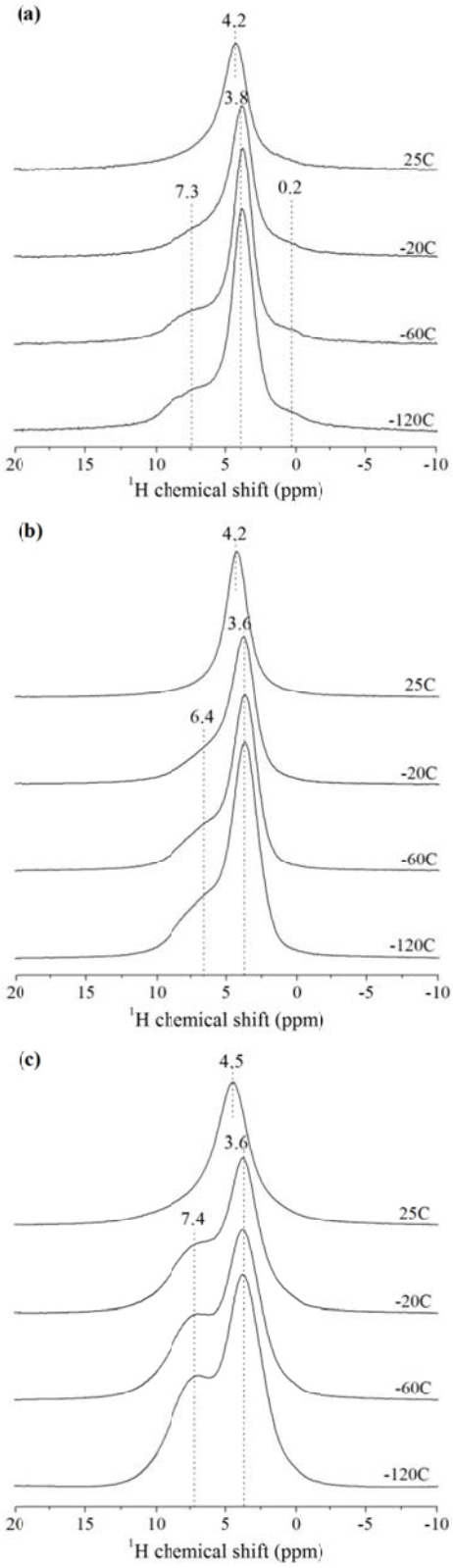

Figure 5.10. ^{1}H NMR of $BaSn_{1-x}Y_xO_{3-x/2-y}(OH)_{2y}$ at low temperatures. (a) x = 0.10, (b) x = 0.30 and (c) x = 0.50. Spectra referenced to TMS.

Figure 5.11 illustrates the spin-spin relaxation behavior of Sn-OH-Sn and Sn-OH-Y at -120°C in $BaSn_{0.50}Y_{0.50}O_{2.75-y}(OH)_{2y}$. The two proton sites have very similar behaviors; one does not seem to relax faster than the other one. This corroborates our assignment, since from the two previous systems a Y-OH-Y environment should be slower to relax due to its higher immobility.

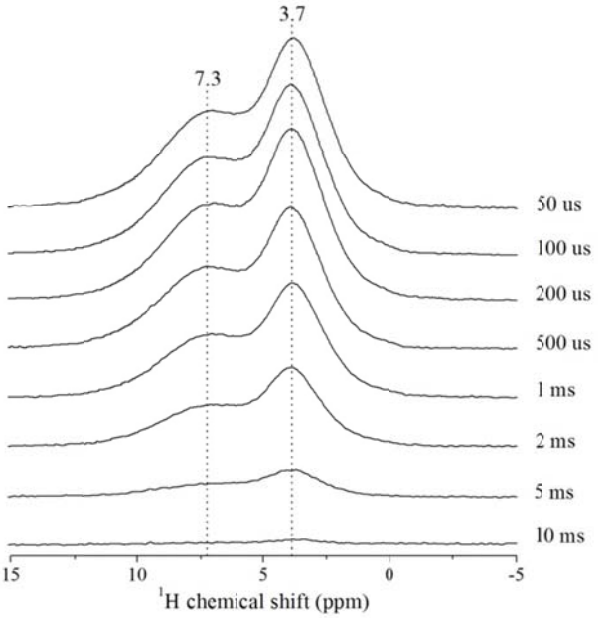

Figure 5.11. ^{1}H spectra recorded with different Hahn echo delays to determine the T_2 relaxation rates for the different proton environments in $BaSn_{0.50}Y_{0.50}O_{2.75-y}(OH)_{2y}$ at -120°C. The values on the right correspond to the delay time between the 90° and the 180° pulses. Spectra referenced to TMS.

E. High temperature ^{1}H NMR

1. $BaZr_{1-x}Y_xO_{3-x/2-y}(OH)_{2y}$

The protonic behavior at high temperatures in $BaZr_{0.70}Y_{0.30}O_{2.85-y}(OH)_{2y}$ is shown in *Figure 5.12*. The spinning speed for high temperature spectra is considerably reduced compared to low temperature results, 6 kHz *vs.* 14 kHz, which explains the lack of resolution observed at room temperature compared to the previous set of results. From room temperature to 250°C, the chemical shift of the observed resonance at 3.5 ppm shifts to higher frequencies. In this temperature range, the samples are not losing water; therefore we can assume that the protons are simply redistributing themselves throughout the structure, more of the Zr-O-Zr environments being occupied as the temperature increases. This illustrates the tendency for protons to conduct

in the material: the protons are leaving the sites with smaller enthalpy but higher activation energy, Zr-O-Y and Y-O-Y, for sites where they can exchange more freely, *i.e.* Zr-O-Zr. Some of the protons are still trapped on the Y-O-Y environments (shoulder at lower frequencies), since the $BaZr_{0.70}Y_{0.30}O_{2.85-y}(OH)_{2y}$ sample does contain a non-negligible amount of such sites. Above 300°C the shift of the protons gradually decreases to 0.9 ppm. According to section III.A this region of chemical shift corresponds to hydroxide species; the structure is now dehydrating as well as conducting protons. Due to the gradual decrease of the chemical shift with temperature, this could be illustrating the opening of the structure with temperature leading to proton environments less hydrogen-bonded to the nearest oxygen atom. The resonance becomes sharper as the temperature of 750°C is reached. The ^1H spectrum after the high temperature experiment, back at room temperature, shows a clear drop in proton concentration and the protons seem to be occupying most of the oxygen sites nearby yttrium, *i.e.* both Zr-O-Y and Y-O-Y.

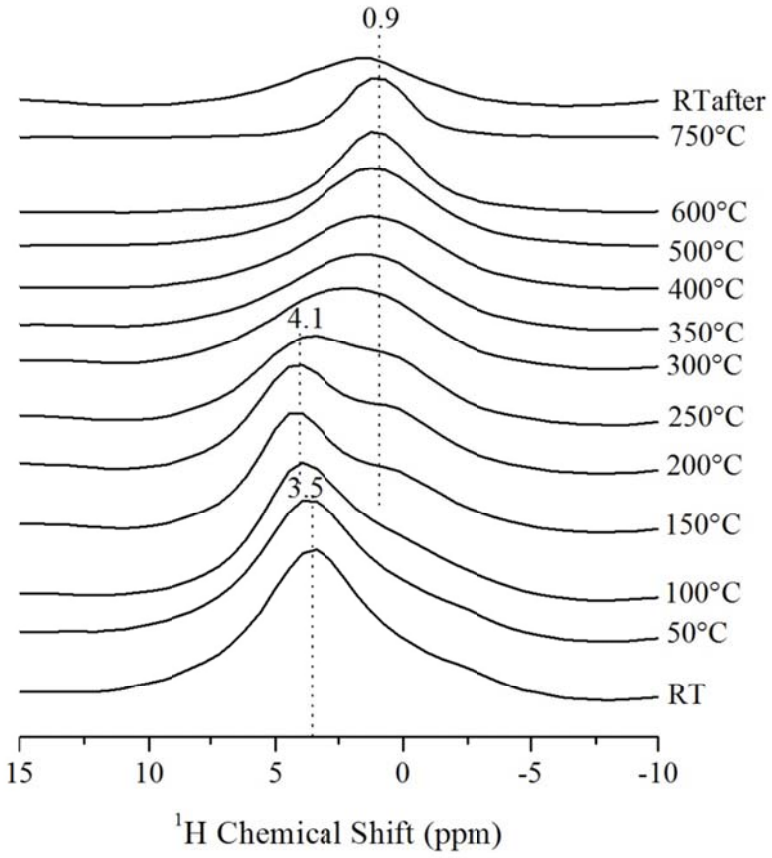

Figure 5.12. High temperature ^1H NMR of $BaZr_{0.70}Y_{0.30}O_{2.85-y}(OH)_{2y}$. Spectra referenced to water.

A similar pattern is observed for protons in $BaZr_{0.50}Y_{0.50}O_{2.75-y}(OH)_{2y}$ (*Figure 5.13*). The protons seem to leave the structure at higher temperatures, starting at 500°C. In the 200°C to 400°C temperature range, we observed an additional resonance at 2.5 ppm indicating that some of the protons are hosted on Y-O-Y. They reside on this site until 500°C, the temperature at which the expansion of the unit cell becomess non-negligeable. Above 500°C, the cell expansion decreases the strength of the hydrogen-bonding leading to a decrease in chemical shift. At 600°C and above, we observe a sharper shift at 1.1 ppm illustrating the higher mobility of the protons, free from hydrogen-bonding. Once again after the experiment, the proton distribution at room temperature seems to be mostly distributed on Y-O-Y environments.

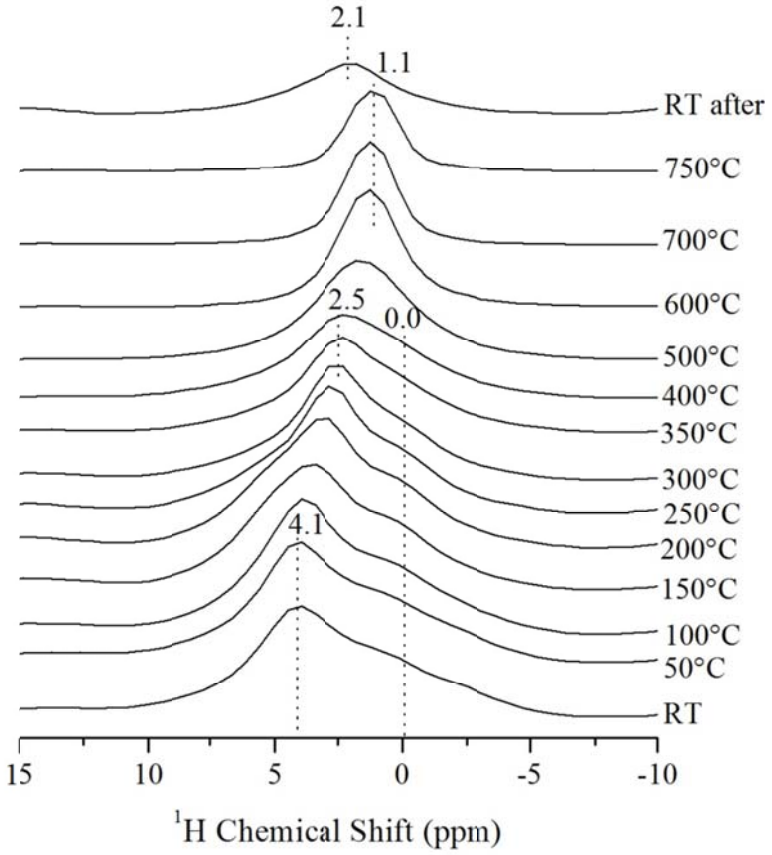

Figure 5.13. High temperature ^{1}H NMR of $BaZr_{0.50}Y_{0.50}O_{2.75-y}(OH)_{2y}$. Spectra referenced to water.

2. $BaSn_{1-x}Y_xO_{3-x/2-y}(OH)_{2y}$

Fewer temperatures were recorded for the $BaSn_{1-x}Y_xO_{3-\delta}$ system. Nevertheless a clear sharpening of the proton resonance is observed for $BaSn_{0.50}Y_{0.50}O_{2.75-y}(OH)_{2y}$ (*Figure 5.14*) with a gradual shift from 3.1 to 1.9 ppm. The protons seem to be hopping in between Sn-O-Y sites until they reach the surface and become hydroxide species (1.9 ppm) before being released in the atmosphere. After the experiment the proton concentration has dropped and is mostly distributed on the Sn-O-Y environments.

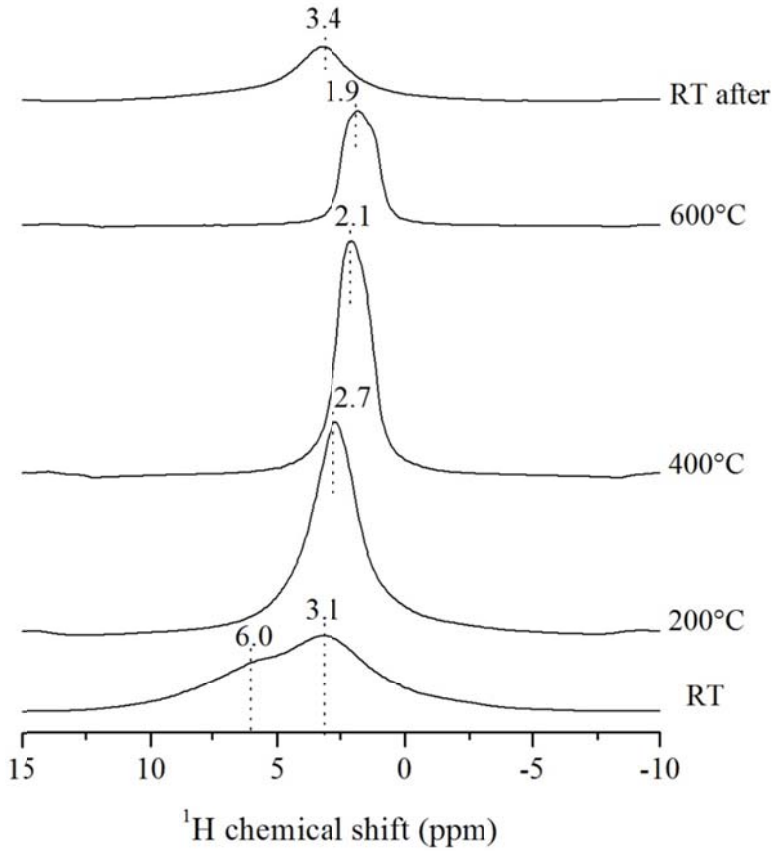

Figure 5.14. High temperature ^{1}H NMR of $BaSn_{0.50}Y_{0.50}O_{2.75-y}(OH)_{2y}$. Spectra referenced to water.

A similar trend is observed for $BaSn_{0.70}Y_{0.30}O_{2.85-y}(OH)_{2y}$ (*Figure 5.15*); however in this case, the structure seems to reach full dehydration close to 600°C. Even after coming back to room temperature, there are barely any protons detected by NMR.

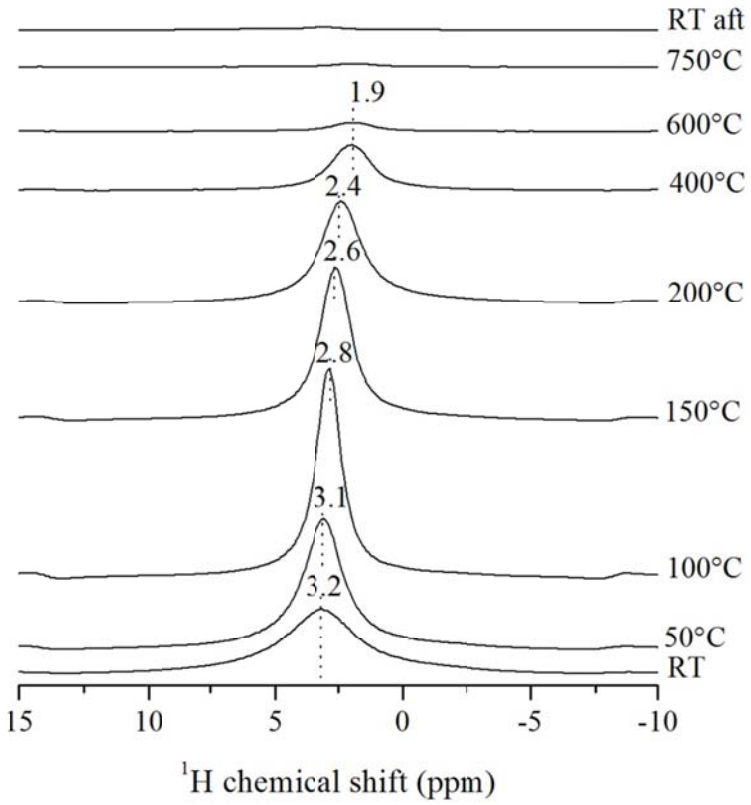

Figure 5.15. High temperature ^{1}H NMR of $BaSn_{0.70}Y_{0.30}O_{2.85-y}(OH)_{2y}$. Spectra referenced to water.

IV. Discussion

The TRAPDOR and low temperature ^{1}H NMR results clearly highlight the structural differences underlying the three protonic conductors studied here and the consequences on their conduction characteristics. The protonic distribution in $BaZr_{1-x}Sc_xO_{3-\delta}$ suggests that the protons exhibit higher affinity to scandium. For the 30% substituted material, the majority of the protons exist on Sc-O-Sc sites. In the case of $BaZr_{1-x}Y_xO_{3-\delta}$ until a substitution level of 30% is reached, we do not observe the presence of Y-OH-Y environments and only a minority of protons are hosted on the Y-O-Y site in $BaZr_{0.80}Y_{0.20}O_{2.90-y}(OH)_{2y}$. From the T_2 experiments it occurs that the "trapping" site, *i.e.* Sc-O-Sc or Y-O-Y, leads to proton species that are much more rigid.

These protons are less likely to participate in the conduction mechanism or will require a lot more energy to escape those sites. In $BaZr_{0.70}Sc_{0.30}O_{2.85-y}(OH)_{2y}$ the majority of the protons exist on Sc-O-Sc environments, which easily explains the lower conductivity observed for $BaZr_{1-x}Sc_xO_{3-\delta}$ compared to $BaZr_{0.70}Y_{0.30}O_{2.85-y}(OH)_{2y}$. Most of the protons in $BaZr_{0.70}Sc_{0.30}O_{2.85-y}(OH)_{2y}$ are immobile and the energy required for conduction will be dedicated to "untrapping" those protons.

Due to the smaller size of scandium compared to yttrium, with respective ionic radii of 0.75 and 0.90 Å,[42] the lattice parameter in $BaZr_{1-x}Sc_xO_{3-\delta}$ is much smaller than in $BaZr_{1-x}Y_xO_{3-\delta}$.[34, 37] If we think of a proton being hosted on a Sc-O-Sc site *vs.* Y-O-Y site, the Sc…Sc atomic distance is much shorter than the Y…Y one, therefore increasing the hydrogen-bonding of the proton with the nearest oxygen which in turn increases the energy for the proton to "escape" from the Sc-O-Sc site. A similar effect noticed by infrared spectroscopy supports the unique behavior upon hydration in $BaZr_{1-x}Sc_xO_{3-\delta}$.[36] In $BaZr_{1-x}Y_xO_{3-\delta}$ the more homogenous repartition of X-O-X distances (X = Zr or Y) keeps the protons more mobile, unless they happened to be hosted by a Y-O-Y environment. It increases the chances for proton to hop around freely as long as the Y concentration stays below 30%, therefore increasing the conductivity of $BaZr_{1-x}Y_xO_{3-\delta}$ compared to $BaZr_{1-x}Sc_xO_{3-\delta}$. The low temperature ^1H NMR experiments also show the need to keep the yttrium substitution to low levels in order to keep the proton mobile. Above 20% substitution a non negligible amount of protons will not actively participate in the conductivity mechanism for extended periods of time and the probability for the more mobile protons to encounter a Y-O-Y site on the way increases with substitution level.

The case of $BaSn_{1-x}Y_xO_{3-\delta}$ is slightly different mostly due to the cation ordering occurring in this structure at substitution levels of 30% and above. The cation ordering should in principle create a network of oxygen sites all identical to one another, Sn-O-Y, preventing the presence of trapping sites, Y-O-Y, and therefore increasing the conductivity, all sites having the same enthalpy. However the presence of Sn clusters distributed throughout the structure considerably reduces the protonic conductivity in the material.

In the end $BaZr_{1-x}Y_xO_{3-\delta}$ with 10 to 20 % of yttrium substitution appears to be the best candidate of all three systems studied for protonic conduction. It presents a limited amount of trapping sites, Y-O-Y, unlike in $BaZr_{0.85}Sc_{0.15}O_{2.925-y}(OH)_{2y}$ where a large portion of the protons occupies Sc-O-Sc sites and becomes immobile. Even though the protons do not tend to be trapped, the material still holds the protons over a large range of temperatures unlike $BaSn_{0.50}Y_{0.50}O_{2.75-y}(OH)_{2y}$ where a high concentration of protons is being released starting at 600°C. This is all the more important since the condition under which these materials will be used, will bring a constant balance between dehydration and faster protonic motion at higher temperature. Y^{3+} is also the cation with the closest radius to Zr^{4+}, hereby limiting the amount of distortion encountered in the structure and facilitating the protonic motion.

In order to propose a better perovskite based protonic conductor, it is important to keep all these requirements in mind. It seems very unlikely to find a substituting element that would leave the $BaZrO_3$ structure or any other perovskite based material as little distorted as possible, provide a limited amount of trapping sites, *i.e.* prevent clustering of the substituting cation, dehydrate at the highest possible temperature, in our case better than 600°C, and finally present a smaller activation energy than the one reported for protons in $BaZr_{1-x}Y_xO_{3-\delta}$. The lanthanide family may contain a possible candidate but it is far from being an easy set of requirements to meet. Further research will be needed in order to evaluate additional candidates.

V. Conclusions

A set of ^{1}H NMR experiments allowed the clarification of the different protonic conduction reported in the literature for $BaZr_{1-x}Sc_xO_{3-\delta}$, $BaSn_{1-x}Y_xO_{3-\delta}$ and $BaZr_{1-x}Y_xO_{3-\delta}$. The clustering of the oxygen vacancies between Sc cations in $BaZr_{1-x}Sc_xO_{3-\delta}$ results in a high concentration of Sc-O-Sc environments in the hydrated structure, the environments which turn out to be the perfect trapping site for proton. The shorter Sc…Sc distance involved in this configuration due to the considerably smaller size of Sc^{3+} compared to Zr^{4+} spatially confines the proton and reduces its acidity. This proton becomes secluded from the rest of the structure and the activation energy required for its motion will be particularly costly to reach, limiting the potential conductivity in $BaZr_{1-x}Sc_xO_{3-\delta}$. Due to the cation ordering present in $BaSn_{1-x}Y_xO_{3-\delta}$ at high substitution levels, one could expect $BaSn_{0.50}Y_{0.50}O_{2.75-\delta}$ to be the perfect protonic conductor. Indeed such an arrangement should leave in theory only one oxygen site, Sn-O-Y, facilitating the motion of protons through the structure as all oxygen sites have the same energy. However this implies the presence of a high 5 coordinate Y concentration, while yttrium is much more comfortable in a 6 coordinate geometry. Therefore in order to avoid a high number of 5 coordinate Y, the oxygen vacancies order in between Sn cations, leading to a non negligible concentration of Sn-O-Sn sites after hydration. The ^{1}H NMR results at 25°C showed that these Sn-rich clusters are limited in size since the protons hosted on Sn-O-Sn environments participate in the local motion at room temperature. However it implies that a considerable amount of these small clusters are distributed throughout the structure to prevent a high concentration of 5 coordinate Y environments and any mobile proton is even more likely to encounter such clusters and be slowed down in their motion. In $BaZr_{1-x}Y_xO_{3-\delta}$ the similar size of Y^{3+} and Zr^{4+} leaves the structure almost undistorted after substitution which results in a more homogeneous distribution of O…O distances. Therefore the protons are less attracted to Y-O-Y environments than to Sc-O-Sc in $BaZr_{1-x}Sc_xO_{3-\delta}$ and remain more mobile at identical substitution levels. However the concentration of Y-O-Y environment will remain related to the yttrium concentration and result in a tendency for protons to locate on Y-O-Y in $BaZr_{0.70}Y_{0.30}O_{2.85-y}(OH)_{2y}$ and $BaZr_{0.50}Y_{0.50}O_{2.75-y}(OH)_{2y}$ since such sites exist; therefore it is only natural to have to limit the concentration of yttrium to low substitution levels to keep the protons mobile. Our ^{1}H NMR results showed that the sample with the highest concentration of mobile protons, Zr-OH-Zr and Zr-OH-Y, is $BaZr_{0.80}Y_{0.20}O_{2.90-y}(OH)_{2y}$ in agreement with reported conduction results. According to our

analysis, it will be quite difficult to find a substituting element more suited than yttrium in $BaZrO_3$ and that will lead to higher conductive performances.

VI. References

1. H. Iwahara, H. Uchida, K. Ono and K. Ogaki, *Journal of the Electrochemical Society*, 1988, **135**, 529.

2. H. Iwahara, T. Yajima, T. Hibino, K. Ozaki and H. Suzuki, *Solid State Ionics*, 1993, **61**, 65.

3. R. C. T. Slade, S. D. Flint and N. Singh, *Solid State Ionics*, 1995, **82**, 135.

4. K. D. Kreuer, *Solid State Ionics*, 1997, **97**, 1.

5. P. Murugaraj, K. D. Kreuer, T. He, T. Schober and J. Maier, *Solid State Ionics*, 1997, **98**, 1.

6. T. Schober, *Solid State Ionics*, 1998, **109**, 1.

7. K. D. Kreuer, *Solid State Ionics*, 1999, **125**, 285.

8. H. G. Bohn and T. Schober, *Journal of the American Ceramic Society*, 2000, **83**, 768.

9. K. Katahira, Y. Kohchi, T. Shimura and H. Iwahara, *Solid State Ionics*, 2000, **138**, 91.

10. K. D. Kreuer, S. Adams, W. Münch, A. Fuchs, U. Klock and J. Maier, *Solid State Ionics*, 2001, **145**, 295.

11. K. D. Kreuer, *Annual Review of Materials Research*, 2003, **33**, 333.

12. O. Parkash, D. Kumar, K. K. Srivastav and R. K. Dwivedi, *Journal of Materials Science*, 2001, **36**, 5805.

13. F. M. M. Snijkers, A. Buekenhoudt, J. Cooymans and J. J. Luyten, *Scripta Materialia*, 2004, **50**, 655.

14. P. Singh, O. Parkash and D. Kumar, *Journal of Materials Science: Materials in Electronics*, 2005, **16**, 145.

15. F. Iguchi, N. Sata, T. Tsurui and H. Yugami, *Solid State Ionics*, 2007, **178**, 691.

16. S. B. C. Duval, P. Holtappels, U. F. Vogt, E. Pomjakushina, K. Conder, U. Stimming and T. Graule, *Solid State Ionics*, 2007, **178**, 1437.

17. S. Tao and J. T. S. Irvine, *Journal of Solid State Chemistry*, 2007, **180**, 3493.

18. Y. Yamazaki, R. Hernandez-Sanchez and S. M. Haile, *Chemistry of Materials*, 2009, **21**, 2755.

19. Y. Yamazaki, R. Hernandez-Sanchez and S. M. Haile, *Journal of Materials Chemistry*, 2010, **20**, 8158.

20. E. Fabbri, D. Pergolesi, S. Licoccia and E. Traversa, *ECS Transactions*, 2009, **25**, 1745.

21. E. Fabbri, D. Pergolesi, S. Licoccia and E. Traversa, *Solid State Ionics*, 2010, **181**, 1043.

22. W. Münch, G. Seifert, K. D. Kreuer and J. Maier, *Solid State Ionics*, 1996, **86-88**, 647.

23. W. Münch, G. Seifert, K. D. Kreuer and J. Maier, *Solid State Ionics*, 1997, **97**, 39.

24. W. Munch, K. D. Kreuer, G. Seifert and J. Maier, *Solid State Ionics*, 2000, **136-137**, 183.

25. M. S. Islam, *Journal of Materials Chemistry*, 2000, **10**, 1027.

26. M. S. Islam, P. R. Slater, J. R. Tolchard and T. Dinges, *Dalton Transactions*, 2004, 3061.

27. M. A. Gomez, M. A. Griffin, S. Jindal, K. D. Rule and V. R. Cooper, *Journal of Chemical Physics*, 2005, **123**, 094703/1.

28. M. E. Bjorketun, P. G. Sundell and G. Wahnstrom, *Physical Review B*, 2007, **76**, 054307.

29. E. Bevillon and G. Geneste, *Physical Review B*, 2008, **77**, 184113/1.

30. B. Merinov and W. Goddard, III, *Journal of Chemical Physics*, 2009, **130**, 194707/1.

31. S. J. Stokes and M. S. Islam, *Journal of Materials Chemistry*, 2010, **20**, 6258.

32. B. Gross, C. Beck, F. Meyer, T. Krajewski, R. Hempelmann and H. Altgeld, *Solid State Ionics*, 2001, **145**, 325.

33. I. Ahmed, S. G. Eriksson, E. Ahlberg, C. S. Knee, H. Goetlind, L. G. Johansson, M. Karlsson, A. Matic and L. Boerjesson, *Solid State Ionics*, 2007, **178**, 515.

34. I. Ahmed, M. Karlsson, S.-G. Eriksson, E. Ahlberg, C. S. Knee, K. Larsson, A. K. Azad, A. Matic and L. Boerjesson, *Journal of the American Ceramic Society*, 2008, **91**, 3039.

35. T. Omata, Y. Noguchi and S. Otsuka-Yao-Matsuo, *Journal of the Electrochemical Society*, 2005, **152**, E200.

36. M. Karlsson, I. Ahmed, A. Matic and S. G. Eriksson, *Solid State Ionics*, 2010, **181**, 126.

37. Y. Yamazaki, P. Babilo and S. M. Haile, *Chemistry of Materials*, 2008, **20**, 6352.

38. C. Karmonik, T. J. Udovic, R. L. Paul, J. J. Rush, K. Lind and R. Hempelmann, *Solid State Ionics*, 1998, **109**, 207.

39. R. Hempelmann, M. Soetratmo, O. Hartmann and R. Wappling, *Solid State Ionics*, 1998, **107**, 269.

40. K. D. Kreuer, W. Munch, M. Ise, T. He, A. Fuchs, U. Traub and J. Maier, *Berichte der Bunsen-Gesellschaft*, 1997, **101**, 1344.

41. K. C. Liang, Y. Du and A. S. Nowick, *Solid State Ionics*, 1994, **69**, 117.

42. R. D. Shannon, *Acta Crystallographica, Section A Crystal Physics, Diffraction, Theoretical and General Crystallography*, 1976, **A32**, 751.

References

Chapter 1

1. S. C. Singhal, *MRS Bulletin*, 2000, **25**, 16.

2. R. M. Ormerod, *Chemical Society Reviews*, 2003, **32**, 17.

3. A. Lashtabeg and S. J. Skinner, *Journal of Materials Chemistry*, 2006, **16**, 3161.

4. D. J. L. Brett, A. Atkinson, N. P. Brandon and S. J. Skinner, *Chemical Society Reviews*, 2008, **37**, 1568.

5. J. C. Ruiz-Morales, D. Marrero-Lopez, M. Galvez-Sanchez, J. Canales-Vazquez, C. Savaniu and S. N. Savvin, *Energy and Environmental Science*, 2010, **3**, 1670.

6. Z. Zhan and S. A. Barnett, *Science*, 2005, **308**, 844.

7. M. D. Gross, J. M. Vohs and R. J. Gorte, *Journal of Materials Chemistry*, 2007, **17**, 3071.

8. W. Jamsak, S. Assabumrungrat, P. L. Douglas, N. Laosiripojana, R. Suwanwarangkul, S. Charojrochkul and E. Croiset, *Chemical Engineering Journal*, 2007, **133**, 187.

9. E. D. Wachsman and S. C. Singhal, *Electrochemical Society Interface*, 2009, **18**, 38.

10. G. W. Crabtree and M. S. Dresselhaus, *MRS Bulletin*, 2008, **33**, 421.

11. J. Larminie and A. Dicks, *Fuel Cell Systems Explained* John Wiley & Sons, 2nd edition, 2003.

12. D. Tucker, M. Shelton and A. Manivannan, *Electrochemical Society Interface*, 2009, **18**, 45.

13. S. M. Haile, *Acta Materialia*, 2003, **51**, 5981.

14. S. Stotz and C. Wagner, *Berichte der Bunsengesellschaft für Physikalische Chemie*, 1966, **70**, 781.

15. T. Takahashi and H. Iwahara, *Revue de Chimie Minerale*, 1980, **17**, 243.

16. H. Iwahara, H. Uchida and S. Tanaka, *Solid State Ionics*, 1983, **9-10**, 1021.

17. H. Iwahara, H. Uchida, K. Ono and K. Ogaki, *Journal of the Electrochemical Society*, 1988, **135**, 529.

18. K. D. Kreuer, S. Adams, W. Münch, A. Fuchs, U. Klock and J. Maier, *Solid State Ionics*, 2001, **145**, 295.

19. K. D. Kreuer, *Annual Review of Materials Research*, 2003, **33**, 333.

20. M. J. Scholten, J. Schoonman, J. C. van Miltenburg and H. A. J. Oonk, *Solid State Ionics*, 1993, **61**, 83.

21. K. H. Ryu and S. M. Haile, *Solid State Ionics*, 1999, **125**, 355.

22. H. Iwahara, T. Yajima, T. Hibino, K. Ozaki and H. Suzuki, *Solid State Ionics*, 1993, **61**, 65.

23. K. A. Furøy, R. Haugsrud, M. Hänsel, A. Magrasó and T. Norby, *Solid State Ionics*, 2007, **178**, 461.

24. M. J. Scholten, J. Schoonman, J. C. van Miltenburg and H. A. J. Oonk, *Proceedings - Electrochemical Society*, 1993, **93-4**, 146.

25. I. Naray-Szabo, *Naturwissenschaften*, 1943, **31**, 202.

26. T. Schober and H. G. Bohn, *Solid State Ionics*, 2000, **127**, 351.

27. H. G. Bohn and T. Schober, *Journal of the American Ceramic Society*, 2000, **83**, 768.

28. A. Magrez and T. Schober, *Solid State Ionics*, 2004, **175**, 585.

29. F. M. M. Snijkers, A. Buekenhoudt, J. Cooymans and J. J. Luyten, *Scripta Materialia*, 2004, **50**, 655.

30. P. Babilo, T. Uda and S. M. Haile, *Journal of Materials Research*, 2007, **22**, 1322.

31. F. Iguchi, N. Sata, T. Tsurui and H. Yugami, *Solid State Ionics*, 2007, **178**, 691.

32. S. B. C. Duval, P. Holtappels, U. F. Vogt, E. Pomjakushina, K. Conder, U. Stimming and T. Graule, *Solid State Ionics*, 2007, **178**, 1437.

33. S. Tao and J. T. S. Irvine, *Journal of Solid State Chemistry*, 2007, **180**, 3493.

34. R. B. Cervera, Y. Oyama, S. Miyoshi, K. Kobayashi, T. Yagi and S. Yamaguchi, *Solid State Ionics*, 2008, **179**, 236.

35. S. Higgins, N. M. Sammes, A. Smirnova, J. A. Kilner and G. Tompsett, *Journal of Fuel Cell Science and Technology*, 2008, **5**, 027001/1.

36. F. Iguchi, T. Tsurui, N. Sata, Y. Nagao and H. Yugami, *Solid State Ionics*, 2009, **180**, 563.

37. Y. Yamazaki, R. Hernandez-Sanchez and S. M. Haile, *Chemistry of Materials*, 2009, **21**, 2755.

38. Y. Yamazaki, P. Babilo and S. M. Haile, *Chemistry of Materials*, 2008, **20**, 6352.

39. S. Imashuku, T. Uda and Y. Awakura, *ECS Transactions*, 2007, **7**, 2321.

40. S. Imashuku, T. Uda, T. Ichitsubo, E. Matsubara and Y. Awakura, *Journal of Phase Equilibria and Diffusion*, 2007, **28**, 517.

41. P. Murugaraj, K. D. Kreuer, T. He, T. Schober and J. Maier, *Solid State Ionics*, 1997, **98**, 1.

42. D. L. Pavia, G. M. Lampman and G. S. Kriz, *Introduction to spectroscopy*, 3rd edn., Hartcourt College Publisher, Orlando, 2001.

43. E. Fukushima and S. B. W. Roeder, *Experimental pulse NMR - A nuts and bolts approach*, Massachusetts, 1981.

44. D. D. Laws, H.-M. L. Bitter and A. Jerschow, *Angewandte Chemie, International Edition*, 2002, **41**, 3096.

45. M. H. Levitt, *Spin Dynamics: Basics of Nuclear Magnetic Resonance*, John Wiley & Sons, 2001.

46. M. J. Duer, *Introduction to Solid-State NMR Spectroscopy*, Blackwell Publishing Ltd, Oxford, 2004.

47. M. E. Smith and E. R. H. Van Eck, *Progress in Nuclear Magnetic Resonance Spectroscopy*, 1999, **34**, 159.

48. K. J. D. MacKenzie, *Solid State Ionics*, 2004, **172**, 383.

49. L. Frydman and J. S. Harwood, *Journal of the American Chemical Society*, 1995, **117**, 5367.

50. C. P. Grey and A. J. Vega, *Journal of the American Chemical Society*, 1995, **117**, 8232.

Chapter 2

1. L. Buannic, F. Blanc, I. Hung, Z. Gan and C. P. Grey, *Journal of Materials Chemistry*, 2010, **20**, 6322.

2. M. J. Scholten, J. Schoonman, J. C. van Miltenburg and H. A. J. Oonk, *Proceedings - Electrochemical Society*, 1993, **93-4**, 146.

3. T. Schober and H. G. Bohn, *Solid State Ionics*, 2000, **127**, 351.

4. H. G. Bohn and T. Schober, *Journal of the American Ceramic Society*, 2000, **83**, 768.

5. A. Magrez and T. Schober, *Solid State Ionics*, 2004, **175**, 585.

6. F. M. M. Snijkers, A. Buekenhoudt, J. Cooymans and J. J. Luyten, *Scripta Materialia*, 2004, **50**, 655.

7. P. Babilo, T. Uda and S. M. Haile, *Journal of Materials Research*, 2007, **22**, 1322.

8. F. Iguchi, N. Sata, T. Tsurui and H. Yugami, *Solid State Ionics*, 2007, **178**, 691.

9. S. B. C. Duval, P. Holtappels, U. F. Vogt, E. Pomjakushina, K. Conder, U. Stimming and T. Graule, *Solid State Ionics*, 2007, **178**, 1437.

10. S. Tao and J. T. S. Irvine, *Journal of Solid State Chemistry*, 2007, **180**, 3493.

11. R. B. Cervera, Y. Oyama, S. Miyoshi, K. Kobayashi, T. Yagi and S. Yamaguchi, *Solid State Ionics*, 2008, **179**, 236.

12. S. Higgins, N. M. Sammes, A. Smirnova, J. A. Kilner and G. Tompsett, *Journal of Fuel Cell Science and Technology*, 2008, **5**, 027001/1.

13. F. Iguchi, T. Tsurui, N. Sata, Y. Nagao and H. Yugami, *Solid State Ionics*, 2009, **180**, 563.

14. Y. Yamazaki, R. Hernandez-Sanchez and S. M. Haile, *Chemistry of Materials*, 2009, **21**, 2755.

15. K. D. Kreuer, S. Adams, W. Münch, A. Fuchs, U. Klock and J. Maier, *Solid State Ionics*, 2001, **145**, 295.

16. K. D. Kreuer, *Annual Review of Materials Research*, 2003, **33**, 333.

17. I. Naray-Szabo, *Naturwissenschaften*, 1943, **31**, 202.

18. Y. Yamazaki, P. Babilo and S. M. Haile, *Chemistry of Materials*, 2008, **20**, 6352.

19. S. Imashuku, T. Uda and Y. Awakura, *ECS Transactions*, 2007, **7**, 2321.

20. S. Imashuku, T. Uda, T. Ichitsubo, E. Matsubara and Y. Awakura, *Journal of Phase Equilibria and Diffusion*, 2007, **28**, 517.

21. N. Kim, C.-H. Hsieh and J. F. Stebbins, *Chemistry of Materials*, 2006, **18**, 3855.

22. K. J. D. MacKenzie and M. E. Smith, *Multinuclear Solid-State Nuclear Magnetic Resonance of Inorganic Materials*, Pergamon Oxford, 2002.

23. A. J. Rossini and R. W. Schurko, *Journal of the American Chemical Society*, 2006, **128**, 10391.

24. N. Kim and J. F. Stebbins, *Chemistry of Materials*, 2009, **21**, 309.

25. N. Kim, J. F. Stebbins, S. Quartieri and R. Oberti, *American Mineralogist*, 2007, **92**, 1875.

26. P. Jain, H. J. Avila-Paredes, C. Gapuz, S. Sen and S. Kim, *Journal of Physical Chemistry C*, 2009, **113**, 6553.

27. D. Riou, F. Fayon and D. Massiot, *Chemistry of Materials*, 2002, **14**, 2416.

28. S. E. Ashbrook and M. E. Smith, *Chemical Society Reviews*, 2006, **35**, 718.

29. A. E. McDermott, F. J. Creuzet, A. C. Kolbert and R. G. Griffin, *Journal of Magnetic Resonance*, 1992, **98**, 408.

30. D. H. Zhou, D. T. Graesser, W. T. Franks and C. M. Rienstra, *Journal of Magnetic Resonance*, 2006, **178**, 297.

31. A. Samoson, *Extended magic-angle spinning*, Wiley, Chichester, UK, 2002.

32. A. Samoson, T. Tuherm, J. Past, A. Reinhold, T. Anupold and I. Heinmaa, *Topics in Current Chemistry*, 2005, **246**, 15.

33. B. C. Gerstein, *CRAMPS*, Wiley, Chichester, U.K., 1996.

34. A. Lesage, *Physical Chemistry Chemical Physics*, 2009, **11**, 6876.

35. P. Babilo and S. M. Haile, *Journal of the American Ceramic Society*, 2005, **88**, 2362.

36. Z. Gan, P. L. Gor'kov, W. W. Brey, P. J. Sideris and C. P. Grey, *Journal of Magnetic Resonance*, 2009, **200**, 2.

37. L. Frydman, *Encyclopedia of Nuclear Magnetic Resonance*, 2002, **9**, 262.

38. Z. Gan and H.-T. Kwak, *Journal of Magnetic Resonance*, 2004, **168**, 346.

39. J.-P. Amoureux, C. Fernandez and S. Steuernagel, *Journal of Magnetic Resonance, Series A*, 1996, **123**, 116.

40. A. Bielecki and D. P. Burum, *Journal of Magnetic Resonance, Series A*, 1995, **116**, 215.

41. J. D. van Beek, *Journal of Magnetic Resonance*, 2007, **187**, 19.

42. K. Eichele and R. E. Wasylishen, Dalhousie University, Halifax, Canada.

43. M. Bak, J. T. Rasmussen and N. C. Nielsen, *Journal of Magnetic Resonance*, 2000, **147**, 296.

44. P. Hodgkinson and L. Emsley, *Progress in Nuclear Magnetic Resonance Spectroscopy*, 2000, **36**, 201.

45. R. D. Shannon, *Acta Crystallographica, Section A Crystal Physics, Diffraction, Theoretical and General Crystallography*, 1976, **A32**, 751.

46. I. Oikawa, M. Ando, Y. Noda, K. Amezawa, H. Kiyono, T. Shimizu, M. Tansho and H. Maekawa, *17th International Conference on Solid State Ionics*, Toronto, 2009.

47. L. Frydman and J. S. Harwood, *Journal of the American Chemical Society*, 1995, **117**, 5367.

48. A. Medek, J. S. Harwood and L. Frydman, *Journal of the American Chemical Society*, 1995, **117**, 12779.

49. I. Hung, J. Trébosc, G. L. Hoatson, R. L. Vold, J.-P. Amoureux and Z. Gan, *Journal of Magnetic Resonance*, 2009, **201**, 81.

50. T. J. Bastow, P. J. Dirken, M. E. Smith and H. J. Whitfield, *Journal of Physical Chemistry*, 1996, **100**, 18539.

51. E. Oldfield, C. Coretsopoulos, S. Yang, L. Reven, H. C. Lee, J. Shore, O. H. Han, E. Ramli and D. Hinks, *Physical Review B Condensed Matter and Materials Physics*, 1989, **40**, 6832.

52. D. S. Middlemiss, F. Blanc, C. J. Pickard and C. P. Grey, *Journal of Magnetic Resonance*, 2010, **204**, 1.

53. M. H. Levitt, *Spin Dynamics: Basics of Nuclear Magnetic Resonance*, John Wiley & Sons, 2001.

54. T. Matzke, U. Stimming, C. Karmonik, M. Soetratmo, R. Hempelmann and F. Güthoff, *Solid State Ionics*, 1996, **86-88**, 621.

55. M. Pionke, T. Mono, W. Schweika, T. Springer and H. Schober, *Solid State Ionics*, 1997, **97**, 497.

56. W. Münch, G. Seifert, K. D. Kreuer and J. Maier, *Solid State Ionics*, 1996, **86-88**, 647.

57. W. Münch, G. Seifert, K. D. Kreuer and J. Maier, *Solid State Ionics*, 1997, **97**, 39.

58. K. D. Kreuer, W. Münch, U. Traub and J. Maier, *Berichte der Bunsen-Gesellschaft*, 1998, **102**, 552.

59. F. Shimojo, K. Hoshino and H. Okazaki, *Journal of the Physical Society of Japan*, 1997, **66**, 8.

Chapter 3

1. H. Iwahara, T. Yajima, T. Hibino, K. Ozaki and H. Suzuki, *Solid State Ionics*, 1993, **61**, 65.

2. R. C. T. Slade, S. D. Flint and N. Singh, *Solid State Ionics*, 1995, **82**, 135.

3. K. D. Kreuer, *Solid State Ionics*, 1997, **97**, 1.

4. K. D. Kreuer, *Solid State Ionics*, 1999, **125**, 285.

5. H. G. Bohn and T. Schober, *Journal of the American Ceramic Society*, 2000, **83**, 768.

6. K. D. Kreuer, S. Adams, W. Münch, A. Fuchs, U. Klock and J. Maier, *Solid State Ionics*, 2001, **145**, 295.

7. K. D. Kreuer, *Annual Review of Materials Research*, 2003, **33**, 333.

8. F. M. M. Snijkers, A. Buekenhoudt, J. Cooymans and J. J. Luyten, *Scripta Materialia*, 2004, **50**, 655.

9. F. Iguchi, N. Sata, T. Tsurui and H. Yugami, *Solid State Ionics*, 2007, **178**, 691.

10. S. B. C. Duval, P. Holtappels, U. F. Vogt, E. Pomjakushina, K. Conder, U. Stimming and T. Graule, *Solid State Ionics*, 2007, **178**, 1437.

11. S. Tao and J. T. S. Irvine, *Journal of Solid State Chemistry*, 2007, **180**, 3493.

12. Y. Yamazaki, R. Hernandez-Sanchez and S. M. Haile, *Chemistry of Materials*, 2009, **21**, 2755.

13. Y. Yamazaki, R. Hernandez-Sanchez and S. M. Haile, *Journal of Materials Chemistry,* 2010, **20**, 8158.

14. P. Babilo and S. M. Haile, *Journal of the American Ceramic Society*, 2005, **88**, 2362.

15. J.-P. Amoureux, C. Fernandez and S. Steuernagel, *Journal of Magnetic Resonance, Series A*, 1996, **123**, 116.

16. A. Bielecki and D. P. Burum, *Journal of Magnetic Resonance, Series A*, 1995, **116**, 215.

17. J. B. Grutzner, K. W. Stewart, R. E. Wasylishen, M. D. Lumsden, C. Dybowski and P. A. Beckmann, *Journal of the American Chemical Society*, 2001, **123**, 7094.

18. G.-J. M. P. van Moorsel, E. R. H. Van Eck and C. P. Grey, *Journal of Magnetic Resonance, Series A*, 1995, **113**, 159.

19. R. D. Shannon, *Acta Crystallographica, Section A Crystal Physics, Diffraction, Theoretical and General Crystallography*, 1976, **A32**, 751.

20. A. Magrez and T. Schober, *Solid State Ionics*, 2004, **175**, 585.

21. Y. Yamazaki, C.-K. Yang and S. M. Haile, *Scripta Materialia*, 2011, **65**, 102.

22. T. Schober and H. G. Bohn, *Solid State Ionics*, 2000, **127**, 351.

23. Y. Yamazaki, P. Babilo and S. M. Haile, *Chemistry of Materials*, 2008, **20**, 6352.

24. E. Fabbri, D. Pergolesi, S. Licoccia and E. Traversa, *Solid State Ionics*, 2010, **181**, 1043.

25. P. Babilo, T. Uda and S. M. Haile, *Journal of Materials Research*, 2007, **22**, 1322.

26. R. B. Cervera, Y. Oyama, S. Miyoshi, K. Kobayashi, T. Yagi and S. Yamaguchi, *Solid State Ionics*, 2008, **179**, 236.

27. A. K. Azad, C. Savaniu, S. Tao, S. Duval, P. Holtappels, R. M. Ibberson and J. T. S. Irvine, *Journal of Materials Chemistry,* 2008, **18**, 3414.

28. F. Iguchi, T. Tsurui, N. Sata, Y. Nagao and H. Yugami, *Solid State Ionics*, 2009, **180**, 563.

29. T. Omata, M. Takagi and S. Otsuka-Yao-Matsuo, *Solid State Ionics*, 2004, **168**, 99.

30. S. Imashuku, T. Uda, Y. Nose, G. Taniguchi, Y. Ito and Y. Awakura, *Journal of the Electrochemical Society,* 2009, **156**, B1.

31. F. Iguchi, N. Sata and H. Yugami, *Journal of Materials Chemistry,* 2010, **20**, 6265.

32. T. J. Bastow, P. J. Dirken, M. E. Smith and H. J. Whitfield, *Journal of Physical Chemistry*, 1996, **100**, 18539.

33. M. H. Levitt, *Spin Dynamics: Basics of Nuclear Magnetic Resonance*, John Wiley & Sons, 2001.

34. M. M. Maricq and J. S. Waugh, *Journal of Chemical Physics*, 1979, **70**, 3300.

35. L. Holmes, L. Peng, I. Heinmaa, L. A. O'Dell, M. E. Smith, R.-N. Vannier and C. P. Grey, *Chemistry of Materials*, 2008, **20**, 3638.

36. S. E. Ashbrook, K. R. Whittle, G. R. Lumpkin and I. Farnan, *Journal of Physical Chemistry B,* 2006, **110**, 10358.

37. R. Dupree and M. E. Smith, *Chemical Physics Letters*, 1988, **148**, 41.

38. A. I. Becerro, A. Escudero, P. Florian, D. Massiot and M. D. Alba, *Journal of Solid State Chemistry*, 2004, **177**, 2783.

39. T. Harazono and T. Watanabe, *Bulletin of the Chemical Society of Japan,* 1997, **70**, 2383.

40. C. P. Grey, M. E. Smith, A. K. Cheetham, C. M. Dobson and R. Dupree, *Journal of the American Chemical Society*, 1990, **112**, 4670.

41. P. Florian, D. Massiot, G. Humbert and J.-P. Coutures, *Comptes Rendus de l'Académie des Sciences, Série IIb: Mécanique,Physique, Chimie, Astronomie,* 1995, **320**, 99.

42. K. Kawata, H. Maekawa, T. Nemoto and T. Yamamura, *Solid State Ionics*, 2006, **177**, 1687.

43. P. Jain, H. J. Avila-Paredes, C. Gapuz, S. Sen and S. Kim, *Journal of Physical Chemistry C*, 2009, **113**, 6553.

44. N. Kim and J. F. Stebbins, *Chemistry of Materials*, 2007, **19**, 5742.

45. S. W. Reader, M. R. Mitchell, K. E. Johnston, C. J. Pickard, K. R. Whittle and S. E. Ashbrook, *Journal of Physical Chemistry C*, 2009, **113**, 18874.

46. E. J. Harvey, S. E. Ashbrook, G. R. Lumpkin and S. A. T. Redfern, *Journal of Materials Chemistry,* 2006, **16**, 4665.

47. K. J. D. MacKenzie and M. E. Smith, *Multinuclear Solid-State Nuclear Magnetic Resonance of Inorganic Materials*, Pergamon Oxford, 2002.

Chapter 4

1. K. D. Kreuer, *Annual Review of Materials Research*, 2003, **33**, 333.

2. P. Murugaraj, K. D. Kreuer, T. He, T. Schober and J. Maier, *Solid State Ionics*, 1997, **98**, 1.

3. I. Naray-Szabo, *Naturwissenschaften*, 1943, **31**, 202.

4. K. V. Paulose, P. Murugaraj, J. Koshy and A. D. Damodaran, *Japanese Journal of Applied Physics, Part 1 Regular Papers, Short Notes & Review Papers*, 1992, **31**, 1323.

5. J. Koshy, K. S. Kumar, J. Kurian, Y. P. Yadava and A. D. Damodaran, *Bulletin of Materials Science*, 1994, **17**, 577.

6. H. D. Megaw, *Proceedings of the Physical Society,* 1946, **58**, 133.

7. N. J. Clayden, C. M. Dobson and A. Fern, *Journal of the Chemical Society, Dalton Transactions Inorganic Chemistry*, 1989, 843.

8. M. R. Mitchell, S. W. Reader, K. E. Johnston, C. J. Pickard, K. R. Whittle and S. E. Ashbrook, *Physical Chemistry Chemical Physics*, 2011, **13**, 488.

9. P. Babilo and S. M. Haile, *Journal of the American Ceramic Society*, 2005, **88**, 2362.

10. A. Bielecki and D. P. Burum, *Journal of Magnetic Resonance, Series A*, 1995, **116**, 215.

11. J. B. Grutzner, K. W. Stewart, R. E. Wasylishen, M. D. Lumsden, C. Dybowski and P. A. Beckmann, *Journal of the American Chemical Society*, 2001, **123**, 7094.

12. G.-J. M. P. van Moorsel, E. R. H. Van Eck and C. P. Grey, *Journal of Magnetic Resonance, Series A*, 1995, **113**, 159.

13. J.-P. Amoureux, C. Fernandez and S. Steuernagel, *Journal of Magnetic Resonance, Series A*, 1996, **123**, 116.

14. J. D. van Beek, *Journal of Magnetic Resonance*, 2007, **187**, 19.

15. M. Bak, J. T. Rasmussen and N. C. Nielsen, *Journal of Magnetic Resonance*, 2000, **147**, 296.

16. P. Hodgkinson and L. Emsley, *Progress in Nuclear Magnetic Resonance Spectroscopy*, 2000, **36**, 201.

17. M. A. Subramanian, *Journal of Solid State Chemistry*, 1994, **111**, 134.

18. K. J. D. MacKenzie and M. E. Smith, *Multinuclear Solid-State Nuclear Magnetic Resonance of Inorganic Materials*, Pergamon Oxford, 2002.

19. S. E. Ashbrook and M. E. Smith, *Chemical Society Reviews*, 2006, **35**, 718.

20. T. J. Bastow, P. J. Dirken, M. E. Smith and H. J. Whitfield, *Journal of Physical Chemistry*, 1996, **100**, 18539.

21. L. Frydman and J. S. Harwood, *Journal of the American Chemical Society*, 1995, **117**, 5367.

22. A. Medek, J. S. Harwood and L. Frydman, *Journal of the American Chemical Society*, 1995, **117**, 12779.

23. S. E. Ashbrook, K. R. Whittle, G. R. Lumpkin and I. Farnan, *Journal of Physical Chemistry B*, 2006, **110**, 10358.

24. R. Dupree and M. E. Smith, *Chemical Physics Letters*, 1988, **148**, 41.

25. A. I. Becerro, A. Escudero, P. Florian, D. Massiot and M. D. Alba, *Journal of Solid State Chemistry*, 2004, **177**, 2783.

26. T. Harazono and T. Watanabe, *Bulletin of the Chemical Society of Japan*, 1997, **70**, 2383.

27. C. P. Grey, M. E. Smith, A. K. Cheetham, C. M. Dobson and R. Dupree, *Journal of the American Chemical Society*, 1990, **112**, 4670.

28. P. Florian, D. Massiot, G. Humbert and J.-P. Coutures, *Comptes Rendus de l'Académie des Sciences, Série IIb: Mécanique,Physique, Chimie, Astronomie*, 1995, **320**, 99.

29. K. Kawata, H. Maekawa, T. Nemoto and T. Yamamura, *Solid State Ionics*, 2006, **177**, 1687.

30. P. Jain, H. J. Avila-Paredes, C. Gapuz, S. Sen and S. Kim, *Journal of Physical Chemistry C*, 2009, **113**, 6553.

31. N. Kim and J. F. Stebbins, *Chemistry of Materials*, 2007, **19**, 5742.

32. S. W. Reader, M. R. Mitchell, K. E. Johnston, C. J. Pickard, K. R. Whittle and S. E. Ashbrook, *Journal of Physical Chemistry C*, 2009, **113**, 18874.

33. E. J. Harvey, S. E. Ashbrook, G. R. Lumpkin and S. A. T. Redfern, *Journal of Materials Chemistry*, 2006, **16**, 4665.

34. Y. Yamazaki, R. Hernandez-Sanchez and S. M. Haile, *Journal of Materials Chemistry*, 2010, **20**, 8158.

35. M. H. Levitt, *Spin Dynamics: Basics of Nuclear Magnetic Resonance*, John Wiley & Sons, 2001.

36. M. S. Islam, *Journal of Materials Chemistry*, 2000, **10**, 1027.

37. M. S. Islam, P. R. Slater, J. R. Tolchard and T. Dinges, *Dalton Transactions*, 2004, 3061.

Chapter 5

1. H. Iwahara, H. Uchida, K. Ono and K. Ogaki, *Journal of the Electrochemical Society*, 1988, **135**, 529.

2. H. Iwahara, T. Yajima, T. Hibino, K. Ozaki and H. Suzuki, *Solid State Ionics*, 1993, **61**, 65.

3. R. C. T. Slade, S. D. Flint and N. Singh, *Solid State Ionics*, 1995, **82**, 135.

4. K. D. Kreuer, *Solid State Ionics*, 1997, **97**, 1.

5. P. Murugaraj, K. D. Kreuer, T. He, T. Schober and J. Maier, *Solid State Ionics*, 1997, **98**, 1.

6. T. Schober, *Solid State Ionics*, 1998, **109**, 1.

7. K. D. Kreuer, *Solid State Ionics*, 1999, **125**, 285.

8. H. G. Bohn and T. Schober, *Journal of the American Ceramic Society*, 2000, **83**, 768.

9. K. Katahira, Y. Kohchi, T. Shimura and H. Iwahara, *Solid State Ionics*, 2000, **138**, 91.

10. K. D. Kreuer, S. Adams, W. Münch, A. Fuchs, U. Klock and J. Maier, *Solid State Ionics*, 2001, **145**, 295.

11. K. D. Kreuer, *Annual Review of Materials Research*, 2003, **33**, 333.

12. O. Parkash, D. Kumar, K. K. Srivastav and R. K. Dwivedi, *Journal of Materials Science*, 2001, **36**, 5805.

13. F. M. M. Snijkers, A. Buekenhoudt, J. Cooymans and J. J. Luyten, *Scripta Materialia*, 2004, **50**, 655.

14. P. Singh, O. Parkash and D. Kumar, *Journal of Materials Science: Materials in Electronics*, 2005, **16**, 145.

15. F. Iguchi, N. Sata, T. Tsurui and H. Yugami, *Solid State Ionics*, 2007, **178**, 691.

16. S. B. C. Duval, P. Holtappels, U. F. Vogt, E. Pomjakushina, K. Conder, U. Stimming and T. Graule, *Solid State Ionics*, 2007, **178**, 1437.

17. S. Tao and J. T. S. Irvine, *Journal of Solid State Chemistry*, 2007, **180**, 3493.

18. Y. Yamazaki, R. Hernandez-Sanchez and S. M. Haile, *Chemistry of Materials*, 2009, **21**, 2755.

19. Y. Yamazaki, R. Hernandez-Sanchez and S. M. Haile, *Journal of Materials Chemistry*, 2010, **20**, 8158.

20. E. Fabbri, D. Pergolesi, S. Licoccia and E. Traversa, *ECS Transactions*, 2009, **25**, 1745.

21. E. Fabbri, D. Pergolesi, S. Licoccia and E. Traversa, *Solid State Ionics*, 2010, **181**, 1043.

22. W. Münch, G. Seifert, K. D. Kreuer and J. Maier, *Solid State Ionics*, 1996, **86-88**, 647.

23. W. Münch, G. Seifert, K. D. Kreuer and J. Maier, *Solid State Ionics*, 1997, **97**, 39.

24. W. Munch, K. D. Kreuer, G. Seifert and J. Maier, *Solid State Ionics*, 2000, **136-137**, 183.

25. M. S. Islam, *Journal of Materials Chemistry*, 2000, **10**, 1027.

26. M. S. Islam, P. R. Slater, J. R. Tolchard and T. Dinges, *Dalton Transactions*, 2004, 3061.

27. M. A. Gomez, M. A. Griffin, S. Jindal, K. D. Rule and V. R. Cooper, *Journal of Chemical Physics*, 2005, **123**, 094703/1.

28. M. E. Bjorketun, P. G. Sundell and G. Wahnstrom, *Physical Review B*, 2007, **76**, 054307.

29. E. Bevillon and G. Geneste, *Physical Review B*, 2008, **77**, 184113/1.

30. B. Merinov and W. Goddard, III, *Journal of Chemical Physics*, 2009, **130**, 194707/1.

31. S. J. Stokes and M. S. Islam, *Journal of Materials Chemistry*, 2010, **20**, 6258.

32. B. Gross, C. Beck, F. Meyer, T. Krajewski, R. Hempelmann and H. Altgeld, *Solid State Ionics*, 2001, **145**, 325.

33. I. Ahmed, S. G. Eriksson, E. Ahlberg, C. S. Knee, H. Goetlind, L. G. Johansson, M. Karlsson, A. Matic and L. Boerjesson, *Solid State Ionics*, 2007, **178**, 515.

34. I. Ahmed, M. Karlsson, S.-G. Eriksson, E. Ahlberg, C. S. Knee, K. Larsson, A. K. Azad, A. Matic and L. Boerjesson, *Journal of the American Ceramic Society*, 2008, **91**, 3039.

35. T. Omata, Y. Noguchi and S. Otsuka-Yao-Matsuo, *Journal of the Electrochemical Society*, 2005, **152**, E200.

36. M. Karlsson, I. Ahmed, A. Matic and S. G. Eriksson, *Solid State Ionics*, 2010, **181**, 126.

37. Y. Yamazaki, P. Babilo and S. M. Haile, *Chemistry of Materials*, 2008, **20**, 6352.

38. C. Karmonik, T. J. Udovic, R. L. Paul, J. J. Rush, K. Lind and R. Hempelmann, *Solid State Ionics*, 1998, **109**, 207.

39. R. Hempelmann, M. Soetratmo, O. Hartmann and R. Wappling, *Solid State Ionics*, 1998, **107**, 269.

40. K. D. Kreuer, W. Munch, M. Ise, T. He, A. Fuchs, U. Traub and J. Maier, *Berichte der Bunsen-Gesellschaft*, 1997, **101**, 1344.

41. K. C. Liang, Y. Du and A. S. Nowick, *Solid State Ionics*, 1994, **69**, 117.

42. R. D. Shannon, *Acta Crystallographica, Section A Crystal Physics, Diffraction, Theoretical and General Crystallography*, 1976, **A32**, 751.